The Institute of Space and Astronautical Science
Report SP No. 10, September 1989

EXECUTIVE SUMMARY

The High Energy Particle Experiment (HEP) for GEOTAIL mission has been designed to understand (1) the particle acceleration mechanism, energy flow, boundary dynamics, magnetic reconnection mechanism in the geotail region, (2) the solar flare particle acceleration mechanism, the propagation mechanism through the interplanetary space, and (3) the origin, lifetime, propagation mechanism of cosmic ray heavy ions. Achieving these objectives, Low Energy Particle Detectors (LD), Burst Detectors (BD), Medium Energy Isotope Telescopes (MI-1 and MI-2), and High Energy Isotope Telescope (HI) will be placed in the spacecraft.

Particles having energy ranges indicated below will be detected by these detectors.

Electron	20 keV	–	2.5 MeV
Proton	2 keV	–	35 MeV
Helium	2 keV	–	220 MeV
Carbon	4.5	–	110 MeV/n
Silicon	6.2	–	180 MeV/n
Iron	7.5	–	210 MeV/n

Characteristics and the main technique used for each instrument to observe high energy particles are summarized in Table ES-1. Details of the scientific objectives, the basic principles of particle identifications, electronics system and data processing system, key parameter information, telemetry data formats, preflight and in-flight calibration method, data analysis plan are described in this document.

Table ES-1 GEOTAIL HEP instrument characteristics and resource requirements.

Sensors	LD	BD	MI-1	MI-2	HI	Electronics	Total
Energy range							
for electrons	20-300 keV	0.12-2.5 MeV	–	–	–		
for protons	2 keV-1.5 MeV*	0.4-35. MeV**	MeV/n	–	MeV/n		
He	2 keV-1.5 MeV*	3.5-35. MeV/n	2.4-20	–	10-55		
	(*1.5MeV-6.MeV/n over flow channel)		(2.4-15)***		(10-40)		
	(**0.4-3.5 MeV proton and He)			MeV/n			
C	–	–	4.5-38	6.5-40	18-110		
			(4.5-38)	(6.5-40)	(18-110)		
Ne	–	–	5.5-50	8.0-52	24-130		
			(5.5-50)	(8.0-52)	(24-130)		
Ca	–			12.0-80	34-210		
				(14.0-74)	(34-210)		
Fe	–	–	7.5-80	3.-80	38-210		
				(16.0-65)	(21-210)		
Z<45	–	–	–	14.-120			
			(***( ) Energy range for nuclear mass)				
Charge range							
for elements	1-20	1-2	2-20	6-45	2-28		
for isotopes	–	–	2-10	6-28	2-28		
Number of sensors	3x4#	3	1	2	1		
	(#3 for electrons, 12 for protons)						
Geometrical factors (cm^2 sr)	0.02 each	0.76 each	4.	30. each	40		
View cone full angle	6°x12° each	30°x45° each	90°x90°	120°x120°	120°x120°		
Orientation to spin axis	30°, 90°, 150°	30°, 90°, 150°	90°	90°	90°		
Main techniques	TOF, ΔExE	ΔExE	PSD, ΔExE	PSD, ΔExE	PSD, ΔExE		
Weight (g)	4150±300	3000±200	3200±640 (MI-1 & MI-2)		2500±500	6200±620	19050
Power (mW)	4770 (3670##)	2808 (936##)	4980(4980##)(MI-1&-2)		2448(2448##)	10620(8700)	25620
	(## save mode)						
Size (mm^3)	200x200x305	210x242x130	440x170x152(MI-1 &-2)		220x180x180	300x260x235	
TLM bit rate (bps)	2560 real 512 record 32kbps RAM check	3100 real 160 record	40W/Isotope (MI-1, -2 & HI)				

1. INTRODUCTION

The GEOTAIL mission, which will be launched in 1992 as one of the spacecraft missions in ISTP (International Solar Terrestrial Physics) program, is placed into an 8 x 250 R_E orbit in the magnetotail for the first two years to study the characteristics of the plasma and field topology in the distant tail region. Then the trajectory will be modified to an 8 x 20 R_E equatorial orbit and the observation of the plasma dynamics in the near tail region and outer magnetosphere is continued for the next one and a half years. GEOTAIL mission has different subsystems to pursue the in-situ observation of plasma, solar wind, magnetic field as well as charged particles to understand the physical processes contributing to the variation of these parameters.

HEP (High Energy Particle) subsystem is designed to observe several species of charged particles in wide energy range in the vicinity of spacecraft to understand charged particle environment. The objectives of the HEP subsystem can be divided into two categories. The first category is the study of plasma dynamics and the second category is the studies of the solar flare mechanism, the anomalous cosmic ray particles and the galactic cosmic ray particles. The HEP consists of 5 different type detectors (LD, BD, MI-1, MI-2, and HI) and a data processing unit (DPU). LD and BD are mainly used to measure low energy particles which reflect plasma dynamics in the tail geomagnetosphere. On the other hand, MI-1, MI-2 and HI are mostly sensitive to solar particles and cosmic rays which reflect physical condition of interplanetary space and the origin of these particles. LD's (= Low energy particle Detectors), are new type ion-mass spectrometers with a small geometric factor, using time of flight technique and the silicon detector system, to identify particle mass and to measure three dimensional distribution of low energy particle flux. BD's (= Burst Detectors) are silicon detector telescopes with a large geometrical factor for measuring three dimensional distribution of burst particle flux in the magnetotail region. MI-1, MI-2 and HI are newly developed ΔE x E silicon detector telescopes with large geometric factor compared with those used in space so far. MI-1 (= Medium energy Isotope detector 1) measures isotope abundances of relatively light solar particles in the medium energy region and MI-2s measure isotope abundances of particles from carbon to iron in the medium energy region as well as element abundances of particles heavier than iron included in the solar flares. HI (= High energy heavy Isotope telescope) measures isotope abundances of high energy particles included in galactic cosmic rays and solar flares. In the section 2, the scientific objectives of the HEP experiment are described. In the section 3, the details of the instruments for these experiments are shown. In the section from 4 to 8, the key parameters, the telemeter data formats, the test and calibration plans and the data analysys scenario for each instrument are described.

2. Scientific Backgrounds and Objectives

The scientific backgrounds and objectives of GEOTAIL HEP instruments LD, BD, MI-1, MI-2 and HI are presented in this section.

2.1 Energetic Particles in the Magnetosphere

A rich variety of energetic particle phenomena have been observed inside and around the magnetosphere. At the earth's bow shock, upstream reflection of solar wind ions and subsequent first-order Fermi acceleration processes accelerate ions up to >100 keV energies. Around the dayside magnetopause, where the solar wind interacts strongly with the earth's magnetosphere, energetic ions are released from the magnetosphere via interacting field lines. These particles provide an excellent diagnostic tool for the study of interaction mechanisms. The solar wind energy imparted to the magnetosphere through the day-side interaction processes is eventually stored in the magnetotail and then released inside the magnetosphere in an explosive way: this phenomenon, known as magnetospheric substorms, leads to very dynamic reconfigurational changes of the magnetosphere. Bursts of ions and electrons extending in energy from a few keV to >1 MeV are observed when the spacecraft encounters the tail plasma sheet in the process of dynamical deformations.

One of the major science objectives of GEOTAIL mission is to investigate the physical mechanisms that are hidden behind the complexity of these strongly time-dependent, spatially non-uniform appearances of energetic particles. The HEP-LD and -BD instruments are designed to complement each other to measure a wide range of energetic particles (2 keV/n to 35 MeV for ions, and 20 keV to 2.5 MeV for electrons) with full angular coverage in velocity space. These instruments will provide a perfect platform to elucidate the roles and fate of energetic particles throughout the solar wind-magnetosphere interaction processes.

Energetic particles also serve as a useful diagnostic tool for remote sensing of boundaries in the magnetosphere. Owing to a finite gyroradius effect, angular anisotropy of energetic ions in the plane perpendicular to the magnetic field reflects spatial gradients in particle density up to two gyroradii from the observation point. For example, under the dayside magnetopause conditions, presence of boundaries at the distance of $0.1R_E$ from the satellite can be sensed by examining the azimuthal anisotropy of 100 keV protons arriving at the position of satellite. Distance, direction and attitude of boundaries can be deduced reliably if ion anisotropies for different energies and different pitch angles are compared. This technique, originally developed by

Williams (1979), has been successfully used for studies of various boundary characteristics, e.g. oscillatory motions and deformation of the dayside magnetopause (Williams, 1980; Fritz et al., 1982), structure of the flux transfer events (Daly and Keppler, 1983), and movement and thickness of the tail plasma sheet boundaries (Andrews et al., 1981).

Another important property of energetic particles is that their phase space density is sensitive to the mirroring conditions at the ends of the field lines; i.e. the problem of whether the local field lines are topologically open or closed can be addressed by looking at the particle anisotropy in the direction parallel to the field line. For example, if some of the day-side geomagnetic field lines become open, particles formerly trapped on the earth's field lines will stream out toward the open end. This produces streaming anisotropies along the reconnected field lines.

Presence of energetic particles is by itself an interesting subject of research. They represent various acceleration processes occurring in the magnetosphere. Acceleration may be caused by quasi-static electric fields (created either through non-adiabatic particle motions or through anomalous resistivity), by inductive electric fields due to rapid changes of the magnetic field structure, or by strong MHD wave turbulence. Therefore, identification of the acceleration mechanism has global importance not only for study of particle dynamics in the magnetosphere but also for clarifying the extreme conditions that can be sustained by the electromagnetic environment in space.

In accordance with the mission objectives of GEOTAIL, our effort will be concentrated on the study of the solar wind-magnetosphere interaction processes and resultant particle energizations occurring in the magnetotail and in the boundary regions of the magnetosphere. We briefly discuss below some of the major topics in recent development of magnetospheric physics, that have close relevance to energetic particle experiments.

2.1.1 Dayside Interaction Regions

2.1.1.1 General Remarks

It is evident from many previous analyses (e.g. Maezawa and Murayama, 1986) that the state of the solar wind and the embedded magnetic field (IMF) is directly associated with the amount of energy that is released in the magnetosphere. The mechanism by which the solar wind energy is transferred to the magnetosphere has long been discussed, but a unified view fully consistent with observations has not been reached yet.

Important keys to this problem should be found in the physical nature of the dayside magnetopause, a natural boundary between the magnetosphere

and the solar wind plasma. In a simplest MHD model of the magnetosphere, the magnetopause is viewed as a tangential discontinuity surface, which allows no normal flow of plasma and no normal component of magnetic field, so that there could be no bulk energy transfer across the boundary.

Two major mechanisms have been proposed that could overcome this constraint. One is the magnetic field reconnection, which locally violates the frozen-in condition. It allows magnetospheric field lines to be connected with solar wind field lines. The other is the so-called "viscous-like" interaction, for which an enhanced plasma viscosity allows an effective transport of tangential momentum at the boundary. So far, both mechanisms have their respective support from observations: the discovery of plasma jetting along the magnetopause with speeds equal to the Alfven velocity (properly calculated at the boundary) supports the reconnection view, while the discovery of the low-latitutde boundary layer, which implies an effective diffusion of particles across the magnetic field, supports the "viscous" view.

The orbit of GEOTAIL in the near-earth observation phase of its mission is ideal for investigating such solar wind-magnetosphere interaction processes. The planned orbit will allow GEOTAIL to skim along the dayside magnetopause and detect various particle and field signatures arising from the interaction processes. Energetic particle experiment will greatly contribute to this kind of analyses, by its remote sensing capability and by detection of particles whose distribution function has been determined by the interaction processes.

2.1.1.2 Flux Transfer Events

The discovery of flux transfer events (FTEs) has largely modified our view on the dayside reconnection processes (Russell and Elphic, 1978; 1979). We have learned that reconnection does not necessarily occur in a large scale configuration but can take the form of small, individually reconnected flux tubes that are convected away past the satellite in a relatively short time period.

The physical picture of flux transfer events has originally been proposed to explain the characteristic magnetic signatures frequently registered at satellites just outside the magnetopause. The hypothesis that these events signify the stressed flux tubes resulting from spatially limited reconnection have been confirmed by detection of ions escaping from the magnetosphere along the magnetic tube.

By examining the field aligned anisotropy of >25 keV ions of magnetospheric origin, the hemisphere to which the flux tubes are connected have been determined (Daly et al., 1984). The result suggests that these flux transfer events have been initiated near the equatorial region rather than at

high latitudes. However, the events analyzed in detail are so far biased towards the northern hemisphere observations, and limited in numbers in the sense that the distribution of IMF directions is uneven, so that thorough determination of their generation sites awaits future observations.

*It is very important to determine the precise locations where the FTEs are initiated. The fast 3D analysis capability of HEP-LD and the favorable orbital configuration will provide us with good statistics of FTE occurrences along the dayside magnetospheric boundary.

2.1.1.3 Large Scale Reconnection

Although FTEs can account for a significant portion of the magnetic flux reconnected on the day side, it is premature to conclude that the FTEs are the only mechanism by which geomagnetic field lines become open to the magnetosheath. It may be that the characteristic features of the FTEs are just easier to recognize than the broader signatures of large-scale, more uniformly occurring reconnection processes. In fact, magnetic structures that are consistent with the magnetopause having the property of a rotational discontinuity surface (as expected from conventional reconnection models) are sometimes observed.

In the case of large-scale, quasi-steady reconnection, the field line geometry is characterized by the presence of a stationary "reconnection line", where, and only where, the field lines can get reconnected. The position of the reconnection line on the magnetopause is of considerable importance, because it significantly affects the speed of reconnection. As in the case of the FTEs, we can determine the relative position of the reconnection line with respect to the satellite from anisotropy measurement of energetic ions. Escape of energetic electrons can also be a useful signature if the satellite is sufficiently near the reconnection line.

*It is important to distinguish various possible types of day side reconnection. Energetic particle experiments will make significant contributions by remote sensing of magnetic structures, by identification of the connectivity of magnetic flux to the IMF, and by direct measurement of accelerated particles.

2.1.1.4 Low Latitude Boundary Layer

It is still unknown how much percentage of the energy transferred from the solar wind to the magnetosphere is to be associated with viscous processes occurring at the day side low-latitude boundary layer (LLBL) (Eastman and Hones, 1976; 1979). Particularly, it is important to see whether layers of

mixed plasma encountered at the magnetopause is produced through the viscous processes or by magnetic reconnection. If magnetic field lines threading the plasma layer are closed ones, the layer is more likely to be associated with viscous processes, while if they are open, it would be associated with reconnection. We should further determine whether such plasma mixing is taking place locally or at some places far from the satellite. Measurement of the directional anistropy of trapped ion component together with that of low energy plasma will give us clues to these questions.

The Kelvin-Helmholtz instability is a candidate mechanism for the viscous momentum transfer at the magnetopause (e.g. Miura and Pritchett, 1982). Although it does not directly lead to particle transport across the magnetopause, the wavy deformations of the magnetopause may profoundly affect the occurrence conditions for other physical processes such as magnetic reconnection. Remote sensing of the magnetopause using energetic particles is just appropriate tool for determination of the wave-length and amplitude of such surface deformations.

*Determination of the field line topology is essential to distinguish viscous processes from reconnection. The pitch angle anisotropy of trapped ions measured by HEP is a useful indicator of the field line topology.

2.1.2 Energetic Particle Bursts around the Magnetosphere

2.1.2.1 General Remarks

Bursts of energetic ions are often observed in the region upstream of the bow shock and in the magnetosheath. To date, there are at least three known sources for these ion bursts; 1) solar energetic particles (SEPs), which will be discussed in detail in Section 2.2, 2) ions accelerated within the magnetosphere and finding their way out to the magnetosheath, and 3) ions accelerated locally around the bow shock. SEPs are easily discernible from other two types of ion events by their much harder spectrum and by the longer decay time. Other two types of ions can be mutually intermixed and it would be difficult to distinguish them. However, there seems to be an upper energy limit of 100–200 keV to the bow-shock associated particles, while particles of magnetospheric origin are often accelerated to well beyond 500 keV.

2.1.2.2 Energetic Ions and Electrons and Electrons Escaping from the Magnetosphere

Fast-rise, Slow-decay type of energetic particle events are observed deep in the magnetosheath (Sarris et al., 1976; 1978; Krimigis et al., 1978). Since their occurrences have close association with substorm periods, they are

thought to represent the particles accelerated within the magnetosphere and somehow escaping the magnetosphere.

Anisotropy measurements have confirmed that these particles are escaping along the field lines from the near-earth magnetosphere, most probably from the near-tail region. When multi-satellite data are available, the burst intensities in the magnetosheath are always lower than those in the magnetosphere thereby confirming the magnetospheric origin of particles.

The energy spectrum of these events has a power law distribution with the spectrum index of $-3 \sim -4$. The spectrum often extends to 500 keV $\sim$ 1 MeV region, which makes sharp contrast with the diffuse ion population accelerated at the bow shock.

A distinct population of very energetic electrons are sometimes observed in the vicinity of the magnetopause, but their sources are unknown (Meng and Anderson, 1970; 1975; Domingo et al., 1977). Statistics of many such events and simultaneous observations with other satellites will show where and how the magnetospheric particles are leaking from the magnetosphere in an effective way.

*In order to differentiate between the magnetospheric and bow shock-associated particles, it is important to perform accurate spectrum and anistropy analyses for ions ranging from <10 keV to 1 MeV. The combination of HEP-LD and -BD instruments will provide such capability. Ion composition measurements provided by HEP-LD will also facilitate the distinction.

2.1.2.3 Particle Acceleration at the Bow Shock

The earth's bow shock is an ideal place where we can test the consequences of well-developed acceleration theories directly against observations. Particularly, theories of first-order Fermi acceleration at the shock have direct applications to many astrophysical problems; it is important to test their assumptions and consequences on the basis of actual measurements. Finite lateral dimension of the bow shock and the spatially varying angle between the shock normal and the incident magnetic field due to the shock curvature give additional ingredients which are not considered in the ordinary shock theories.

Two distinct energetic ion populations (beam-type and diffusive-type) have been discovered in the upstream region (Scholer et al, 1979; Paschmann et al., 1981; Ellison, 1985).

Beam-type ions are found on the field lines connected to the quasi-perpendicular shock regions. They are less energetic and have been reflected from the bow shock in the direction of magnetic field. On the other hand, diffusive-type ions are found on the field lines that are connected to the

quasi-parallel regions of the bow shock. They are more energetic and have broader distribution in phase space. Although these two groups of ions were initially thought to occur in mutually exclusive regions of space, it is now thought that there is a continuous transition from one to the other.

It has been suggested that the diffusive-type component originates from the beam-type component through strong scattering by ULF waves. However, detailed evolution processes in the ion velocity space has not been traced yet, because temporal variations in the direction of the IMF causes too rapid changes in the field line connectivity between the satellite and the bow shock.

*GEOTAIL has unique opportunities to skim along the bow shock surface monitoring the distribution function of ions accelerated in the vicinity of the bow shock. This will greatly contribute to the study of the response of bow-shock aceleration processes to time-varying IMF conditions.

2.1.2.4 Jovian Electrons

The earth's magnetospheric environments are also populated by particles that are emitted from distant acceleration sites such as the solar atmosphere and the magnetospheres of the outer planets. Among them, solar energetic particles (SEP) are principally measured by HEP-MI and -HI sensor systems, and their physics will be described in later sections. Another important particle population found in our environment is Jovian electrons, which escape from the Jovian magnetosphere along the interplanetary magnetic field (Chenette et al., 1977; Chenette, 1980). Although their intensity around the earth's magnetosphere is such that they are often masked by substorm-associated bursts or by solar particles, the quiet level of >1 MeV energy electrons in the magnetosheath is strongly modulated by Jovian particles. These particles have a hard energy spectrum with a power law index of $-1.5 \sim -2$, which makes sharp contrast with electron bursts of (the earth's) magnetospheric origin.

*As compared to energetic electrons of local origin, Jovian electrons are relatively low in intensity, but they have a harder spectrum extending to more than a few MeV. The combination of a large area and a good azimuthal angular resolution (16 sectors) of HEP-BD will facilitate the distinction of Jovian electrons from local particles.

2.1.3 Energetic Particles in the Magnetotial

2.1.3.1 General Remarks

A wealth of energetic particle phenomena are known to occur during the rapid deformation of the magnetosphere in the expansion/recovery phases

of the substorm. Generally speaking, there are two different possibilities for a sudden appearance of these particles at the spacecraft:

1) Sudden onset of a particle acceleration mechanism(s) in the magnetotail (temporal effects).

2) Motion of magnetic structures relative to the satellite which brings the satellite into a preexisting layer of energetic particles (spatial effects).

Observationally, it has been suggested that the direct causes of energetic particle events in the distant tail are mostly due to condition 2). These events are closely associated with the passage of the plasmoid, which pushes the plasma sheet boundary layer (PSBL) locally outward then inward across the satellite.

However, from the theoretical view point, condition 1) is the more fundamental cause of the energetic particle events. The leading theory of substorms suggests that ions streaming in the plasma sheet boundary layer at the expansion phase of substorms are originally accelerated at the near-earth neutral line, which is formed at the onset of substorms.

2.1.3.2 Origins of the Plasma Sheet Boundary Layer Particles

Plasma sheet boundary layer (PSBL) is a unique place where characteristic ion beams with energies 30–300 keV are encountered directed either tailward or earthward (Williams, 1981; Spjeldvik and Fritz, 1981; Richardson and Cowley, 1985). According to the reconnection model of substorms, the source of these ions is associated with the particle acceleration mechanisms occurring at the magnetic neutral lines.

The reconnection model of substorms has been successful in explaining the timing of the PSBL encounter as a function of the satellite location and the substorm phases. The polarity of the field aligned anisotropy of energetic ions are also explicable by the relative location of the satellite with respect to the neutral line. Thus, the ion beams observed at the time of plasmoid passage are directed tailward, as the near-earth neutral line is still earthward of the satellite. On the other hand, when the near-earth neutral line retreats tailward during the recovery phase of substorm, predominantly earthward streaming of energetic ions are observed at PSBL.

Even with the extensive studies made by the ISEE satellites, many questions remain unsolved about the origin of ion beams at PSBL. Some of them are listed below.

1) What is the acceleration mechanism(s) that produces a nearly power law energy spectrum at higher energies (10 keV – 500 keV) coexistent with the shifted Maxwellian distribution of low energy plasma?

2) Do the acceleration processes operate at the distant neutral line even when the magnetosphere is in a relatively quiet state?

3) Can the PSBL particles be identified as a major source of central plasma sheet particle population? If so, where and how do these particles get scattered in velocity space to form more or less isotropic distribution of plasma sheet population.

4) How do these particles interact with auroral arcs? What is the relationship between the low-altitude field-aligned acceleration of electrons and the earthward-directed ion beams in the PSBL?

5) Can all the multiple ion beams observed at the PSBL be explained by the mirror reflections at low altitudes?

*A precise determination of the distribution function is needed to distinguish the source energy spectrum from various propagation effects. Continuous coverage of ion energy from thermal energies to MeV range would be essential to study possible breaks in the spectrum corresponding to the presence of multiple acceleration mechanisms.

2.1.3.3 Plasmoids in the Tail

The strongest signature of substorms in the distant tail regions is the passage of the plasmoid, which is the locally expanded region of plasma sheet containing hot plasma jetting anti-sunward (e.g., Hones, 1979; Baker et al., 1984; Hones et al., 1984). Some of the particles accelerated in the near-earth tail region have been trapped in the closed magnetic loops of plasmoid; these particles are observed to have isotropic distribution in the moving frame of reference. Local acceleration may be still occurring at the O-type neutral line of the plasmoid.

On the other hand, along the open field lines adjacent to the plasmoid (i.e. near the PSBL), the particles that have been accelerated at the near-earth neutral line are observed to flow out freely in the anti-sunward direction. These particles show a characteristic velocity dispersion as a function of distance across the plasmasheet boundary; this is due to the fact that particles undergo electric-field drifts perpendicular to the field lines as they travel along the field lines. The effect of the electric-field drifts is less for higher energy particles, because they can promptly propagate from the source region to the observation site.

*Measurement of velocity dispersions of energetic ions allows an estimate of the speed of electric field drift, which in turn reflects the speed of reconnection occurring at the near-earth neutral line.

2.1.3.4 Direct Probing of the Explosive Processes Occurring in the Near-Earth Tail

Near-earth reconnection is one of the most promising mechanisms for the

explosive energy release during the substorm expansion phase (e.g., Russell and McPherron, 1973; Nishida and Nagayama, 1973; Hones et al., 1974). However, direct in-situ measurement of the near-earth reconnection has been very scarce (Terasawa and Nishida, 1973), due partly to the orbital constraint of the previous satellites. The orbit of GEOTAIL during the near-earth observation phase of its mission is designed to fill this gap: when the apogee is on the nightside, the satellite will spend majority of its time within the radial distance range of 10–30 R_E in the tail, where occurrences of the near-earth neutral line will be constantly monitored with higher probability than ever.

Our knowledge about the mechanism of particle acceleration operating at the near-earth neutral line is sparse. It is important to identify first the spatial scale and time duration of the acceleration processes. In this regard, it is important to determine in situ the upper limit of the energy obtained by the particles, and how it varies with time. The upper limit and time evolution of spectrum can be a key to the spatial and time scales of acceleration, respectively.

Although energy spectra of energetic particles that are injected earthward (e.g. those observed at the synchronous orbit) have been well documented, these particles have gained most of their energy through betatron acceleration as they were rapidly convected earthward. Therefore, the source energy spectra should be investigated in situ in the vicinity of the neutral line beofore they are modified by convection effects.

By the same token, ions observed at the plasma sheet boundary layer in the distant tail do not carry direct information on the source mechanism. Their spectrum have been severely modified by the velocity dispersion effect.

*It is important to determine the energy spectrum of accelerated particles by in situ observations. Fast analysis in 3D velocity space by HEP-LD and -BD is prerequisite for accurate analyses of time-varying spectra.

2.1.3.5 Particle Acceleration at the Distant Neutral Line

ISEE-3 magnetic field measurements suggested an almost permanent presence of the distant neutral line at >100 R_E down the tail (Slavin et al., 1983; Tsurutani et al., 1984; Baker et al., 1984). However, energetic particle aspects of the distant neutral line is far from being established. This situation is probably because during disturbed times, the effect of the near-earth neutral line predominates in the tail. During quiet times, the tail magnetic structure does not change much so that the satellite has less probability to encounter the field lines connected to the distant neutral line.

It remains to be verified how the distant neutral line contributes to the energetic particle population in the plasma sheet. It is also uncertain how

this neutral line behaves during substorms and how it is related to the auroral zone precipitation.

*Detailed examination of quiet time characteristics of energetic particles would be necessary to clarify the role of the distant neutral line in the magnetospheric physics.

2.1.4 Ion Composition Measurements and Other Additional Remarks

In all of the examples listed above, ion composition measurement is an indispensable part of our analysis for several reasons. First, it will give us a clue to the particle source. Oxygen to proton ratios can be used to distinguish ionospheric sources from the solar wind sources. Two of the examples where ion composition measurements play a crucial role are: 1) the source of plasma sheet ions, particularly those at the recovery phase of substorms, and 2) origin of the bursty energetic ions in the magnetosheath and in the upstream regions.

Second, in the case of the drifting Maxwellian distribution, (and for any plasma distribution moving with respect to the observer for this matters), the energy associated with the drift motion is proportional to the particle mass, so that when the drift (flow) speed becomes large, a small population of heavier ions can affect appreciably the total energy spectrum in the satellite frame of reference. In the near-earth plasma sheet, under severe geomagnetic activity, the density of oxygen ions can sometimes be even comparable to that of protons, so that this is really a significant effect.

Thirdly, in some of the theoretical acceleration mechanisms, efficiency of energization depends on the particle rigidity, so that the comparison of energy spectra for different ion species can provide crucial information for identification of the mechanisms.

*Composition measurement of HEP-LD will help greatly to identify the sources of plasma sheet ions for various phases of substorms. Alpha to proton ratio at the MeV range measured by HEP-BD will help identify the acceleration mechanisms of ions at this energy range.

Finally, we briefly comment on the absolute flux and energy ranges of the energetic particle events that we will observe. Figure 2.1.4-1 shows the representative differential energy spectra for some of the known energetic electron populations in and around the magnetosphere. Their abbreviations are:

PS: Quiet time plasma sheet population in the near-earth tail
MP: Electrons at the dayside magnetopause
TB: Bursty appearances of electrons in the tail including those at the time of plasma sheet recovery
JE: Jovian Electrons.

For the sake of comparison, the energy and sensitivity ranges of HEP-LD

and -BD are shown by two shaded boxes. Lower and upper borders of the shaded boxes correspond to 1 c/s and 3×10^5 c/s levels, respectively, for each instrument, assuming that the electron energy spectra obey a power law with index -4.

Figure 2.1.4-2 gives the same sort of information for protons, as a representative case of ions. Abbreviations are:

MP: Protons at the dayside magnetopause
UP: Upstream protons
TB: Bursty appearances of protons in the tail including those at the time of plasma sheet recovery
SP: Solar proton events

The energy and sensitivity ranges of HEP-LD and -BD sensors are shown by shaded boxes in the same way as in the case of electrons.

It is evident that the large detection area of the BD subsystem contributes greatly to the analysis and statistics of ions and electrons at energies greater than a few hundred keV. On the other hand, the LD subsystem are designed to achieve an excellent combination of time and angular resolutions for relatively abundant particles at lower energies.

2.2 Solar Energetic Particles

The solar energetic particle (SEP) compositions provide rich information concerning source region, particle injection/acceleration mechanisms, and transport mechanisms occurring in the solar atmosphere and interplanetary space.

2.2.1 Samples of Solar Atmospheric Material

Solar particle events transport a sample of the solar atmosphere into interplanetary space. The direct measurement provides unique information about the solar atmospheric composition, and physical process operating in the chromosphere and/or corona. SEP observations offer the best method for determining the solar elemental and isotopic composition, thereby greatly strengthening our knowledge of the solar system composition which is primarily based on the measurements of terrestrial, lunar and meteoritic abundances.

Fractionation processes operate in SEP acceleration, thereby biasing the energetic particle population. These effects are systematic and appear to be well organized by particle mass-to-charge state ratio, if one observes a large number of different particle events over a broad energy range.

Different kinds of SEP flares sample different coronal sites. Large particle flare events appear to sweep up large volumes of coronal material. Small

^{3}He rich events may sample small, compact, hot sites in the corona. By comparing the composition at various flare sites along with e.g., solar wind and photospheric composition, it is possible to gain key insights into the physical mechanism which transport heavy ions into corona and then accelerate and transport into the interplanetary space.

2.2.1.1 Large Particle Events

[A] Elemental Composition in Large SEP Events

Comprehensive studies of SEP compositions were carried out by IMP-7 and -8 at 1AU, and Voyager 1 and 2 spacecrafts moved from 1 to 11 and 15 AU, respectively. Now the major elements in the range below Zn, including some rare elements (e.g. P, K, Cl etc.), are measured (Cook et al.,1984; Breneman and Stone, 1985a, b; McGuire et al., 1986). SEP abundance obtained by seven flare events and other solar abundances (the photosphere, corona and solar wind) is shown in Fig. 2.2.1-1.

Heavy ion abundances for major species in large particle events exhibit strong variations from one event to another which are ordered by Z or A of the ions. Differing species exhibit different energy spectra. Thus the abaundance variation are also energy dependent (Mewaldt, 1980). Nevertheless, observing a large number of flares, it is possible to average out these fluctuations in order to obtain a set of relative abundances for major species which are independent of energy (1 – 20 MeV/n) (Fan et al., 1984; Meyer, 1985a; Mason, 1987). Over a more limited energy range, the variations in spectral shape are organized by particle magnetic rigidity, which suggests that shock acceleration mechanisms are responsible for accelerating particles.

The observations which have been done before are still limited in the number of species, accuracy, the energy range and the number of particle events.

*By observing a large number of species over a broad energy range with high statistical accuracy, a more complete and comprehensive explanation for SEP abundance and/or solar atmospheric composition and physical processes occurred at flare sites will be given. GEOTAIL mission in orbit in the phase of solar maximum, will give us a great opportunity to observe them.

The average SEP abundances observed in large flares differ from photospheric and universal abundances in a manner ordered by first ionization potential (FIP). SEP abundances of elements with FIP $<$10 eV ("low FIP") are overabundant by a factor of 3 to 4 compared with elements with FIP $>$ 10 eV ("high FIP"). This same trend is seen in the composition of the solar corona and solar wind (SW), although the coronal and SW composition are not well enough determined to make a definitive remark because of a limited

number of observed species (Fig. 2.2.1-2). It is also seen in the galactic cosmic ray source (Meyer, 1985b; Mason, 1987). It is not clear whether the enhancement function is a exponential or a step function at about 10 eV, so it would be premature to form a conclusion. There is a much better chance of defining the nature of the FIP enhancement function using SEPs than the GCRs, and this will gives crucial insights into the GCR interpretation. Clearly, studies of the SEP composition and physics of the corona will be vital area for obtaining an understanding of physical processes essential to solar studies, and to GCRs as well.

The FIP-bias seen in SEP seems to imply a preferential increase of ionized heavy ions relative to neutral heavies from the underlying cool chromosphere (Meyer, 1985a, b; Montmerle, 1988a, b). Apparently heavy elements with low FIP are easily ionized and then a selection takes place between ionized and neutral heavies. The ionized material would be then transported into the corona with a higher efficiency by a factor of three or four.

*The information obtained by measurements of various species should make it possible to provide discriminating constraints on models for transport of photospheric heavies into the corona.

*Elemental and isotope measurement will provide especially interesting information since one has two or more different ions with different ionization properties.

*The HEP package will make the first systematic measurement with high sensitivity of SEP elemental and isotopic abundances, covering a broad energy range.

[B] Isotopic Composition in Large SEP Events

The measurement of the isotopic composition offers the best hope for obtaining the isotopic composition of the solar atmosphere. This information cannot be obtained by spectroscopic observation. Fractionation effects, which depend primarily on atomic properties, should be relatively unimportant in the determination of isotopic ratios for most elements accelerated in large flares.

A knowledge of the isotopic composition of the solar atmosphere will give key insights into the origin and evolution of the solar system, and into the related problem of determining local intersteller medium and local galactic abandances.

At the present stage, this rich source of the information has been only once obtained with high resolution observation in a single particle event by the CALTEC-HIST instrument on board the ISEE-3 (Althouse et al., 1978). Nevertheless, this single observation (Mewaldt et al., 1984) showed that the SEP $^{20}Ne/^{22}Ne$ ratio was significantly different from that of the solar wind

(Geiss et al., 1982). This difference in Ne isotope ratio between SEP and SW suggests that a different mechanism for the injection and/or acceleration of SEP vs. SW neon. The major elements C, O, Ne, Mg and Si observed by the ISEE-3 instrument in this flare were consistent with the solar system abundance. The statistical uncertainties for rare isotopoes ^{13}C, ^{18}O etc., were too large to identify whether significant anomalies as seen in meteorites and lunar fines may exist. Comparisons of isotopic abundances measured for solar particles with the solar system are shown in Fig. 2.2.1-3.

*Measurement of isotopic composition with high sensitivity and mass resolution over a broad range of energy is required to determine isotope abundance not only of major species C, O, Ne, Mg, Si etc., but also to explore many minor ones as well. SEP abundance observation with higher precision by HEP instruments especially MI and HI will gain key insights into the origin and evolution of solar system, and into the problem of ISM and universal abundances, stellar nucleosynthesis, and chemical evolution of the galaxy.

[C] Correlation between SEP Composition and GCR Composition

As the spallation products such as D, Li, Be, B, are not observed in SEP, the energy loss effects should be negligible because SEP's observed in the interplanetary space have traversed <0.03 g/cm^2 of matter. Therefore, the SEP composition may be discusssed without the need to apply the difficult and uncertain corrections for spallation which play so a crucial role in the interpretation of the GCR data. The knowledge obtained from the SEP observation is basis to discuss the GCR source and genesis.

A striking similarity exists between the SEP and GCR composition, which is the linear correlation in the range of C through Zn. The close resemblance between the SEP and GCRS composition means that the ratio of SEP/Solar System shows a correlation with FIP or chemical property (Fig. 2.2.1-2). Thus the study of SEP composition and coronal processes can yield insights of direct relevance to the physics of GCRS. But we must pay special attention to the points that hydrogen, and to a lesser extent, helium are more abundant in the SEP composition than in the GCR source.

The two clues described above, that is, the close resemblance of elemental abundance between SEP and GCRS, and FIP-bias, suggest that most of the GCR heavy nuclei, which have therefore a solar-like composition, belong originally to a plasma with temperature of <8000K, corresponding to the chromosphere of F to M type stars (Meyer, 1985a, b; Montmerle, 1988a, b).

The isotopic abundance, on the other hand, is the signature of stellar nucleosynthesis. Then we can study even the minor trend, i.e., only slight deviations from the general "normal abundance" which is the signature of quantitatively minor contributors. The overabundance of Ne isotope ratio,

Mg and Si isotope ratio (still ambiguous), along with the excess of C and O, are known up to date (Fig. 2.2.1-3). These nuclides are not originated from cool stars in GCR source but probably produced during the helium-burning stage of massive stars (hot stars) (Montmerle, 1988a, b).

The precise measurement of isotopic composition provides us crucial insights into the connection between the stars and GCR. Since the sun is a typical star in those kinds of cool stars and SEP is the direct sample from the sun, the abundance in SEP should be investigated most elaborately as a standard.

*The HEP instruments have a very large geometric factor and a high mass resolution to determine elemental and isotopic abundances not only for major species but also to explore the minor ones. It will provide the systematic exploration of the rich storage bank of solar information.

2.2.1.2 ^{3}He Rich Flare Composition

There exists a distinctly separate class of events with $^3He/^4He$ ratios of order 1, that is, enriched by factor of 1000 – 10000 over photospheric abundance (or coronal abundance). Studies had shown that these events were also enriched in heavy nuclei compared with large solar flares. Ionic charge-state measurements showed that the source region for ^{3}He rich flares has a temperature of about 10^7 K, well above the about $2x10^6$ K temperature inferred for normal large particle events (Kocharov and Kocharov, 1984; Mason et al., 1986).

Masone et al. (1986) reported a survey of heavy ion enhancement near 1 MeV/n in 66 ^{3}He rich flares observed with the instrument on ISEE-3. They compared the heavy ion enrichments (factor of 10–20) with the ^{3}He enrichment (Fig. 2.2.1-4), and the less variability than the $^3He/^4He$ ratio, and concluded that they were uncorrelated with the ^{3}He enrichment. They argued that the heavy ion enrichment was not due to the acceleration mechanism that enriches the ^{3}He. Rather, it was suggested that the plasma resonance mechanism (Fisk, 1978; Vargoglis and Papadopoulos, 1983) that enriches the ^{3}He occurred only in coronal sites where the ambient plasma was already enriched in heavy ions, perhaps due to thermal and pressure gradient effects. It is interesting that the heavy ion enrichment pattern does not correlate well with FIP for these events; for example, Ne with a high FIP is enhanced about as much as Mg, a low FIP element.

Measurements of ionization state show that the heavy ions in these events are ejected from hotter coronal sites than ions accelerated in large flares. While the heavy nuclei enrichments might also be caused by the plasma heating which enriches the ^{3}He, other evidence indicates that these heavy

ion enrichments are due to thermal diffusion (Nakada, 1970) which could be expected to be important at high temperature sites in the corona (Mason et al., 1986). Thus, ^{3}He rich flares sample a distinctly different coronal location than large particle events.

Our knowledge of ^{3}He rich flare up to date are based only on a few major heavy elements. Abundances of heavy isotopes except He are not known at all now.

*Probing the ions with high sensitivity and mass-resolution is required to study them. HEP-MI and -HI will provide accurate determination of additional species with high precision in these events. The abundance patterns possibly seen in other elements, or the presence or lack of isotopic abundance anomalies other than He, could give new insights into the plasma processes operating at these flare sites.

Reames et al. (1985) systematically studied 187 solar electron events and found ^{3}He events present in over half of the events and suggested that ^{3}He events would be found in all electron events if the detection sensitivity were better. Reames and Stones (1986) showed that in the absence of electron data, the km wavelength Type III radio burst could be used to identify the associated flare events at the Sun.

They have shown that ^{3}He rich events occur more often than once a month, and are associated with impulsive keV electron events, and therefore also with Type III radio bursts (Reames et al., 1985; Reames and Stone, 1986). And it has made us accessible to often identify the source regions. The acceleration mechanism in these flares appears to be different with the one operating in large solar flares, and seems to be the same mechanism which impulsively accelerates keV electrons. Since keV electron events are observed with a frequency of >1/day, it is reasonable to anticipate that advanced instruments with a very wide aperture may detect ^{3}He rich events with a similar frequency. We may expect to measure the extent where these ion events frequently occur in the coronal region.

*It is exciting to study the association between the ^{3}He rich events and impulsive electron events using the high sensitive sensor. A package of HEP instruments will carry out the systematic observation of these events along with the correlative study with radio observations, and X-ray observations by other spacecrafts.

2.2.2 *Energy Release and Ion Acceleration in the Solar Atmosphere*

The coronal structure of flares has been studied by soft X-ray imaging telescopes aboard the Skylab. They find that two classes of flares can be distinguished in the soft X-ray images:

(1) Impulsive events; impulsive, compact, low lying ($<10^4$ km) flares with small volume (10^{26} - 10^{27} cm^3, high energy density (100 – 1000 ergs/cm^3), and durations of <tens minutes in soft X-rays.

(2) Long duration events; long duration (hours) of flares with larger volumes (10^{28} – 10^{29} cm^3), lower energy density (10 – 1000 ergs/cm^3) located high in the corona ($5x10^4$ km). These long duration events are known to accompany coronal mass ejections (CME).

The processes of particle acceleration occurring in the solar atmosphere have wide variations in time scale, atmospheric height, location, the structure of the associated magnetic field, and the size of the acceleration region. Distinct acceleration processes suggested are mainly:

- Impulsive (short time scale) acceleration related to the flash phase,
- Second order Fermi (stochastic) acceleration in turbulent regions generated after a flare,
- Low coronal shock acceleration generated immediately after the impulsive phase,
- High coronal shock associated with large flare events, and with CMEs.

These four processes operate in different coronal sites, and energize different particle populations. And then distinct suprathermal and energetic particle signatures are created.

Impulsive particle accelerations is most likely due to fast magnetic field reconnection. Particle acceleration by shock waves is important not only because they play the central role in particle acceleration, but also because much of the shock energy eventually converts to thermal energy and may be a significant contributor to corona heating.

*The full-range of observations from radio to gamma-ray, along with particle observation will clear the dynamical processes occuring in the solar atmosphere. By the measurements of energy spectra, time profiles, and compositions of electrons, protons, and heavies in the broad energy range by the HEP instruments with high sensitivity and mass resolution, the GEOTAIL HEP experiment will provide a comprehensive picture of the energetic particles accelerated at the corona, which is still incomplete understanding of the dynamical processes in the corona. This can be realized by the corporation of radiation (radio, X- and γ-ray) observation.

2.2.2.1 Impulsive Events

During the solar maximum, impulsive solar particle events occur about once per day, and generally produce relatively small fluxes of SEPs and low maximum particle energies, which are associated with short-duration X-ray events generated in compact regions in the lower part of the corona (Pallavicini et al., 1977).

The events are thought to begin with the release of energy via magnetic field annihilation over an active region, which impulsively energizes electrons to 10–100 keV. A substantial fraction of the total energy released in the annihilation is imparted to these electrons. Shock wave acceleration, at least, appears to be absent on a large scale. Accelerated electrons produce Type III and, occasionally, Type V radio bursts as they move through the corona and into the interplanetary space. Heavy ions are also energized with a low abundance.

The particles associated with some impulsive events are enriched in ^{3}He and heavy ions which come from hotter coronal regions than the large particle events (Klecker et al., 1984). These flares accelerate electrons to 10–100 keV simultaneously with the ^{3}He population (Reames et al., 1985). Both the ^{3}He rich and electrons exhibit nearly scatter-free propagation in the interplanetary space, and the times of onset and maximum for the ^{3}He and electron increases are closely related by velocity dispersion. These ^{3}He rich events are mostly not associated by shock waves which differs from the large particle events (Lin, 1985).

The ^{3}He rich events have distinct feature in respect of particle acceleration mechanism.

– They require a plasma resonance process to preferentially heat the ^{3}He in the corona before the occurrence of the impulsive event.

The heavy ions are highly enriched irrespective of the variability of ^{3}He/^{4}He ratios.

– They may provide the nearly "pure" signature of the impulsive acceleration processes since shocks do not appear to be involved.

– They operate in unusual, hot coronal sites.

Another class of impulsive particle events is associated with the observation of nuclear gamma-ray continuum and line emission (Chupp, 1984). According to the gamma-ray observations, electron and ion acceleration during these events is simultaneous and time scale of acceleration is seconds or less. Gamma-ray flares are accompanied with coronal shock waves unlike the ^{3}He rich flare. Gamma-ray flares may be discerned from other flares by a different acceleration mechanism. First, protons are accelerated within closed magnetic loop, and produce gamma-rays by interacting with the solar atmosphere (Bai, 1986). Then, an additional proton component is accelerated by a shock wave in the high corona and escapes into interplanetary space.

*GEOTAIL HEP instruments have outstanding sensitivity over a broad range of energy. The HEP experiments will help characterize impulsive stage acceleration, by observing e, p, He and heavy ions with a more frequency for impulsive events.

2.2.2.2 Long Duration Events

Long duration SEP events associated with soft X-ray emission are generally characterized by large fluxes of relativistic electrons, energetic protons, helium and heavy ions observed in interplanetary space (Cane et al., 1986; Bai, 1986). They are observed roughly once per month during the solar maximum.

First Phase Acceleration:

These events start with "first phase" acceleration of electrons, and subsequent interactions with the solar atmosphere produce other phenomena associated with the flare including the H-alpha flash, etc. The explosive heating at solar atmosphere produces a shock wave which propagates to the upper corona generating Type II radio bursts. These processes are closely related with the CME (Kahler et al., 1984). As the CME moves away from the Sun, it triggers further magnetic field annihilation at high altitudes, producing the soft X-ray emission which lasts for hours.

Second Phase Acceleration:

The high coronal shock is most likely the process in the accelerating mechanism in these events (Ellison and Ramaty, 1985). An important property of large particle events is that SEPs reach the Earth from flares occurring over the entire visible disk of the Sun (Reinhard and Wibberenz, 1974; Mason et al., 1984; Schellert et al., 1985). Since particles are closely bound to magnetic field lines in interplanetary space, this implies the existence of some mechanism operating close to the Sun which permits transport over heliolongitude ranges of up to about 150 deg. This is a controversial thing whether coronal transport of energetic particles or large scale size of the acceleration process is responsible for these events.

- *The package of HEP instruments will measure the electron and ion spectra from hydrogen to nickel over a broad energy range with high sensitivity, including intensity time profile measurements as a function of energy. Obviously simultaneous observation of energy spectra of electron, proton, helium, and heavy species over a broad energy range will give key insights into understanding of the acceleration processes operating in these events.
- *The broad range of ion species and energies covered by the HEP instruments in single S/C is particularly suited to distinguish between various models of acceleration and/or coronal transport.

2.2.3 Physical Conditions in the Solar Atmosphere

The elements, Li, Be and B, are not observed in SEP and the equilibrium abundances of D and T in the solar atmosphere are very small with respect to H. Then, if significant fluxes of these species are detected, they would

have been produced by inelastic collisions with energetic particles in the solar atmosphere. These fluxes can be used to infer the thickness of traversed matter, since the cross sections of their production are known.

In general, different ionic species are observed to have different arrival time at 1 AU even when they are at the same velocity. This occurs for ions with different mass-to-charge ratios which result from incomplete ionization at coronal temperature. Since the temperature gradient in the coronal region is large, Q/M ratios in SEP have a large dependence on temperature in the source region.

*The HEP experiments will be able to characterize the such conditions as temperature and coronal height of the source plasma region.

2.2.4 Other Energetic Particles

The interplanetary space is filled with magnetic field and there are planets with a large magnetosphere (ex., Jupiter). Interplanetary shock waves frequently formed accelerate electrons and ions to MeV/n or more in Interplanetary Magnetic Field (IMF). HEP instruments will make a comprehensive measurement of energetic particle events from interplanetary or planetary origin (ex., CIR ions or Jovian electrons). Energetic particle observation, moreover, can be used to study the propagation of ions from the Sun to the earth, and it is very useful in the investigation of the structure and properties of the interplanetary medium.

[A] Corotating Interaction Regions

Corotating Interaction Regions (CIRs) are typically observed for several years around solar minimum when the polar coronal holes expand to the equator, and the fast solar wind streams from those coronal holes are maintained without much evolution for several solar rotations.

Due to solar rotation, the high speed streams eventually collide with slow speed solar wind emitted earlier from an adjacent longitude. At a few AU heliocentric distance, a compressed interaction region develops, bounded on the front side by a forward shock where the slow wind is accelerated, and on the back side by a reverse shock where the fast stream is decelerated. Since the configuration of the corona holes at the sun can be nearly stationary for several rotations, the configuration of the interaction region can be nearly stationary. Accordingly, the interaction region is known as a corotating interaction region (CIR). The associated MeV ion energy events are known as corotating events.

Originally observed at 1 AU in the fast stream and assumed to be a solar origin, the corotating ion events were observed by Pioneer 10 and 11 to increase in intensity with increasing heliocentric distance to about 4 – 5 AU

and subsequently to decrease in intensity, thus establishing their interplanetary origin.

Periodic streams of energetic particle events which are diffusing back toward the Sun from the site with the intensity maximum can be observed at 1 AU. The leading candidate for the seed population of CIR associated particle events is the solar wind.

The composition of the ions observed at 1 AU appears to be similar to that of the solar wind, though the enhancements of He and CNO relative to protons are observed. As heavy ions in CIR events have not been observed sufficiently yet, we must wait the further observations in the future mission, with instrument having a gathering power of ions.

*During the GEOTAIL mission or extended mission, solar activity decreases toward solar minimum, detailed measurement of energetic CIR particles will be made by GEOTAIL HEP instruments with high sensitivity and mass resolution.

[B] Others

Flare-associated SEPs are accelerated at the Sun, and subsequently propagated through the corona and interplanetary space. It is, however, a complicated task to separate the effects of the three processes from the observations because of the uncertainties and great variability from event to event in the flare process, and in the conditions of the corona and the interplanetary space.

Coronal propagation has been studied by finding the dependence of the observed onset times, rise times, energy spectra and the abundance ratios of SEP events on heliographic angular separation from the flare site. This angular dependences are deduced by statistical analysis of single spacecraft data from many events and by concurrent multi-spacecraft data of individual events.

After escaping from the corona, SEPs are guided and focused by the large-scale IMF and scattered by small-scale magnetic irregularities. Time-Intensity and Time-Anisotropy profiles during solar flares contain information on the acceleration and release processes at the Sun as well as on the interplanetary medium between the Sun and Earth. The SEP propagation process has been modeled as a diffusion process where the scattering mean free path depends on the particle gyroradius and on the power in the fluctuations of the IMF.

*Energy spectra, compositions, time-intensity profiles and anisotropy observations made near at 1 AU by HEP instruments can be used to study both large and small scale properties of the interplanetary medium.

2.3 Galactic Cosmic Ray Particles and Others

2.3.1 Galactic Cosmic Ray Particles

Cosmic ray research involves the study of astrophysical systems ranging from solar system to our galaxy, and focuses on the high energy processes occurring in these environments. Central objectives in this research are the study of galactic cosmic ray (GCR) particles to determine their origin, nucleosynthesis, particle acceleration and propagation, and their role in the dynamics of our galaxy.

The elemental component in GCR particles has been measured at 1 AU by satellite and/or balloon-borne instruments. Galactic cosmic rays are distributed throughout the galaxy as suggested by the gamma-ray observation. The bulk of nuclear component in GCR below about 10^{15} eV has its origin in our galaxy, and is confined to propagate through our galaxy. The lifetime of the confinement time in interstellar magnetic fields is about 10^7 years, as measured by the surviving fraction of the radioactive secondary nuclei ^{10}Be (half-life = 1.5 x 10^6 y).

Since the particle motion is greatly changed in its orbit by the irregularity of the interstllar magnetic fields, the GCR particles are highly observed isotropic. Indeed, a charged particle with a rigidity R = pc/Ze has a Larmor radius r = R/cB, which numerically gives r = about 1 AU for the particle of 1 TeV in the interstellar magnetic fields of a few μG, much smaller than the thickness of the galactic disk. Thereby, the galactic cosmic ray source (GCRS) cannot be seen. In this sense, we have to gain insights from the indirect evidence to understand the origin of GCRs.

Although the astrophysical sites and the acceleration processes for GCRs are not firmly established yet, they have turned out to be a vital contributor carrying the useful information of interstellar medium, nucleosynthesis, and chemical evolution of our galaxy etc. Advances in the development of high sensitive detectors have made possible the precise determination of elemental compositions and spectra of heavy particles over a broad range of energy, which provides key insights on their unsolved matters.

The study of the elemental composition of GCR nuclei had been pursued as a means of investigating the nature of cosmic ray sources and the physical conditions under which GCRs are transported from the source to our solar system. Until recently the instrumental capabilities allowed only the identification of the nuclear charge of GCRs. By the late 1970's, the experimental techniques had been improved that the isotopes of various elements below the iron peak could be observed. This progress has turned the focus of GCR research toward the "Isotope astrophysics" which provides the rich potential of astrophysical environments using the substantial information on GCRs.

Although high resolution observation of GCR isotopes become experimentally possible, high resolution observations to date have been statistically limited and only the major species have so far been measured.

The elemental abundances in GCRS are well organized by the atomic properties of the elements like those for SEP and solar wind (Meyer, 1985a, b). However, the isotopic abundances of a given element should be approximately conserved in the extraction, injection and acceleration processes since the selection effects seem to involve predominantly the atomic or chemical processes of the elements. Only the difference in charge to mass ratio between adjacent isotopes should affect the isotopic composition of the relatively light nuclei. Therefore, isotopic ratios are the most genuine clues to the origin of GCR nuclei.

*Our GEOTAIL HEP team have developed high sensitivity and mass resolution instruments combined with new-type of position-sensitive silicon detectors, which provide the improvement of about 100 times in collecting power for heavy ions in GCRs. The detailed and comprehensive comparison of GCRS and solar system isotopic abundance would shed light on the nucleosynthetic origin and the history of GCR species.

Some of the major objectives of GCR studies are summarized in the next.

2.3.1.1 Nucleosynthesis and Chemical Evolution of the Galaxy

[A] Galactic cosmic ray nuclei represent a direct sample of matter from astrophysical sites before acceleration, which provides the direct observation of the products of nucleosynthesis from outside the solar system. Among the limited number of GCR isotopes so far measured (Fig. 2.2.1-3), it has been discovered that ^{22}Ne is at least a factor of 3 times more abundant in GCR matter than in solar system (Mewaldt, 1983; Wiedenbeck and Greiner, 1980, 1981a, b; Simpson, 1983a, b). The GCRS abundances of ^{25}Mg, ^{26}Mg and ^{29}Si, ^{30}Si seem to be all enhanced by a factor of about 1.6, but recent observation by Webber et al. (1985) and cross section data experimentally obtained by Webber and Kish (1985) lower significantly the source abundances of those isotopes, thereby even if real, the excess could be small. For other isotopes, it is not yet sufficient to know whether the GCRs and the solar system compositions are different, because of the poor statistical accuracy in the observation.

So far a variety of suggestions have been made to explain the neon observations (Casse, 1981, 1983; Casse and Paul, 1982; Woosley and Weaver, 1981). However no consensus has been reached on the origin of ^{22}Ne anomaly up to now. The leading suggestions (Casse, 1981, 1983) include: 1) explosive hydrogen burning in supernovae and/or nova events, 2) metal-rich supernovae, 3) carbon-rich Wolf-Rayet stars and 4) the possibility that the solar

system composition is not standard but anomalous with respect to the bulk of the galaxy. For testing these models, precise measurement of GCR isotopes, including C, O, S, Ar, Ca and Fe isotopes other than Ne, Mg and Si, is necessary.

*HEP-MI and -HI will make possible the precise measurement of not only elemental composition in GCR but also isotopic composition ranging from He to Ni isotopes, which progresses the cosmic ray studies as isotope astrophysics.

Cosmic or Universal abundances compiled by Cameron and other investigators, are based on measurements of composition of not only the Sun but also the earth, the moon and the meteorites (Cameron, 1982; Anders and Ebihara, 1982; Anders and Grevesse, 1984). The universal abundances are considered as the representatives of the average composition of matter in the interstellar matter (ISM). The ISM is the largest storage of matter in our galaxy, and the GCR composition would be similar to that of the ISM (Wiedenbeck, 1984).

Unfortunately we cannot measure the detailed composition of the ISM directly. The best sample of the ISM is thought to be the solar system, which was condensed out of the primitive solar nebula in the interstellar gas about 45 billion years ago. But the validity that the universal composition represent the bulk composition of the galaxy is not obvious, because the solar system was formed from a small spatial reservoir of matter in the galaxy. There is no evidence, moreover, that the composition in the ISM is homogeneous throughout the galaxy. In addition, our galaxy is still evolving by the repeated processing of matter through the various stage of evolving stars and the ejection of the more processed materials into the ISM, which alters the abundances of heavy elements (Wiedenbeck, 1984; Schramm, 1984).

At the present stage, the detailed analysis of the bulk compositions of GCR nuclei leads the conclusion that the GCRs are not originated from the matter ejected from the supernovae. The bulk of the GCRs likely originate in cool stars (F to M stars) associated with their surface activities, while anomalous or exotic composition of GCR species seems to associate with the hot stars (massive O and/or B stars) (Meyer, 1985a–c; Montmerle, 1988a, b). The composition, elemental as well as isotopic, gives strong constrains on the nature of the cosmic ray sources.

The theories of stellar nucleosynthesis and the chemical evolution of the galaxy are greatly influenced by the universal abundance table based on the solar system materials, especially solid matters of the carbonaceous meteorites considered as the least chemical processed matters. The information on the elemental composition in various astrophysical sites is now available. Only the elemental abundances are, however, inadequate for checking the

theories. In order to study nucleosynthetic processes and the chemical evolution of the galaxy, it is important to use the isotopic abundances.

*The HEP instruments with unprecedented excellent sensitivity and mass resolution will make excellent isotopic measurements for the first time. The measurement will give crucial constraints on the nature of the GCRS and reveal the nucleosynthesis in the process of stellar evolution.

[B] The elemental source composition of GCRs is known for most elements between Z = 1 to 60 (Meyer, 1985c). The observation errors, however, vary widely one by one, depending on the relative abundance. Although most of the compositions for GCR heavy nuclei have solar system composition in general, C and O are overabundant and N is depleted among some major elements. And anomalies of heavy nuclei (Z>30) other than CNO are seen in GCR observation.

Elements in the range Z = 30 to 38, and in particular $_{38}$Sr, are not enhanced. The excesses of $_{42}$Mo and $_{58}$Ce are probably certain, and $_{40}$Zr and some s-, and r-process elements, $_{52}$Te, $_{54}$Xe, $_{56}$Ba are probable overabundant. So the excesses seem to start abruptly at Z = 40. The Mo excess is certain, while Zr excess is not yet certain. It is worth an effort to confirmed.

If $_{40}$Zr excess is indeed confirmed, the sharp onset of the excesses between $_{38}$Sr and $_{40}$Zr, right after the neutron magic number N = 50, is almost a signature of a s-process contribution.

Implying that a specific component has undergone strong irradiation, the excesses of Mo, Ba and Ce seem to be due to the same intense neutron-irradiation. There seems to be also an r-process excess, as judged from $_{52}$Te and $_{54}$Xe, though the excesses are not established (Meyer, 1985c).

If, on the contrary, the Zr excess is not present, the interpretation of the various excesses in terms of s- and/or r-process excesses is much confused, since Mo and Ce have both significant s- and r-process components in "solar mix" material. If r-process excesses are present, there may be related to a possible excess of Pt-group elements.

*HEP-MI instrument is designed to measure the elements up to Z = 45 with increased sensitivity. It would be possible to measure the abundances of those nuclides which are important to the nucleosynthetic studies.

2.3.1.2 The Characteristic Time of GCR

GCR nuclei observed near the earth are composed of so called 'primary' and 'secondary' components. The primary particles are those which are accelerated at the GCRS and have survived during the propagation in the galaxy without undergoing a nuclear transformation. The secondary particles are fragments produced by the destructive interactions with atoms in the

ISM. Radioactive isotopes produced as either primary or secondary, decay with different life-times and the measurement of their fraction relative to stable isotopes provides the characteristic time of GCRs (Simpson, 1983a, b; Simpson et al., 1988; Wiedenbeck, 1983).

[1] The Time between Nucleosynthesis and Acceleration

The fundamental question of cosmic ray astrophysics is when the GCRs are accelerated and where the source of GCR is. The question in this measurement is whether GCRs represent a matter freshly synthesized in the evolved stars, perhaps supernova explosions, or whether they might be older species, perhaps a sample of the ISM. If cosmic ray source material synthesized in stellar interior or surface is not accelerated for a long time it is synthesized in the stellar interior and ejected it from a stellar surface back into the ISM, we may expect the ISM as the GCRS.

The time delay between the nucleosynthesis and acceleration can be determined by the measurement of isotopic abundance of electron capture radionuclides which are synthesized at the GCR source, but which can survive in the GCRs if they are accelerated at the source before decaying. These nuclides do not decay once they have been accelerated to high energies and stripped of all orbital electrons.

During explosive nucleosynthesis, heavy nuclides including radionuclide such as ^{56}Ni, ^{57}Co and ^{59}Ni are produced, and they can use as the probe to determine the characteristic time (Soutoul et al., 1978). Figure 2.3.1-1 shows that how the surviving cosmic ray isotopic abundances in the iron-cobalt-nickel group are expected to vary with the delay time between nucleosynthesis and acceleration.

Isotopes	Life
^{56}Ni	6.1 d
^{57}Co	270 d
^{59}Ni	8 x 10^4 y

Isotopic observations up to now have shown that ^{56}Fe is the dominant iron isotope, implying that the ^{56}Ni decay has already occurred and the time delay is thereby longer than a few ten days. The direct confirmation of ^{57}Co and/or ^{59}Ni decay would give the discrimination between a supernova origin and an ISM one.

*Although the flux of those isotopes is weak, the geometric factors for HEP instruments with high mass resolution have been improved by a factor of about 100, so this will shed light on this problem.

[2] Storage Time during Propagation in the Galaxy

One of the principal goals in cosmic ray astrophysics is the study of GCR propagation in the Galaxy. From the measurements of different secondary-to-primary ratios such as B/C and (Sc+Ti+V+Cr+Mn)/Fe, the cosmic rays traverse about 7 g/cm^2 of ISM in traveling from their source to the earth's neighborhood (Protheroe et al., 1981; Garcia-Munoz et al., 1977, 1981, 1984, 1987; Wefel, 1988). To measure the confinement time in the galaxy, it is necessary to employ GCR isotopes with half lives of the same order as the anticipated age.

Radionuclides are useful for the determination of propagation time in the Galaxy include ^{10}Be, ^{26}Al, ^{36}Cl and ^{60}Fe. These nuclides except for ^{60}Fe are expected to be formed in collisions of the primary cosmic rays with the ISM, while ^{60}Fe might be a significant primary component.

Isotopes	Life	
^{10}Be	1.6 x 10^6 y	Secondary
^{26}Al	7.4 x 10^5 y	Secondary
^{36}Cl	3. x 10^5 y	Secondary
^{54}Mn	1.5 x 10^5 y	Secondary
^{60}Fe	3. x 10^5 y	Primary/Secondary

Abundance measurements of ^{10}Be in the about 100 MeV/n have given a cosmic-ray age of about 10^7 years and a density 0.2 – 0.3 atoms/cm^3 on the basis of a homogenous propagation model, which is not inconsistent with the result obtained by ^{26}Al measurement but poor in statistics (Wiedenbeck and Greiner, 1980; Garcia-Munoz et al., 1977, 1981; Webber et al., 1977, 1978) (see Fig. 2.3.1-2). This density is significantly lower than the values of a few atoms/cm^3 determined for the ISM in the disk of the galsxy by astronomical technique. Various possible means of confining GCRs in regions of low-average density have been considered for the interpretation of the abundances of radioactive GCR isotopes. A comparison of the cosmic ray age measured by clocks with different radionuclides would probe the homogeneity of the matter traversed, when we combine with the pathlength distribution determined by stable secondaries such as Li, Be, B, F and the iron secondaries. The better statistics is also needed for the observation of ^{26}Al and ^{36}Cl.

*The HEP instruments will make possible the precise determination of the abundances of those radionuclides because of their high sensitivities and mass resolution. This will make great progress in studies of GCR propagation in the galaxy.

B and ^{15}N are considered to be purely secondary products. The species are close in mass, so that the compared propagation predictions for the ratios, B/C and $^{15}N/O$, are not sensitive to exact for the shape of the path-length-distribution. But both the B/C and $^{15}N/O$ cannot fit simultaneously with standard propagation models. The contradiction is well beyond reasonable errors on both the GCR data and the cross sections. The nuclei concerned are also too close in mass for refinements of the propagation model to have any chance to solve the problem (Meyer, 1985a-c).

*Further measurements of GCR secondaries, ^{6}Li, ^{7}Li, ^{7}Be, ^{9}Be, ^{10}Be, ^{10}B, ^{11}B, ^{15}N, ^{17}O, ^{19}F at low energy, can add a new dimension to studies of GCR propagation. Measurements of key unmeasured cross sections below a few 100 MeV/n down to the threshold energy, and studies of the energy loss problem for heavier nuclide are required simultaneously. The HEP instruments have such a sufficient collecting power that they will make possible the systematic survey of those nuclides.

2.3.2 Anomalous Cosmic Ray Events

Energy spectra of ions have valley in the energy region of MeV/n. And the depth of the valley depends on the solar activity. The energy spectra for specific ions such as He, N, O and Ne have a hump or plateau in the spectral valley in the energy range from a few MeV/n to a few tens MeV/n (Fig. 2.3.2-1). This excess, called "anomalous cosmic ray component", is striking in the phase of solar minimum. This component was observed for the first time in 1972 near the beginning of the last solar minimum (Garcia-Munoz et al., 1973; Hovestadt et al., 1973; Cummings et al., 1984). Recently the existence of anomalous cosmic ray hydrogen around 60 MeV/n has been shown by the measurements of Voyager 1 and 2 near the time of maximum fluxes in 1985 to 1987 (Christian et al., 1988).

According to the leading theory for the origin of the anomalous cosmic ray (Fiske et al., 1984; Pesses et al., 1981), these ions are originated from intersteller neutral gases which penetrate deep into the heliosphere before being singly ionized by solar UV or charge exchange. The neutral gasses with a high FIP are able to invade the inner system of heliosphere. The ions are then carried to the outer heliosphere by the solar wind.

Acceleration may occur at the heliospheric termination shock, with subsequent easy propagation back into the inner solar system, because they have the high magnetic rigidity of the singly ionized anomalous component in comparison with the fully ionized galactic cosmic rays with the same energies.

The question on the anomalous cosmic ray events is whether only those elements involved are essential or due to the lack of instrumental capabilities. The scenario about the origin and the acceleration mechanism is not yet established.

*The GEOTAIL HEP-MI with unprecedented sensitivity and mass resolution will make possible the detail measurement of the heavy isotope composition in the anomalous cosmic ray component at the next solar maximum and the decreasing phase of the solar activity. There is the probability that Ar and its isotopes, and other rare elements can be detected in the GEOTAIL mission.

REFERENCES

Althouse, W. E. et al., *Geosci. Geoelectr.*, **16** (1978) 204.
Anders, E., and M. Ebihara, *Geochim. et. Cosmochim. Acta.*, **46** (1982) 2363.
Anders, E., and N. Grevesse, *Geochem. Cosmochem. Acta*, **53** (1984) 197.
Andrews, M. K., E. Keppler, and P. W. Daly, *J. Geophys Res.*, **86** (1981) 7543.
Bai, T., *Ap. J.*, **308** (1986) 912.
Baker, D. N., and E. C. Stone, *J. Geophys. Res.*, **82** (1977) 1532.
Baker, D. N., S. J. Bame, J. Birn, W. C. Feldman, J. T. Gosling, E. W. Hones, Jr., R. D. Zwickl, J. A. Slavin, E. J. Smith, B. T. Tsurutani, and D. G. Sibeck, *J. Geophys. Res.*, **11** (1984) 1042.
Breneman, H. H., and E. C. Stone, *19th ICRC Conf. Papers*, **4** (1985a) 213.
Breneman, H. H., and E. C. Stone, *Ap. J. Lett.*, **299** (1985b) L57.
Cammeron, A. G. W., in Essays in Nuclear Astrophysics, ed., C. A. Barnes et al., (Cambridge Univ. Press) (1982) 23.
Cane, H. V., S. W. Kahler, and N. R. Sheeley, Jr., *J. Geophys. Res.*, **91** (1986) 1321.
Casse, M., *17th ICRC Conf. Papers*, **13** (1981) 111.
Case, M., in *Composition and Origin of Cosmic Rays*, ed., M. M. Shapiro, (Dordrecht Reidel) (1983) 193.
Casse, M., and J. A. Paul, *Ap. J.*, **258** (1982) 860.
Chenett, D. L., *J. Geophys. Res.*, **85** (1980) 2243.
Chenette, D. L., T. F. Conlon, K. R. Pyle, and J. A. Simpson, *Ap. J. Lett.*, **215** (1977) L15.
Chupp, E. L., *Ann. Rev. Astron. Astrophys.*, **22** (1984) 359.
Cook, W., E. C. Stones, and R. E. Vogt, *Ap. J.*, **279** (1984) 827.
Cristian, E. R., A. C. Cummings, and E. C. Stone, *Ap. J.*, **334** (1988) L77.
Cummings, A. C., E. C. Stone, and W. R. Webber., *Ap. J. Lett.*, **287** (1984) L99.
Daly, P. W., and E. Keppler, *J. Geophys. Res.*, **88** (1983) 3971.
Daly, P. W., M. A. Saunders, R. P. Rijnbeek, N. Sckopke, and C. T. Russell, *J. Geophys. Res.*, **89** (1984a) 3843.
Daly, P. W., K.-P. Wenzel, and T. R. Sanderson, *Geophys. Res. Lett.*, **11** (1984b) 1070.
Domingo, V., D. E. Page, and K.-P. Wenzel, *J. Geophys. Res.*, **82** (1977) 2327.
Eastman, T. E., L. A. Frank, and C. Y. Huang, *J. Geophys. Res.*, **90** (1985) 9541.
Ellison, D. C., *J. Geophys. Res.*, **90** (1985) 29.
Ellison, D. C., and Ramaty, *Ap. J.*, **298** (1985) 400.
Fan, C. Y., G. Gloeckler, and D. Hovestadt, *Space Sci. Rev.*, **38** (1984) 143.
Fisk, L. A., *Ap. J.*, **224** (1978) 1048.
Fisk, L. A., B. Kozlovsky, and R. Ramaty, *Ap. J. Lett.*, **190** (1974) L35.
Fritz, T. A., D. J. Williams, G. Paschmann, C. T. Russell, and W. N. Spjeldvik, *J. Geophys. Res.*, **87** (1982) 2133.
Garcia-Munoz, M., G. M. Mason, and J. A. Simpson, *Ap. J. Lett.*, **182** (1973) L31.
Garcia-Munoz, M., G. M. Mason, and J. A. Simpson, *15th ICRC Conf. Papers*, **1** (1977) 301.
Garcia-Munoz, M., G. M. Mason, and J. A. Simpson, *Ap. J.*, **217** (1977) 895.
Garcia-Munoz, M. et al., *17th ICRC Conf. Papers*, **2** (1981a) 192.
Garcia-Munoz, M. et al., *Ap. J. Lett.*, **280** (1984) L13.
Garcia-Munoz, M. et al., *Ap. J. Suppl.*, **64** (1987) 269.
Geiss, J., *Space Sci. Rev.*, **33** (1982) 201.
Gloeckler, G., *Rev. Geophys. and Space Phys.*, **17** (1979) 569.
Hones, E. W., Jr., *J. Geophys. Res.*, **82** (1977) 5633.
Hones, E. W., Jr., in Dynamics of the Magnetosphere, ed., S.-I. Akasofu, D. Reidel, p.545 (1979).
Hones, E. W., Jr., D. N. Baker, S. J. Bame, R. D. Belian, W. C. Feldman, J. T. Gosling, D. J. McComas, R. D. Zwickl, J. A. Slavin, E. J. Smith, and B. T. Tsurutani, *Geophys. Res. Lett.*, **11** (1984) 5.

Hovestadt, D. et al., *Phys. Rev. Lett.*, **31** (1973) 650.
Klecker, B. et al., *Ap. J.*, **281** (1984) 458.
Kocharov, L. G., and G. E. Kocharov, *Space Sci. Rev.*, **38** (1984) 89.
Krimigis, S. M., D. Venkatesan, J. C. Barichello, and J. C. Sarris, *Geophys. Res. Lett.*, **5** (1978) 961.
Lin, R. P., *Solar Phys.*, **100** (1985) 537.
Maezawa, K., and T. Murayama, in Solar Wind Magnetosphere Coupling, ed., Y. Kamide and J. A. Slavin, p.59 (1986).
Mason, G. M. et al., *Ap. J.*, **303** (1986) 849.
Mason, G. M., *Rev. Geophys. Space Phys.*, **25** (1987) 685.
McGuire, R. E., T. T. von Rosenvinge, and D. V. Reames, *Ap. J.*, **301** (1986) 938.
McGuire, R. E., *Rev. Geophys. Space Phys.*, **21** (1983) 305.
Meng, C.-I., and K. A. Anderson, *J. Geophys. Res.*, **75** (1970) 1827.
Meng, C.-I., and K. A. Anderson, *J. Geophys. Res.*, **80** (1975) 4237.
Mewaldt, R. A., in *Ancient Sun*, ed., Pepin et al., (1980 81.
Mewaldt, R. A., *Rev. Geophys. and Space Phys.*, **21** (1983) 295.
Mewaldt, R. A., J. D. Spalding, E. C. Stone, *Ap. J.*, **283** (1984) 450.
Meyer, J. P., *Ap. J. Suppl.*, **57** (1985a) 151.
Meyer, J. P., *Ap. J. Suppl.*, **57** (1985b) 171.
Meyer, J. P., *19th ICRC Conf. Papers*, **9** (1985c) 141.
Miura, A., and P. L. Pritchett, *J. Geophys. Res.*, **87** (1982) 7431.
Montmerle, T., in Gensis and Propagation of Cosmic Rays, ed., M. M. Shapiro and J. P. Wefel, (Reidel Pub. Comp.), (1988a) 105.
Montmerle, T., in Gensis and Propagation of Cosmic Rays, ed., M. M. Shapiro and J. P. Wefel, (Reidel Pub. Comp.), (1988b) 131.
Nakada, M. P., *Solar Phys.*, **14** (1970) 457.
Nishida, A., and N. Nagayama, *J. Geophys. Res.*, **78** (1973) 3782.
Ormes, J. F., M. Israel, M. Wiedenbeck, and R. Mewaldt, The Particle Astrophysics Magnet Facility ASTROMAG. (1986).
Pallavicini, R., S. Serio, and G. S. Vaiana, *Ap. J.*, **216** (1977) 108.
Paschmann, G., N. Sckopke, I. Papamastorakis, J. R. Asbridge, S. J. Bame, and J. T. Gosling, *J. Geophys. Res.*, **86** (1981) 4355.
Pesses, et al., *Ap. J.*, **246** (1981) L85.
Protheroe, R. J., J. F. Ormes, and G. M. Comstock, *Ap. J.*, **247** (1981) 362.
Reames, D. V., T. T. von Rosenvinge, and R. P. Lin, *Ap. J.*, **292** (1985) 716.
Reames, D. V., and R. G. Stone, *Ap. J.*, **308** (1986) 902.
Reinhard, R., and G. Wibberenz, *Solar Phys.*, **36** (1974) 473.
Richardson, I. G., and S. W. H. Cowley, *J. Geophys. Res.*, **90** (1985) 12133.
Russell, C. T., and R. C. Elphic, *Space Sci. Rev.*, **22** (1978) 681.
Russell, C. T., and R. C. Elphic, *Geophys. Res. Lett.*, **6** (1979) 33.
Russell, C. T., and R. L. McPherron, *Space Sci. Rev.*, **15** (1973) 205.
Sarris, E. T., S. M. Krimigis, and T. P. Armstrong, *J. Geophys. Res.*, **81** (1976) 2341.
Sarris, E. T., S. M. Krimigis, and C. O. Bostrom, *J. Geophys. Res.*, **83** (1978) 4289.
Schellert, G., G. Wibberenz, and H. Kunow, *19th ICRC*, **4** (1986) 305.
Scholer, M., G. Gloeckler, F. M. Ipavich, D. Hovestadt, and B. Klecker, *Geophys. Res. Lett.*, **6** (1979) 707.
Schramm, D. M., in Nucleosynthesis, (The Univ. Chicago Press), ed., W. D. Arnett and J. W. Truran, (1984) 106.
Simpson, J. A., *Ann. Rev. Nucl. Part. Sci.*, **33** (1983a) 323.
Simpson, J. A., in Composition and Origin of Cosmic Rays, ed., M. M. Shapiro, (Dordrecht Reidel) (1983b) 193.
Simpson, J. A. and M. Garcia-Munoz, *Space Sci. Rev.*, **46** (1988) 205.
Slavin, J. A., B. T. Tsurutani, E. J. Smith, D. E. Jones, and D. G. Sibeck, *Geophys. Res. Lett.*, **10** (1983) 973.
Soutoul, A. et al., *Ap. J.*, **219** (1978) 753.
Spjeldvik, W. N., and T. A. Fritz, *J. Geophys. Res.* **86** (1981) 2480.
Terasawa, T., and A. Nishida, *Planet. Space Sci.*, **24** (1976) 855.
Tsurutani, B. T., J. A. Slavin, E. J. Smith, R. Okida, and D. E. Jones, *Geophys. Res. Lett.*, **11** (1984) 1.
Vargoglis, H., and K. Papadopoulos, *Ap. J. Lett.*, **270** (1983) L95.

Webber, W. R. et al., *Ap. J.*, **18** (1977) 125.
Webber, W. R. and J. Kish, *16th ICRC Conf. Papers*, **1** (1979) 389.
Wefel, J. P. et al., *19th ICRC Conf. Papers*, **2** (1985) 88.
Wefel, J. P., in Genesis and Propagation of Cosmic Rays, ed., M. M. Shapiro, and J. P. Wefel, (Reidel Pub., Comp.) (1988) 1.
Wiedenbeck, M. E., and D. E. Greiner, *Ap. J. Lett.*, **239** (1980) L139.
Wiedenbeck, M. E., and D. E. Greiner, *Phys. Rev. Lett.*, **46** (1981a) 682.
Wiedenbeck, M. E., and D. E. Briner, *Ap. J. Lett.*, **247** (1981b) L119.
Wiedenbeck, M. E., in *Composition and Origin of Cosmic Rays*, ed., M. M. Shapiro, (Dordrecht Reidel) (1983b) 193.
Wiedenbeck, M. E., in Nucleosynthesis (The Univ. Chicago Press), (1984) 89.
Williams, D. J., *J. Geophys. Res.*, **84** (1979) 101.
Williams, D. J., *J. Geophys. Res.*, **85** (1980) 3387.
Williams, D. J., *J. Geophys. Res.*, **86** (1981) 5507.
Woosley, S. E., and T. A. Weaver, *Ap. J.*, **243** (1981) 651.

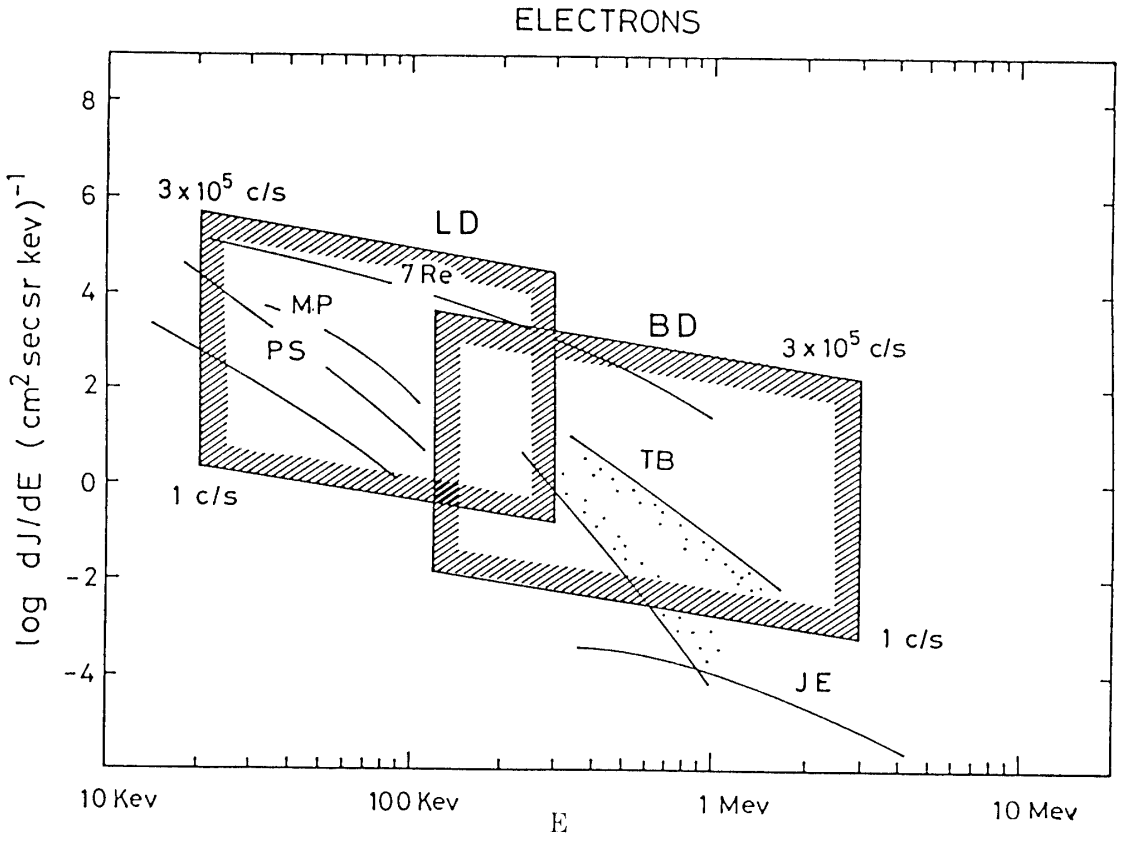

Fig. 2.1.4-1 Energy range and sensitivity of HEP-LD and -BD detectors are indicated by shaded boxes. Lower and upper boundaries of the boxes correspond to 1 c/s and 3×10^5 c/s levels, respectively, assuming that electron distribution is given by a power law with index -4. Representative energy spectra for some of the known electron populations are also shown. Their abbreviations are;

PS: Quiet time plasma sheet population in the near-earth tail
MP: Electrons at the dayside magnetopause
TB: Bursty appearances of electrons in the tail including those at the time of plasma sheet recovery
JE: Jovian Electrons.

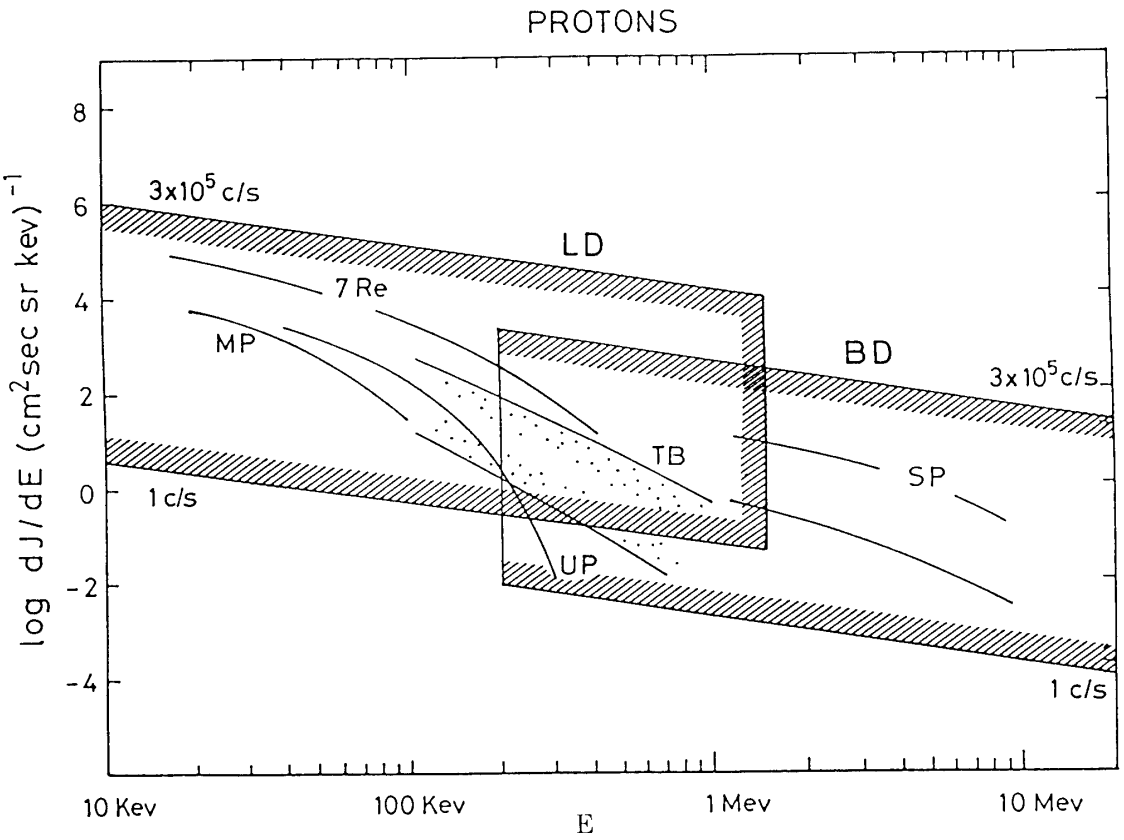

Fig. 2.1.4-2 Same as Fig. 1 but for protons. The lower energy threshold of the BD sensor may be subject to change due to the selection of film for shelding sunlight. Abbreviations are:
MP: Protons at the dayside magnetopause
UP: Upstream protons
TB: Bursty appearances of protons in the tail including those at the time of plasma sheet recovery.

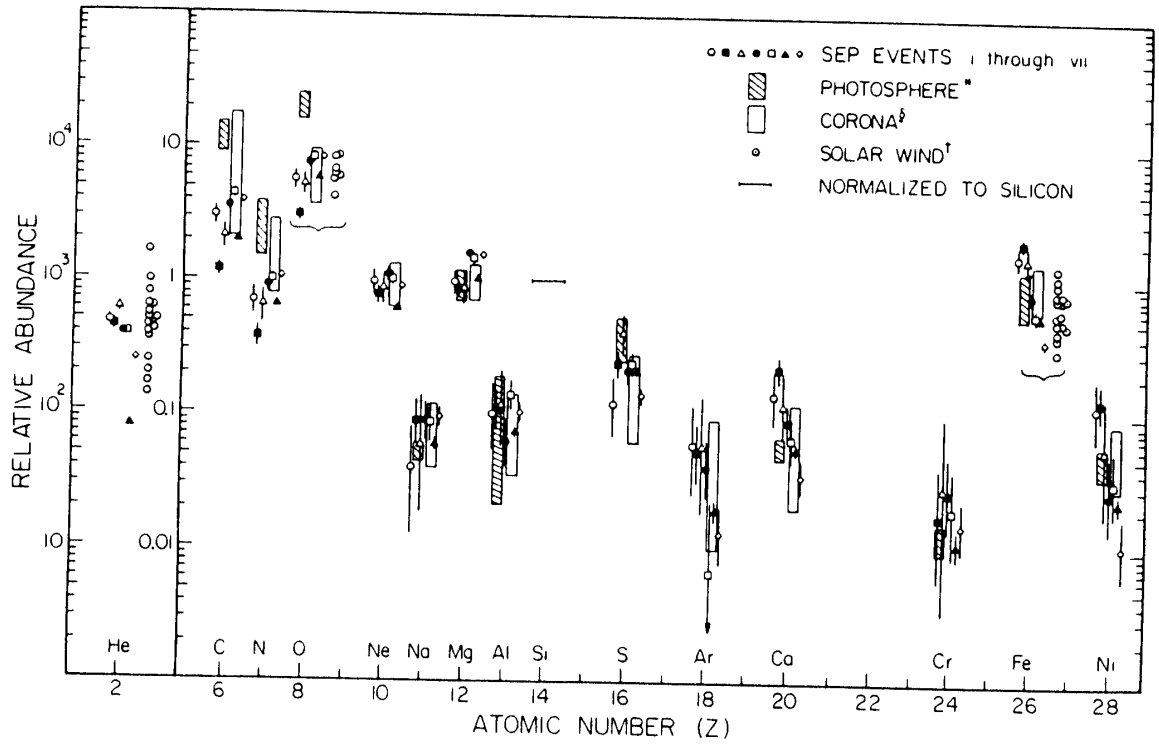

Fig. 2.2.1-1 An overview of the SEP abundance in comparison with the solar photosphere, corona and solar wind. All abundances are normalized to Si (Cook et al., 1984).

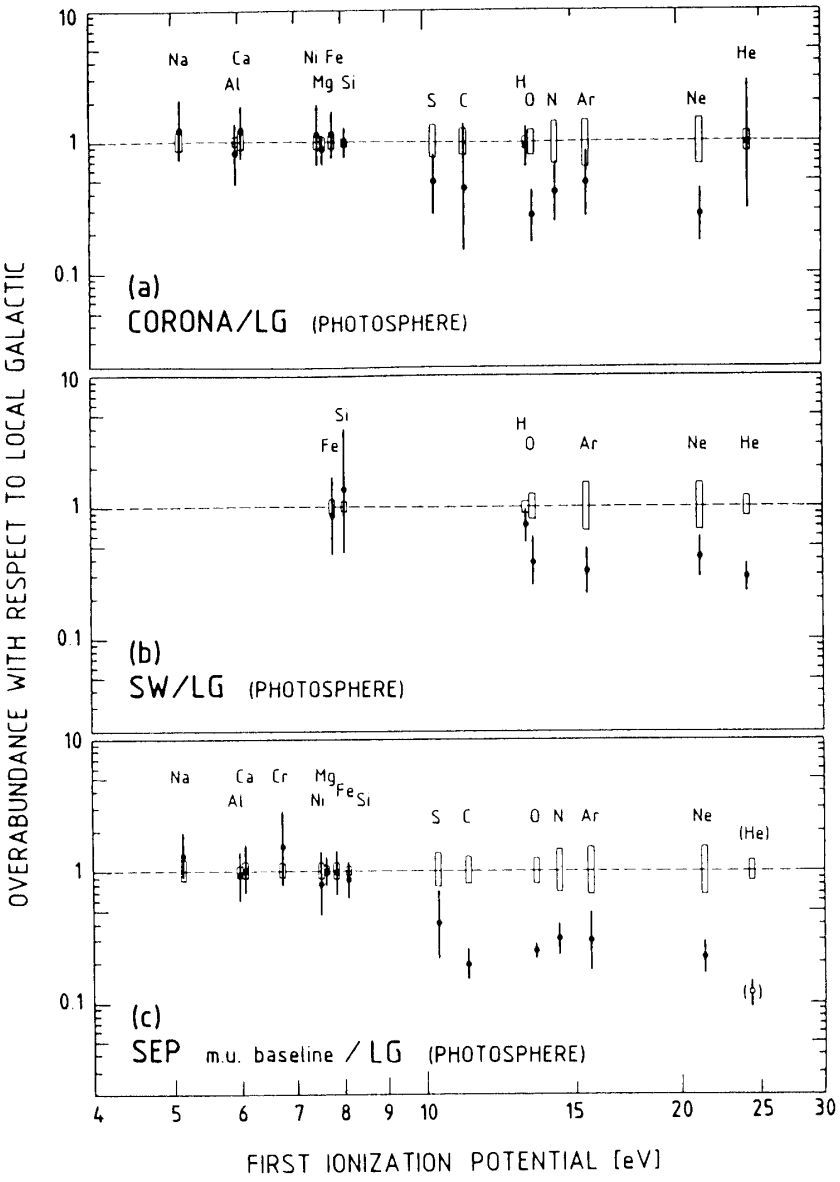

Fig. 2.2.1-2 Elemental abundance ratios with respect to Local Galactic abundance as a function of first ionization potential (FIP). (a) solar corona; (b) solar wind; (c) solar energetic particle (SEP); vs. FIP for $Z < 30$ (Meyer, 1985a, b, c).

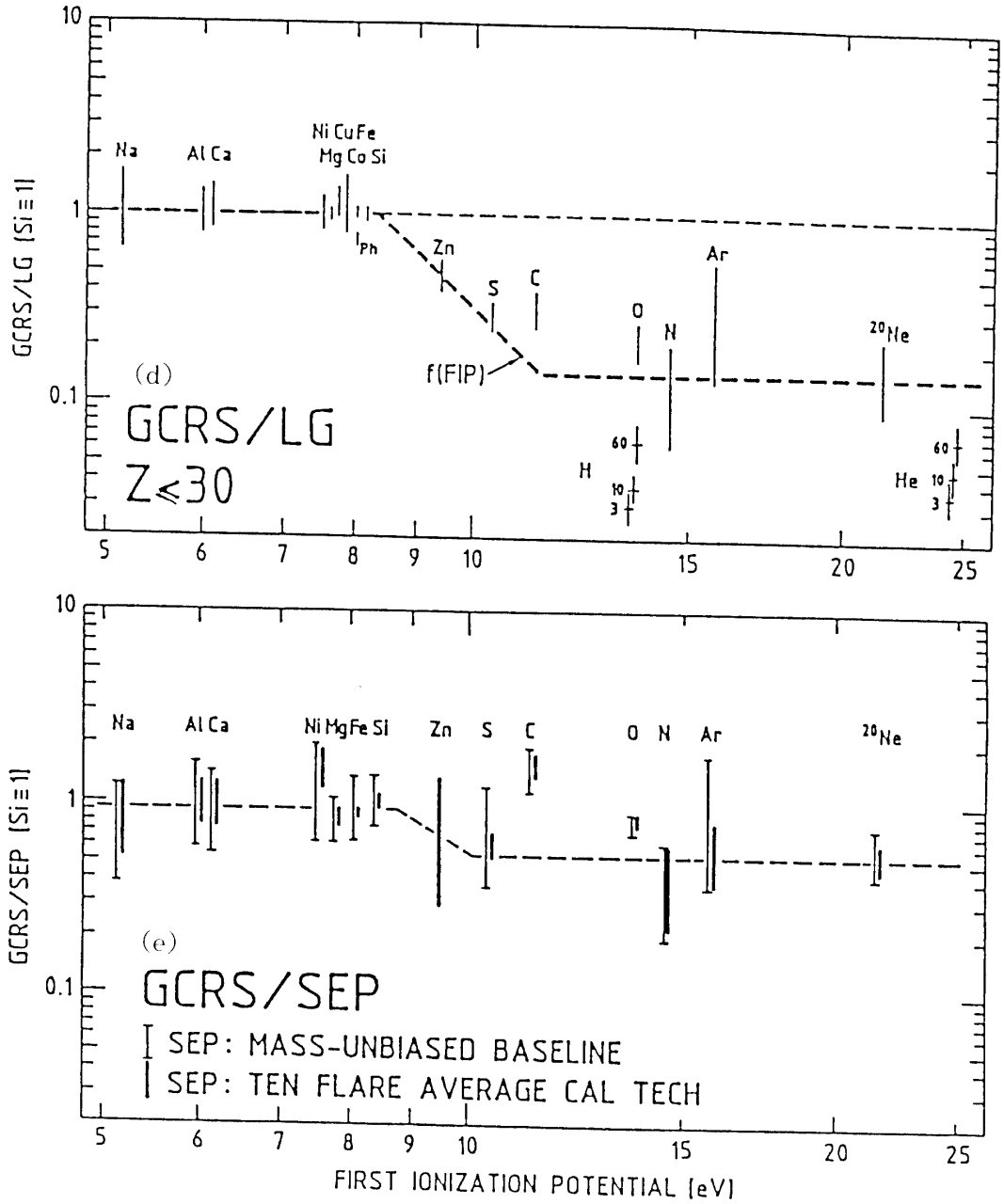

Fig. 2.2.1-2 (continued) Elemental abundance ratios with respect to Local Galactic abundance as a function of first ionization potential (FIP). (d) galactic cosmic ray sources; (e) GCRS/SEP abundance ratios vs. FIP for Z < 30 (Meyer, 1985a, b, c).

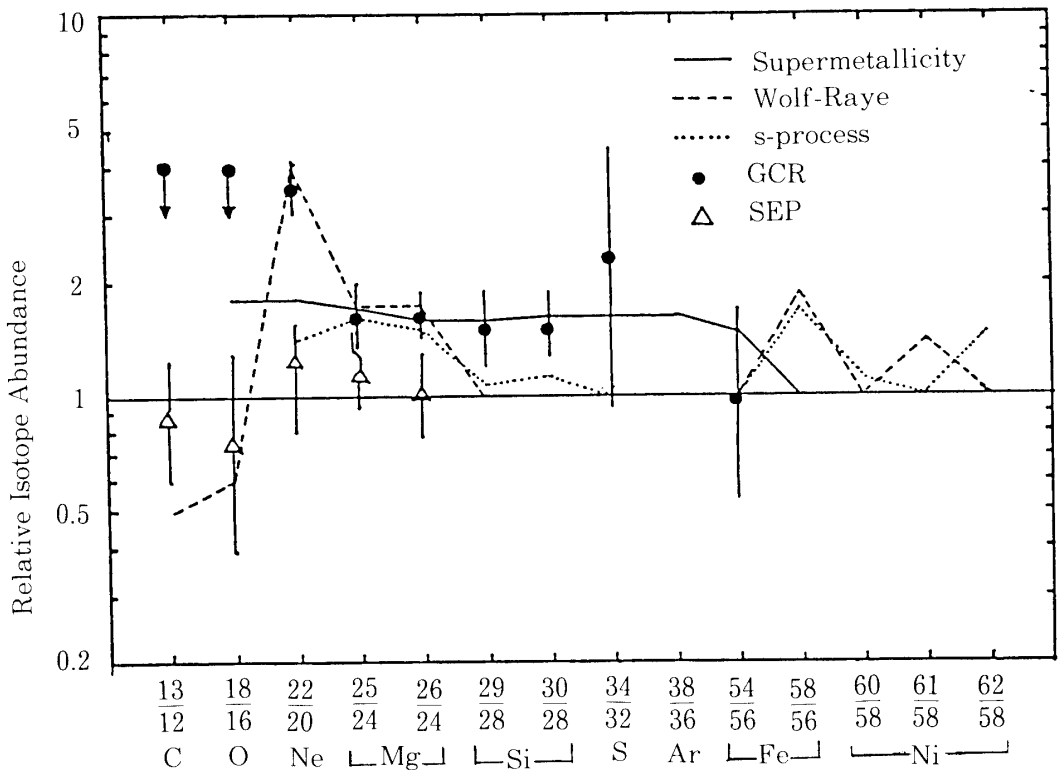

Fig. 2.2.1-3 Comparisons with isotopic abundances measured for SEP and GCRS normalized to the solar system composition.

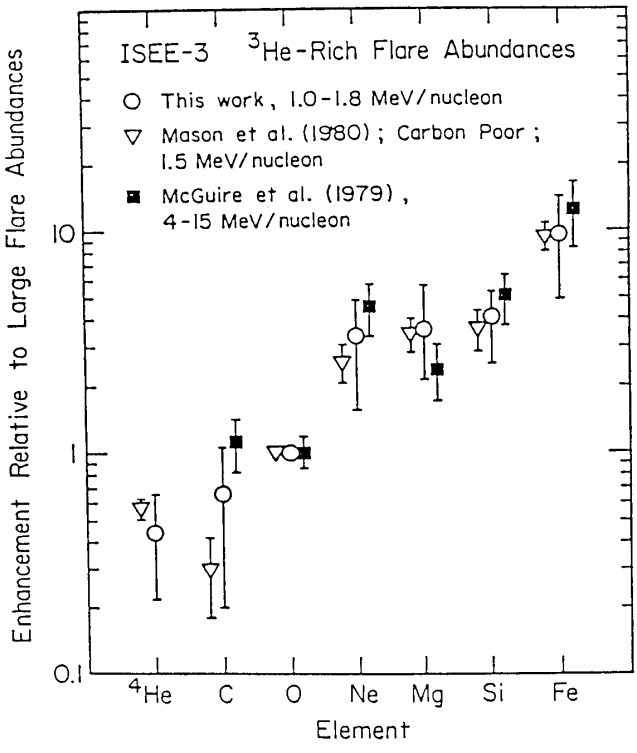

Fig. 2.2.1-4 Enhancement of heavy elemental abundances in ^{3}He- rich events compared to large solar particle events. Data are normalized to oxygen (Mason et al., 1986).

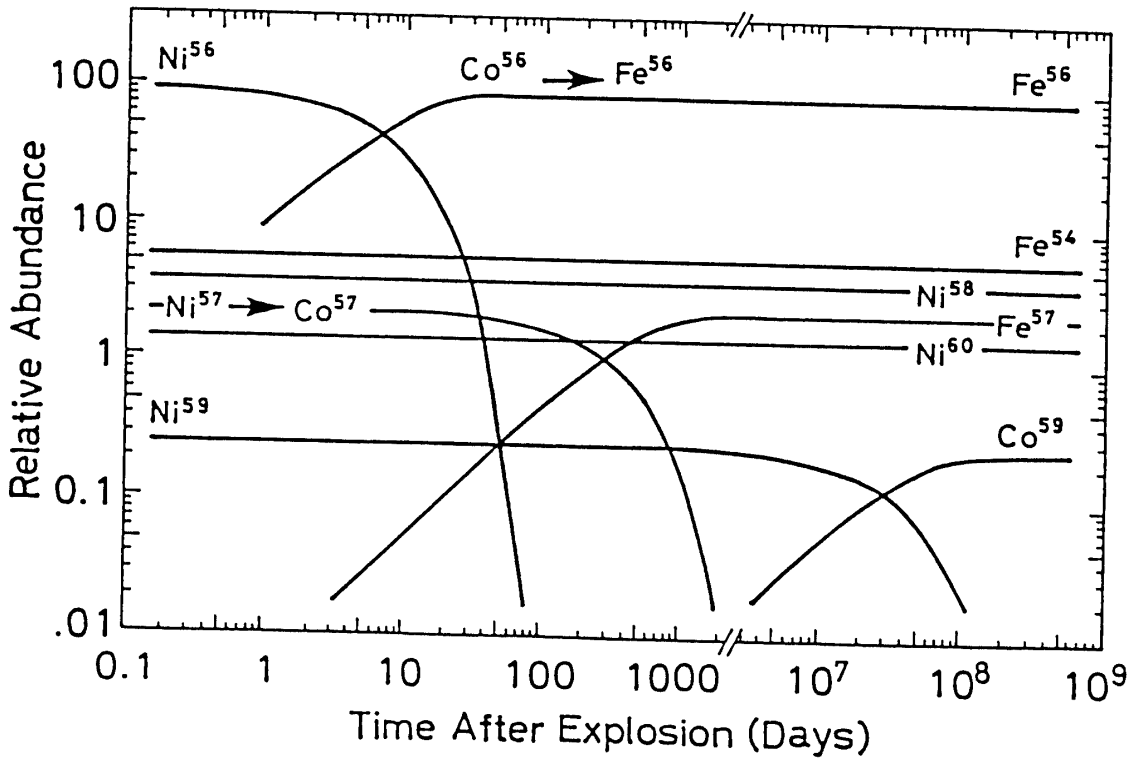

Fig. 2.3.1-1 Cosmic ray isotopic abundances of explosively synthesized electron capture isotopes, iron-cobalt-nickel group as a function of the time after explosion (Ormes et al., 1986).

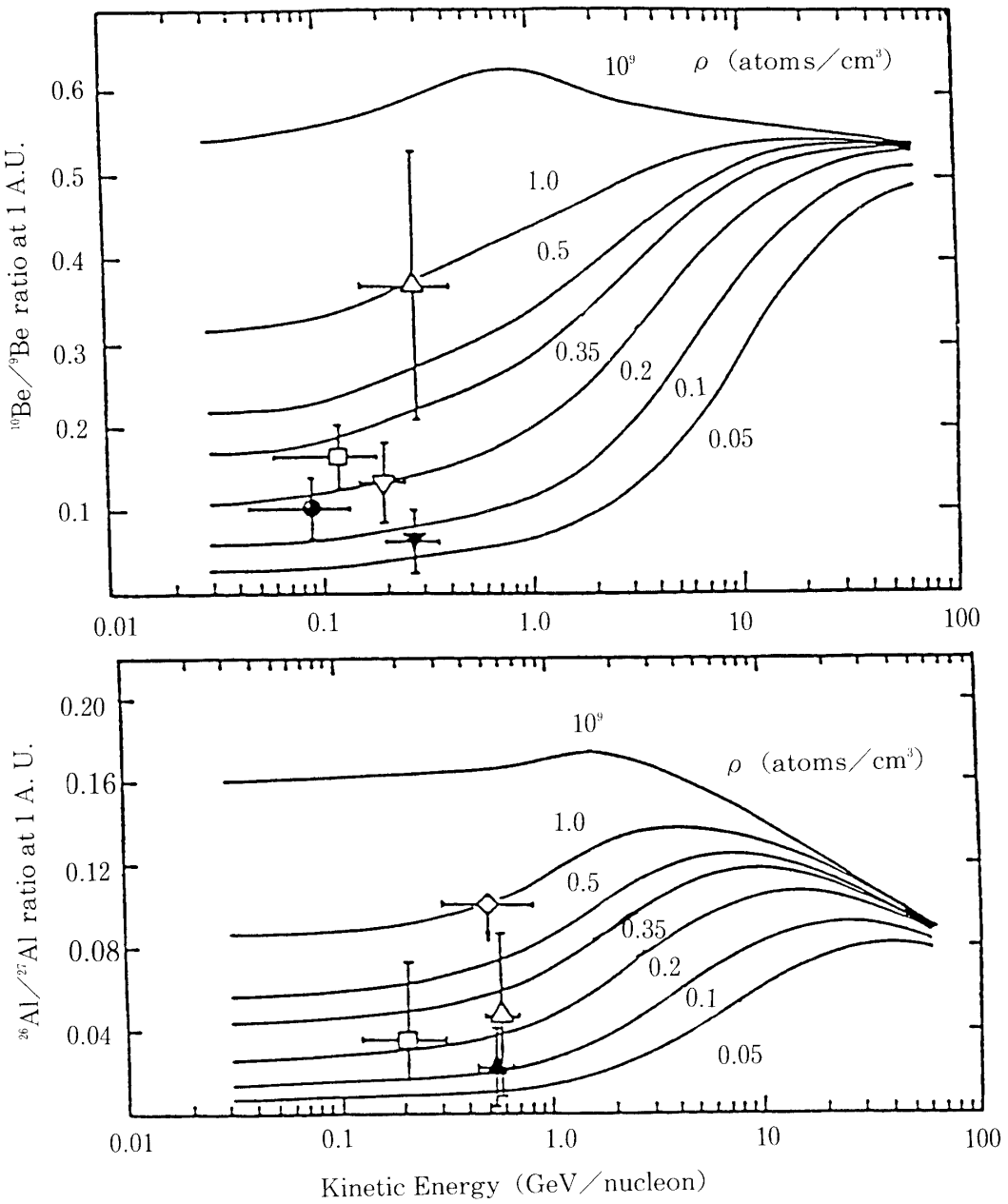

Fig. 2.3.1-2 Comparison of experimental measurements of the radioactive isotopes ^{10}Be and ^{26}Al to predictions of a standard propagation model, parametrized by the mean density of the matter traversed (Wefel, 1988).

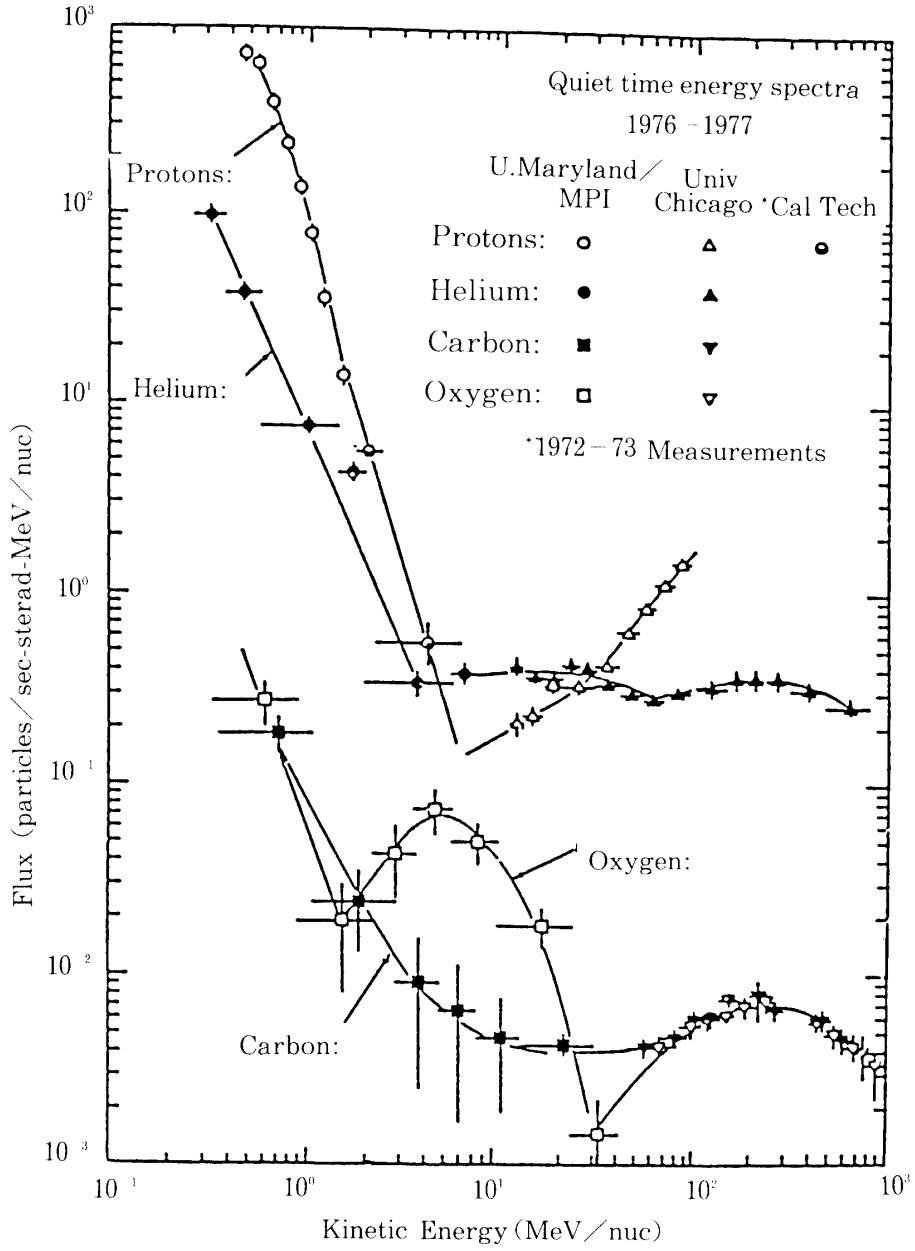

Fig. 2.3.2-1 Differential energy spectra of hydrogen, helium, carbon and oxygen observed near 1 AU during the solar minimum in 1976–1977 during quiet times. Anomalous cosmic ray spectrum peaks for He near 20 MeV/n and O near 5 MeV/n (Gloeckler, 1979).

3. INSTRUMENTS DESCRIPTIONS

Details of GEOTAIL HEP instrument LD, BD, MI-1, MI-2 and HI are presented in this chapter.

3.1 Low Energy Particle Detectors LD

3.1.1 Introduction

The HEP-LD ion-mass spectrometer is based on the well established time-of-flight (TOF) technique in combination with an energy analysis in solid state detectors. The particle's mass A (in amu) is then determined from the two-parameter time-energy analysis. Derivation of timing signals for the TOF spectroscopy from ion induced secondary electron mission (SEE) made this technique an indispensable scientific tool for the spectroscopy of thermal and suprathermal plasmas in planetary magnetospheres and interplanetary space.

Introduction of position sensing on the entry element of the TOF system adds the capability to determine the particle's direction of motion with moderate but sufficient angular resolution. This novel concept allows a 180° angular opening for the entrance collimator of LD and to sample a solid angle of 4π in velocity space as the instrument rotates with the spin motion of the GEOTAIL spacecraft. The detection principle used for LD primarily identifies heavy ions with respect to their mass, energy and direction. Swift electrons with energies between 20 and 300 keV are uniquely distinguished from nuclei, by a valid (T, E) signature with $T \sim 1$ ns. The following is a brief report on the instrumental techniques employed in HEP-LD and the principal data structure of the spectrometer.

3.1.2 Principle of Measurements

The HEP-LD spectrometer is designed for the analysis of energetic electrons and ions with a complete coverage of the unit sphere in phase space. State-of-the-art techniques are employed to accomplish particle discrimination and three dimensional analysis in phase space. Physically the instrument consists of a single box which contains the sensor system (composed of three identical Imaging Ion Mass Spectrometer IIMS detectors), and the Digital Preprocessing Unit (HEP-LD/DPU). Figure 3.1-1 shows the instrument configuration and illustrates orientation and viewing angles on the spacecraft.

3.1.3 The Sensor System

The HEP-LD sensor system consists of three identical IIMS detectors which cover angular interval of 180° in the polar angle of the spectrometer.

The IIMS is an energetic ion spectrometer which derives its particle identifier function $A \sim E \cdot T^2$ from a time-of-flight/energy measurement (particle mass A in amu). Figure 3.1-2 is an illustration of the two-dimensional mass analysis showing the sorting of ions along hyperbolic curves in the E-T plane. Comprehensive description of this detection technique and its application in space research has been published in the literature (e.g., Gloeckler and Hsieh, 1979; Wilken, 1984). The principle of IIMS is related to a family of instruments which uses secondary electron emission (SEE) from matter for obtaining timing signals: The flight time T of a swift particle is obtained by detecting secondary electrons (SE) released from a thin START foil (thickness 5–20 $\mu g/cm^2$) and from the surface of a solid state energy detector (SSD) which is located at a distance behind the foil. Secondary electrons ejected from the foil and the SSD are deflected onto microchannel plates (MCP) to obtain timing signals for the T measurement.

An essential step in the technical evolution of this detection technique is the addition of position sensing on the entrance foil (START foil): The secondary electron transport to the MCP is not only isochronous but also image forming. The principle of proximity focusing is used to create an one-to-one image of the foil on the MCP. The particle's direction of incidence is then obtained from the pinhole effect associated with the small geometry of the SSD as the back element in this imaging ion mass spectrometer (IIMS).

A schematic representation of the IIMS-detector is shown in Fig. 3.1-3. The secondary electrons released from the foil (or from the SSD) are accelerated over a distance of 3 mm to about 1 keV. Except for the 90° reflection in the electrostatic mirror field the electron drift in a potential free cavity towards the respective MCP.

The number of secondary electrons arriving at the MCP is amplified in a two-stage channelplate assembly by a factor of $\sim 5 \cdot 10^6$. A one dimensional four-element anode array behind the START channelplate with a digital read-out system determines the position of the electron cloud on the exit side of the MCP. Each anode element corresponds to an area on the MCP face which in turn projects back to an area on the START foil by virtue of the electron optics. The particular potential distribution in the IIMS detector requires novel design approaches for the signal read-out system. The mandatory condition to keep the solid state detector at ground potential results in a high positive voltage for the exit surface of the microchannelplate. As a result the fast channelplate output pulses have to be isolated from this high potential before timing and position information can be extracted. The principle of the capacitor coupled read-out system is shown in Fig. 3.1-3(b). The position of the activated anode element is obtained from a slow low-power charge

integration whereas the timing pulse is derived from the fast current waveform generated by the channelplate. The time constant for the position determination is about 1μs. If only a single anode was simulated by a particle the follow-on electronics encodes the event in a 2 bit binary address (events for which the MCP output current is split between two adjacent anodes are eliminated from the evaluation process). The fast timing pulse for the time-of-flight measurement is obtained from the common signal path as indicated in Fig. 3.1-3(b). At the end of the flight path (s=3 cm) the incident particle impinges on the small solid-state detector (SSD) as shown in Fig. 3.1-3. Secondary electrons ejected from the SSD surface upon impact of the ion are transferred to a circular STOP microchannel plate without position sensing. The residual ion energy is deposited in the SSD and provides the energy (E) signal for the mass analysis.

The START foil with position sensing and the narrow SSD (active diameter 8 mm) form a particle imaging system similar to a pin-hole camera: The position of intersection on the entrance foil and the SSD define the particle's direction of incidence. The position sensing system forms four angular intervals over a range of 60° as sketched in Fig. 3.1-3. This only moderate angular resolution corresponds to requirements formulated for investigations in geospace with energetic particle distribution functions.

The described system allows the identification of ions over an energy range of 5 keV/n to 1500 keV total energy with a mass resolution of about 4 (at A = 16 amu). The mass-energy range covered by the detector is shown in Fig. 3.1-4. Electrons are identified for energies between 20 keV and 300 keV with the upper energy limit defined by the thickness of the SSD. A veto signal from a second anticoincidence detector identifies high energy electrons (E > 300 keV) and ions (E > 6.5 MeV/nuc) and prohibits their analysis.

The integrated sensor system of HEP-LD consists of three identical sensor units which cover a 180° fan in the polar plane with 12 contiguous angular intervals (15° x 12° each). The collimator of each sensor unit has a built-in plasma rejecter and its sensitivity can be adjusted to the particle flux by an adaptive aperture system. In this case the individual geometric factor (0.02± 20%) cm^2 sr.

3.1.4 The Electronics

The HEP-LD Signal Conditioning Unit (HEP-LD/SCU)

Principle components of the Signal Conditioning Unit are shown in Fig. 3.1-5. Upon arrival of a particle the detector unit generates three analog signals (START, STOP and energy E) and a digital position signal. A hy-

bridised position sensor transforms the primary position signal (MCP output signal on one of the four discrete anodes) into a logic pulse for further analysis in the Position Sensor Logic (PSL). The PSL inspects the event associated information pattern and releases it for further processing only if

a single detector was the source for the position information, and
the coincident time-of flight T and/or signal E were received from the same detector.

When these conditions are met the PSL transmits the valid position code θ_I and stimulates the ion preprocessor IPP in HEP-LD/DPU to accept the valid analog T and/or E signals for digitization and evaluation.

Multiplexers (MUX), controlled by the HEP-LD/DPU, operate the detector set in two fundamental modes:

Parallel or FIND mode: All three detectors are active simultaneously. Incident particles are accepted and processed on a first-come first-serve basis. The high sensitivity of the LD spectrometer is not compromised by duty cycle effects.

Serial or SCAN mode: The IIMS detectors are activated in a serial fashion. At any given time the LD sensitivity equals the sensitivity of a single IIMS detector (1/3 of the total sensitivity). The 180° angular range LD is sampled in a sequence, with each step covering 60°.

The Digital Processing Unit (HEP-LD/DPU)

To make optimum use of the LD spectrometer within constraints imposed by limited telemetry capacity the measured primary E and T event rates must be reduced by partial conversion to physical quantities using proper algorithms and by compression techniques prior to transmission to the main DPU (HEP-E). The conversion and compression is done by the event driven preprocessor IPP. The preprocessor is served and controlled by a (80C86) microprocessor system. A block diagram of the HEP-LD/DPU is shown in Fig. 3.1-6.

The preprocessed data will be further compressed by forming the following data sets: Three-dimensional angular distributions, ion mass and energy spectra, electron energy spectra, ion and electron flux obtained at specific pitch angles such as 0°, 90° and 180° with respect to the S/C spin. These various data sets of LD are defined in section 6.2.

Proper sampling of the energetic particle data over 4π in velocity space requires a set of reference signals from the satellite. The azimuthal phase can determined from a spin sector clock (4096 pulses/spin). A sun pulse from the spacecraft will provide an appropriate reference for the azimuthal sectoring of ion and electron data. The sector clock will also be used to sort the so-called "direct events" (DE) described in section 6.2 and enable reconstruc-

tion of the DE angular distributions. The HEP-LD/DPU uses the spin sector clock to divide the satellite rotation into 32 equally spaced sectors. This becomes the maximum azimuthal sampling resolution for the data. Usually, except in burst mode or other special modes, the data from two of these adjacent sectors are combined to provide a total of 16 equally spaced samples in the azimuthal directions.

The Ion Preprocessor (IPP)

The Ion Preprocessor (IPP) (Fig. 3.1-6) performs the real time processing of the HEP-LD data. It provides

interface to the sensor electronics (SCU),
analog-to-digital conversion of E and T signals,
ripple counters for auxiliary data rates (maximum count rate: 1 MHz),
real time classification of ions into a three-dimensional (A-(E/A)-θ_I-matrix (maximum event rate: 2 x 10^5 events per seconds), and
counting channels for major ion species (16 azimuthal sectors x 12 polar directions x 85 M-E/M channels = 16,320 counting channels).

Each ion is sorted into a 16 by 64 A vs E/A matrix in the A versus E/A plane (Fig. 3.1-4). According to the event pattern, two principle regions (I, II) and two emergency regions (II_a, II_b) with the following definitions are marked in Fig. 3.1-4:

Region I: Signal parameter events (valid T signal, no E signal) allowing (E/A) analysis only.
Region II: Two-parameter events with unique mass identification (valid E and T signals).
Region II_a, II_b: Reserved for single parameter analysis in case the E or T measurement should fail.

In addition to the evaluation of mass and energy per nucleon, individual events are selected according to a prescribed priority scheme and offered to the microprocessor system to be inserted into the Direct Event (DE) section of the experiment data block.

The IPP of LD provides further forty-two 24-bit ripple counters for auxiliary data rates (such as START rate, STOP rate, coincidence rate, SSD rate, and anticoincidence rate) which are incremented at a maximum frequency of 10^6 counts per second. Analog E and T signals are simultaneously digitized by two ADC's in the IPP. To obtain the high speed classification required for the ions, RAM based "look-up-tables" are used to quickly associate the digital E-T-θ_I triplet with an appropriate counting channel. The mass class A (0...15) is a function of the energy E and the time-of-flight T. Adjacent A-(E/A) classes can be combined to form a matrix rate-channel

(MR-data) by means of additional look-up tables. The contents of all these tables will be calculated and periodically checked by the microprocessor. Algorithms and coefficients are stored in the microprocessor program. The coefficients can be changed by telecommands. Final adjustments or unexpected substantial adaptions to mission objectives can be implemented via telecommand.

Operational Modes and Data Rates

The HEP-LD spectrometer has two principle operational modes:

a) The Normal Mode (NM) with a total of 2560 bps in RTT or 512 bps in RT. A RAM Check Mode (RCM) with a bit rate of 32 Kbps in RTT and a Standby Mode (SM) are only used for occasional health checks. RCM and SM are not considered "routine" operational modes.

b) The (internal) Burst Mode (BM) with a burst buffer memory is planned but not yet defined. With either mode HEP-LD can be operated in a multitude of submodes since the DPU can select any subset of detectors and activate them in a serial or parallel fashion. However, most of these modes will only be used for check-out phases or in case of emergency. For all practical purposes and in order to facilitate the data analysis phase HEP-LD will be operated in the "routine" Normal Mode. It is quite possible, however, that scientific considerations require in-flight mode changes because of new or changing scientific emphasis. For this reason the HEP-LD/DPU has access to programmed pairs of NM and BM. Both in NM and BM the instrument can be configured such that the three detector systems are operated either simultaneously (FIND-Mode) or sequentially (SCAN-Mode).

Operational mode: Turn-off LD and BD $>30°C$
Turn-off LD and BD et eclipse.

Science and Housekeeping Data Volume

The standard operational mode for HEP-LD is the Normal Mode (NM). The Burst Mode (BM) is an internal high speed mode which does not change the data output (details of the BM are still under consideration).

a) Scientific Data Sources

Ion Data

I-SPECT = 8 energy channels for each of three ion masses (nominally, H, He and O), integrated over all view directions. This provides a set of omnidirectional energy spectra. The burst mode is identical.

I-FB = 2 integral energy channels for 1 mass (nominally H). These data are taken from the polar angles viewing parallel and antiparallel with respect to

the spin axis. This provides a measure of fast temporal variations. The burst mode provides additional mass information.

I-PITCH = 6 different energies for a single mass (nominally H) and three angles relative to the magnetic field direction (nominally 0°, 90°, and 180° pitch angle). This provides a measure of the shape of the pitch angle distribution every spin period. The burst mode obtains these rates twice as often.

I-3D = 8 energy channels per nucleon for 4 masses are obtained for each of 16 x 12 = 192 different view directions on the unit sphere. These are accumulated over 64 satellite spin periods (192 sec) in the slow form. This is the most detailed representation of the full distribution function for all ions. The burst mode provides the same full spherical coverage in 8 spin periods (24 sec.) In the fast form 2 integral energy channels for the 4 masses but in fewer different view directions (pixels are summed) are provided in 2 satellite spin periods (6 sec). This emphasizes the ion angular distribution temporal changes. The associated burst mode data provides additional energy coverage in one spin period. The combined telemetry that required to transmit the data necessary to form the fast and slow outputs without redundancy.

I-DE = the T, E, and sensor ID for ions, selected on a priority basis, are transmitted at the rate of 4 ions/second in regular mode and 32 ions/second in burst mode. These data are used to search for rare ions and also used to monitor IPP M and E/M processing.

I-SINGLES = the rates from the individual detectors before processing. These are used to monitor sensor performance, reform "dead time" correc tions and check for background contamination.

I-MATRIX DATA = represent the complete M, E/M parameter space in the IPP. These data used to verify that proper processing is performed and to check for contamination of the data spurious events.

Electron Data

E-SPECT = 12 energy channels each integrated over all view directions. It takes at least 2 spin periods to sample them. This gives a set of fast omnidirectional energy spectra. The burst mode integrates over a limited number of azimuthal sectors to provide information on the fast azimuthal spectral changes.

E-FB = 2 energy channels from each of 3 detectors. Additional energies are obtained in the burst mode along with more values per spin parallel to the spin axis.

E-PITCH = 3 energy channels at 30°, 90°, and 120° with respect to the spin axis. In the burst mode these pitch angles are sampled more often to examine the azimuthal pitch angle asymmetries.

E-3D = 4 energy channels are obtained at each of the 96 different view directions on the unit sphere (average values). In burst mode fewer energy channels are taken 6 times as fast. Intensive compression techniques are applied to obtain these T/M rates.

E-SINGLES = Average rates from the lowest threshold of the 3 detectors (i.e. the input rates to the energy ADC). These are used to monitor detector performance and perform "dead time" corrections on the data.

b) Engineering Housekeeping Data Sources

HK-Analog = Analog monitor voltages (0–5V) digitzed in the HEP-LD DPU.

HK-Digital = Digital status information.

Table 3.1-1 Science and Housekeeping (analog) bit rates.

Ch.-Nr	Data Type	Normal Mode			
		Sample Rate # of Spins/Set	Telemetry Rate 8 bit Words/Spin	bps	Remarks
	Science				
0	I-SPECT	1	24	64	
1	I-FB	1/16	32	85	
2	I-PITCH	1/4	96	256	
3	I-3D (slow)	32	192	512	
4	I-3D (fast)	2	132	352	
5	I-DE	1/16	75	200	
6	I-Singles	1	72	192	
7	I-Matrix	64	22	59	
8	E-SPECT	1	12	32	
9	E-FB	1/4	96	256	
10	E-PITCH	1/4	48	128	
11	E-3D (slow)	8	144	384	interchangeable not simultaneously
12	E-3D (fast)	(2)	(144)		
13	E-Singles	1	3	8	
	Subtotal		948	2528	

	Housekeeping (Analog)	Sample Rate # of Spins/Set	Telemetry Rate 8 bit Word/Spin	bps
0	Voltages: +12V			
1	+ 5V			
2	− 5V			
3	−12V			
4	Currents: +12V			
5	+ 5V	8	2	5.5
6	− 5V			
7	−12V			
8	Detector Bias			
9	CHPS A-Monitor			
10	CHPS B-Monitor			
11	Deflect Voltage-Monitor			
12	Temp 1 (Sensor)			
13	Temp 2 (Electr.)			
	Subtotal		2	5.5

Table 3.1-1 (continued)

Ch.-Nr	Data Type	Normal Mode			
		Sample Rate # of Spin/Set	Telemetry Rate 8 bit Words/Spin	bps	Remarks
	Housekeeping				
	Digital				
0	CHPS safe/arm				
1	Aperture A open/closed				
2	Aperture B open/closed				
3	Aperture C open/closed				
4	Aperture A wide/small				
5	Aperture B wide/small				
6	Aperture C wide/small				
7	CHPS A ON/OFF + STEP				
8	CHPS B ON/OFF + STEP	8	2	5.3	
9	Deflection Vol.				
10	Aperture wide/small				
11	Trigger Status				
12	Multiplexer Status				
13	Channel Selection $E_1/E_2/E_3$				
14	Channel Selection $T_1/T_2/T_3$				
15	Channel Selection $P_1/P_2/P_3/P_4$				
16	TAC-Slope				
	DPU Status	8	4	10.6	
	EDB-Identifier	1	2	5.3	Exp.-Datablock Identifier
	Int. Timing	1	2	5.3	
	Subtotal		10	26.5	
	Total Science, HK(A), HK(D)		960 (bit Word/Spin)	2560 (bps)	

3.1.5 Size, Weight, Power and Telemetry Requirements

The physical properties of the HEP-LD unit are:

Size: 200 x 200 x 305 mm (H x W x L) (compare Fig. 3.1-1)
Mass: 4150 gr ± 300 gr
Power: 4.8 W (regulated at HEP-LD input)

The telemetry and telecommand requirements are:

Real Time Telemetry: 2560 bps (32 kbps in the RAM check mode)
Record Telemetry: 512 bps
Telecommand: Discrete and block commands (specifications are given in the HEP instrument interface document)

3.1.6 Special Requirements for HEP-LD

Instrument Configuration and View Directions

The HEP-LD unit is mounted on the spacecraft platform such that plane containing the 180° angular opening is perpendicular to the spin plane and contains both the spin vector and the radius vector to the instrument position. The ±6° x 180° field of view should be unobstructed, (compare Fig. 3.1-1b).

Because of the delicate nature of the particle detectors (MCP, SSD) and their susceptibility to contaminants and because of the use of thin foils the following special protective design features and operational precautions are required:

The IIMS sensors are closed by dust/acoustic doors. In orbit release is performed by sublimation actuators. Chemical: Biphenyl ($C_{12}H_{10}$), ρ = 0.87 g/cm^3, m.p. at 71°C; about 0.5 g per actuator.

Dry nitrogen purge for ground operations. Interface will be provided on the front side of HEP-LD.

Thermal control on the ground and in-orbit: Operational and storage temperature range: −40°C to +35°C, preferred operational range −20°C to +20°C.

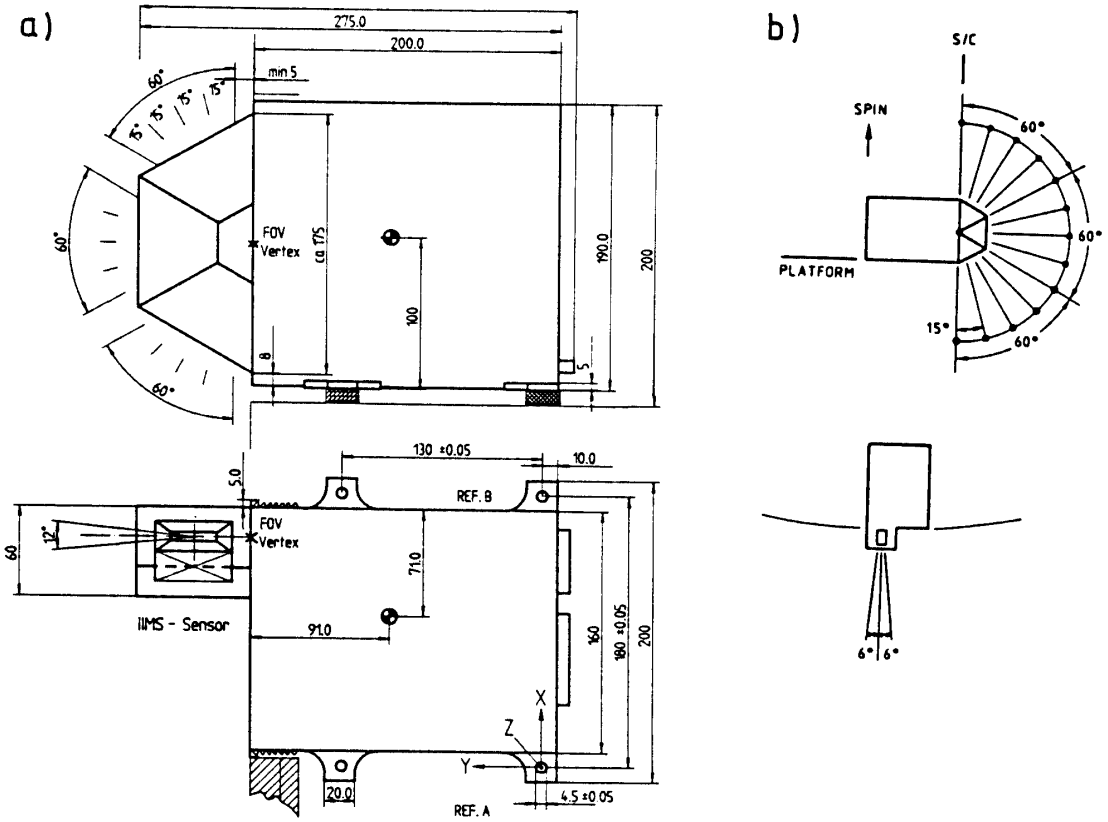

Fig. 3.1-1 (a) The HEP-LD spectrometer with physical dimensions and field of view.
(b) Orientation and viewing direction on the spacecraft.

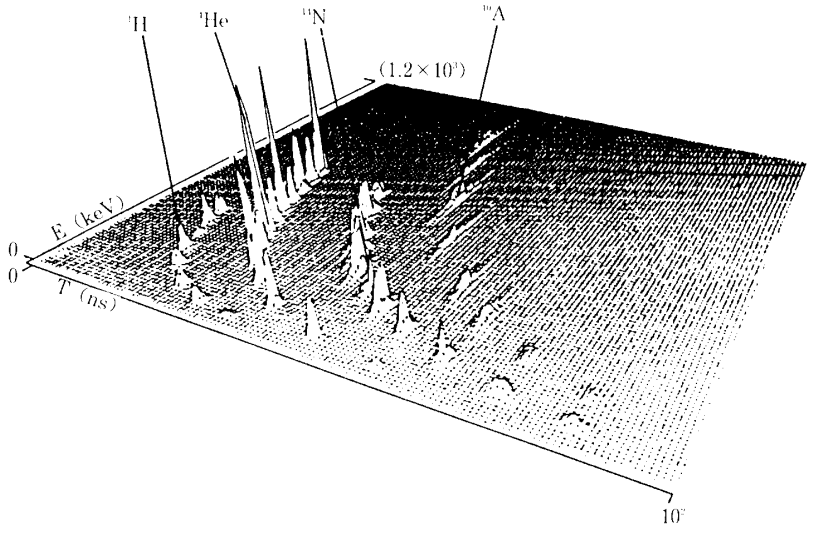

Fig. 3.1-2 Illustration of the two-parameter ion mass analysis used in IIMS. Particles with equal mass follow hyperbolic curves in the E-T plane as shown for hydrogen, helium, nitrogen and argon.

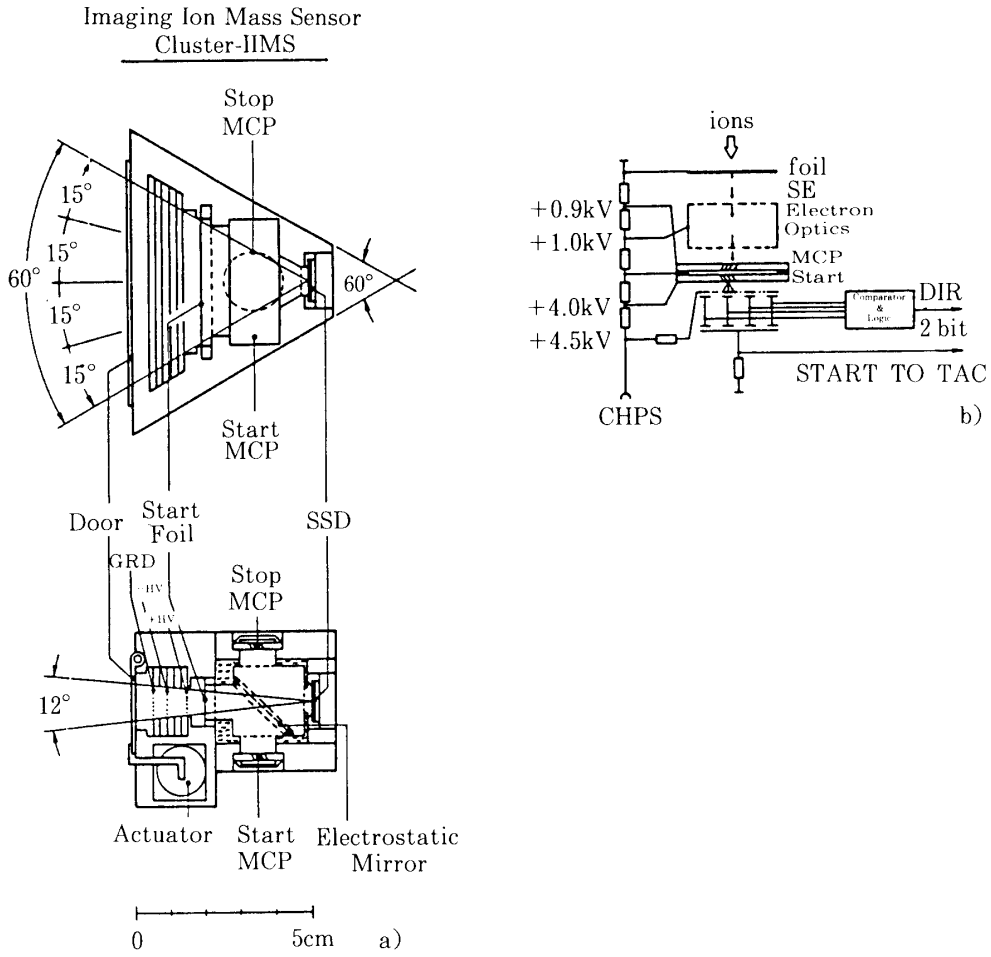

Fig. 3.1-3 (a) Cross sectional view of the IIMS detector unit.
(b) Potential distribution in the time zero detector and the signal read-out system.

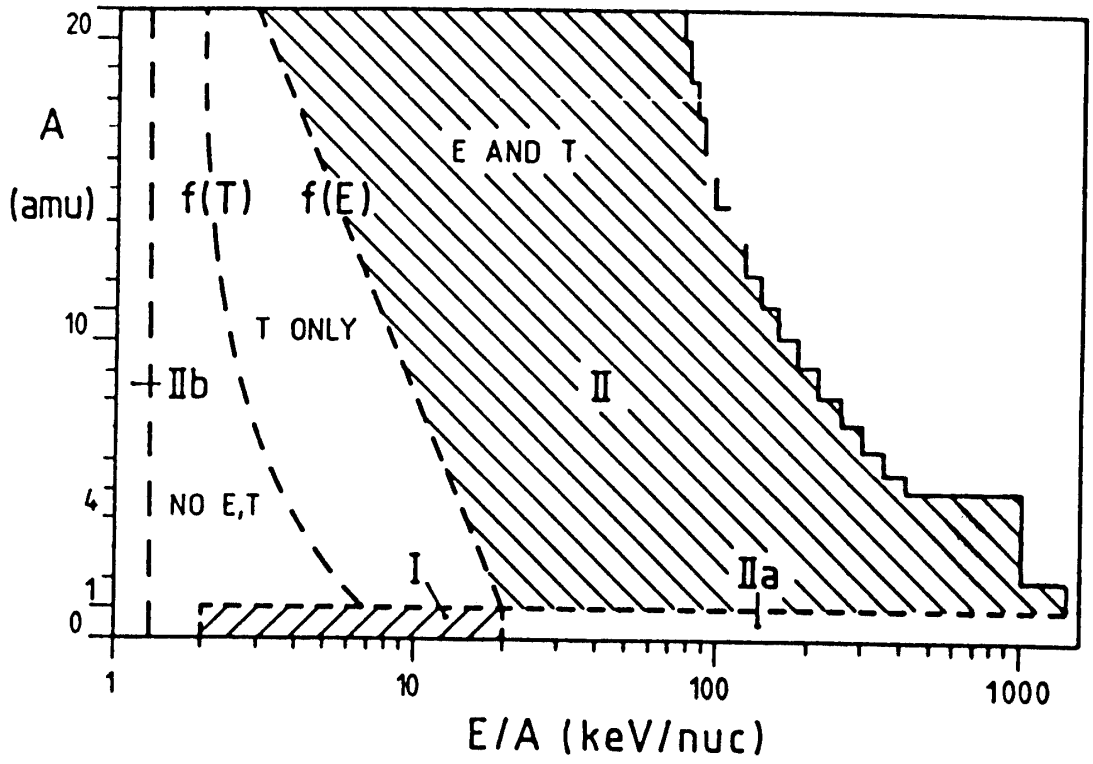

Fig. 3.1.4 Mass (A) versus energy per mass (E/A) matrix illustrating the mass classification in the IPP. The upper boundary (L) reflects the constant total energy limits for all species except for $2 \leqslant A \leqslant 4$ particles. The curves f(T) and f(E) indicate the limits for single and dual parameter analysis, respectively. The corresponding principle regions (I and II) and emergency regions (IIa, IIb) are marked.

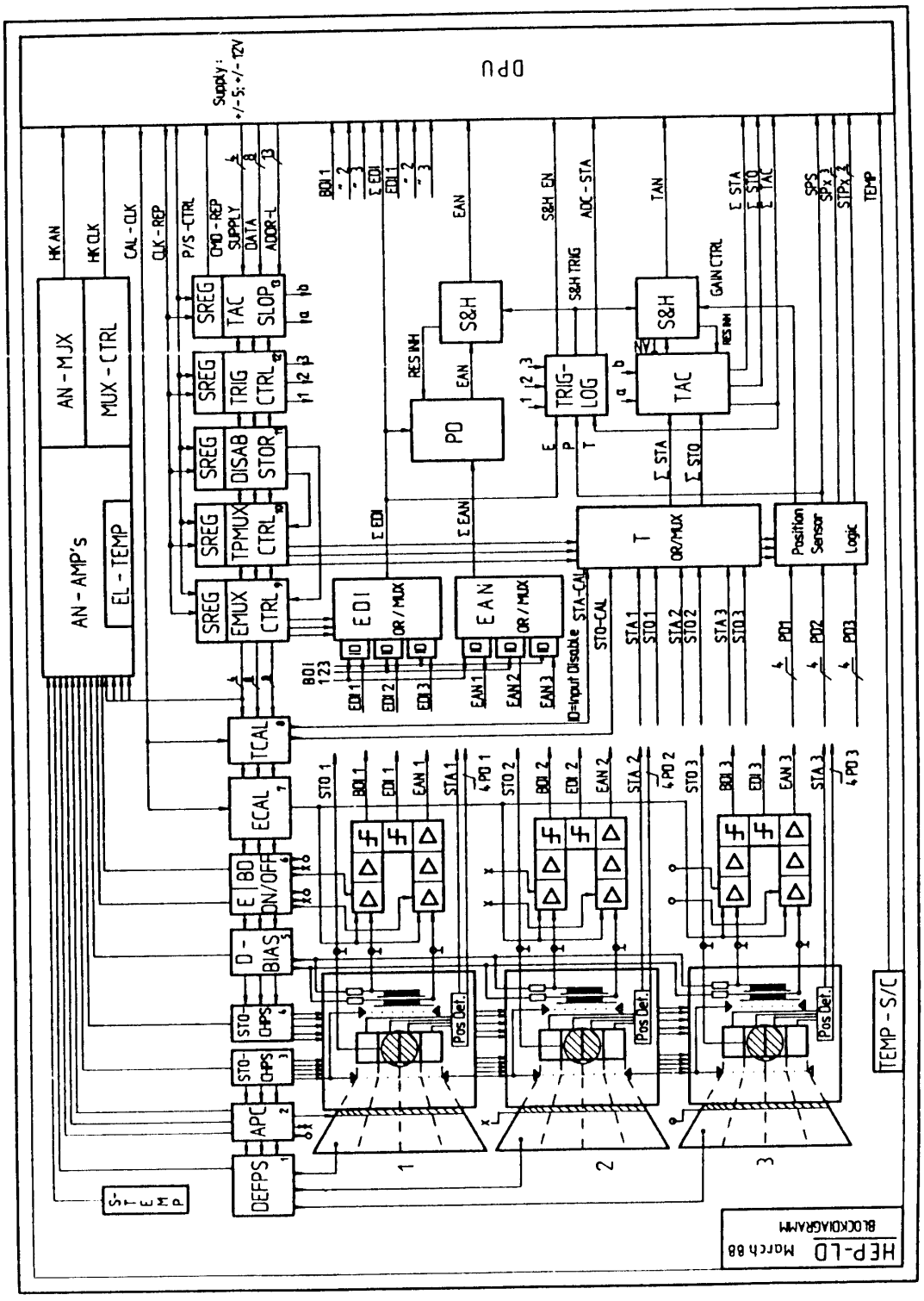

Fig. 3.1.5 Block diagram of the signal conditioning unit showing the functional principle and signal processing.

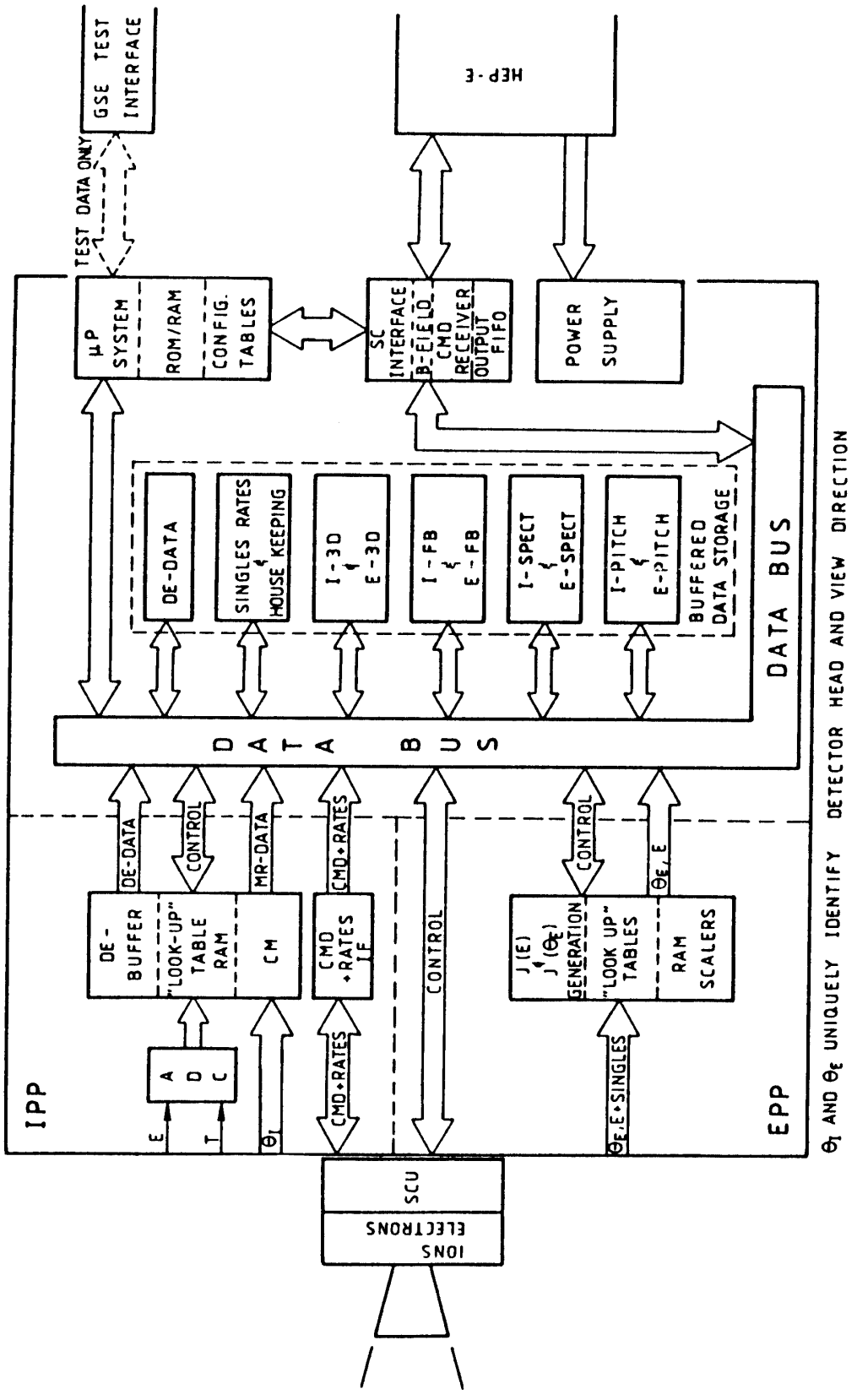

DPU BLOCK DIAGRAM

Fig. 3.1-6 Block diagram of the digital processing unit delineating the principle flow of information. IPP and EPP are the ion and electron preprocessor sections. Description of the data structure is given in section 3.1.4.

3.2 Burst Detectors (BD)

3.2.1 Introduction

To perform the objectives described in section 2, the HEP-BD instruments are designed to observe the high energy electrons, protons and heliums. The objectives are to observe the energy spectra and three dimensional distributions of the high energy particles mainly in the geotail region. The HEP-BD instrument has a large geometrical factor $S\Omega$ to obtain high time/energy/angular resolutions for low intensity particles. A few observations of the magnetospheric geotail regions were made by IMP-8 and ISEE-3. The orbit of the IMP-8 was 23 x $46R_E$, and that of ISEE-3 was $220R_E$. The ISEE-3 measurement was not systematic observations in the geotail region. The characteristics of the spectrometers EPE and CPME of IMP-8, and ULECA and ULEWAT of ISEE-3 are shown in Table 3.2-1. The energy coverages of LD and BD are 20 keV–2.5 MeV for electron, 2 keV–35 MeV for proton and 3.5–140 MeV for helium ions. The geometrical factor of each unit sensor in LD and BD are 2.0 x 10^{-2} cm^2 sr and 0.76 cm^2 sr, respectively. These wide coverage of energy and geometrical factors make possible to observe the large intensity variations in the geotail region.

The BD sensor consists of three silicon ΔE x E detector telescopes and measures in the energy range 0.12–2.5 MeV for electrons, 0.4–3.5 MeV for the mixture of protons and helium ions, 3.5–35 MeV for protons, and 3.5–140 MeV for helium ions. The instruments have rectangular opening angles 30° x 45° and their look directions are 30°, 90° and 150° to spin axis, respectively.

Table 3.2-1 Comparison of spectrometers for observations of magnetospheric geotail region.

Spacecraft	Launch	Orbit	Spectrometers	Specifications
IMP 8[(a)]	1973	23x46R_E	EPE	Sweep Magnet & Semiconductor Detectors Electron 0.03 – 0.20 MeV Proton 0.05 – 0.80 MeV $Z \geq 2$ > 0.6 MeV G.F. = 0.97–1.5 cm^2 sr 16 sectors
			CPME	E x dE/dx method Electron 0.22 – 2.5 MeV Proton 0.29 – 1.80 MeV/n Alpha 0.59 – 1.80 MeV/n $Z \geq 3$ 0.77 – 3.2 MeV/n G.F. = 1.5 cm^2 sr 8 sectors
ISEE-3[(b)]	1978	220R_E	ULECA	Electrostatic Deflection & Semiconductor Detectors Proton, Alpha & Heavy ions 33, 66, 134 keV/Q View angle 9° x ±30° 8 sectors
			ULEWAT	Proportional Counter & Semiconductor Detectors Electron 0.075 – 1.3 MeV Proton 0.2 – 0.3 MeV Opening angle 52° 8 sectors
GEOTAIL	1992	8-250R_E	LD	TOF & Semiconductor Detectors Electron 20 – 300 keV Proton 2 keV – 1.5 MeV Alpha 4 keV/n – 1.5 MeV G.F. = 2 x 10^{-2} cm^2 sr (each) x 12 16 sectors
			BD	Semiconductor Detectors E x dE/dx method Electron 0.12 – 2.5 MeV Proton 0.4 – 35 MeV Alpha 3.5 – 140 MeV G.F. = 0.79 cm^2 sr (each) x 3 16 sectors

Ref. a) Sarris et al., J.G. R., **81**, 2341 (1976).
Kirsch et al., J. G. R., **89**, 1002 (1984).
b) Hovestadt et al., IEEE Trans. Geosci. Ele., GE-**16**, No. 3, 166 (1978).

3.2.2 Principle of Sensors

Identification of electron, proton and helium ions by the BD instrument is based on the silicon ΔE x E detector telescope system. The amount of energy deposited in the passing detector is denoted by ΔE and the amount of energy deposited in the stopping detector is denoted by E. The total energy is then $E_o = \Delta E + E$.

The energy loss ΔE of a charged particles with the energy E_o, mass M and charge Z in the thin passing detector is;

$$\Delta E \sim MZ^2 / E_o.$$

This relationship is used to identify electron, proton and helium particles. The telescope consists of a thin ΔE passing detector, and three stopping E detectors and an anticoincidence detector.

3.2.3 The Sensors

The BD sensors consists of three ΔE x E telescopes (BD-A, -B, and -C). The basic principle of ions identifications is to measure the energy loss rate ΔE for particles and residual energy E.

The cross-sectional view of the telescope is shown in Fig. 3.2.3-1. An 80 μm silicon ion implanted junction detector with the sensitive area 20 x 30 mm^2 is used as a ΔE detector (BD-1), the stopping E detector are a 0.4 mm thick silicon ion implanted junction detector (BD-2) with the sensitive area of 22 x 32 mm^2 and two 3 mm thick Si(Li) detectors (BD-3, -4) with the sensitive area of 27 x 43 mm^2, and 0.4 mm silicon surface barrier detector (BD-5) with the sensitive area 27 x 43 mm^2 which is used as an anticoincidence detector. The characteristics of the detectors are shown in Table 3.2.3-1, and the BD-1 and BD-3 detectors are shown in Fig. 3.2.3-2. Structure of one of the BD telescopes is shown in Fig. 3.2.3-3. There are insulators (marked T's in the figure) between detectors.

The result of the theoretical calculation on the energy losses of electrons, protons and helium ions in the ΔE detector is shown in Fig. 3.2.3-4. The lines 0.48 mm and 6.48 mm in the figure show the energy region corresponding to the detector thicknesses. The energy ranges in normal incident particles are;

electron	0.12 – 2.5 MeV,
proton	0.40 – 35. MeV
helium ion	3.50 – 35. MeV/n.

The BD system consists of three ΔE-E unit telescopes. The aperture of telescope defines an opening angle 30° x 45° and the geometrical factor is

0.76 cm^2 sr each. The three telescopes are mounted to look 30°, 90° and 150° to spin axis. The characteristics of the BD telescopes are shown in Table 3.2.3-2.

3.2.4 The Electronics

The f nctional diagram of HEP-BD system is shown in Fig. 3.2.4-1. One of the three BD telescopes (BD-A) is shown in the figure. The unit of the telescopes and the preamplifiers is separated from the electronics and data processing unit (HEP-E).

The output signals from the two Si(Li) E-detectors are connected to one preamplifier to save the electronics power and weight of sensors. The output signals from the low-level discriminator amplifiers (LLD-Amp) and the summation amplifiers (Sum-Amp) are fed to shaping amplifiers and slant discriminator to identify the electrons, protons and helium ions. The energy spectrum are obtained by 16 channels pulse height analyzers. The particle data are synchronized to the spin phase signals.

3.2.5 Size, Weight, and Power

The figure of the BD sensor box is shown Fig. 3.2.5-1. The weight and power of HEP-BD sensors are shown in Table 3.2.3-2.

3.2.6 Special Requirements

The following precautions are required because the characteristics of silicon detectors are highly sensitive to humidity, temperature and surface contamination.

Dry nitrogen purge (on-ground)		
Temperature	operating	<20°C,
	non-operating	<35°C.
Switch on temperature in-orbit		<20°C.
Humidity		<60%.
No water on silicon surface.		

Table 3.2.3-1 Each HEP-PD telescope consists of five silicon detectors. The characteristics of the five detectors are shown.

GEOTAIL HEP-BD Si DETECTORS

Crystal (mm x mm)	Size (mm x mm)	Sensitive Area*	Sensitive Depth (mm)	Type**	Bias (volt)
BD-1	22 x 32	20 x 30	0.08	II	50
BD-2	24 x 34	22 x 32	0.4	II	180
BD-3	30 x 46	27 x 43	3.0	Li	330
BD-4	30 x 46	27 x 43	3.0	Li	330
BD-5	30 x 46	27 x 43	0.4	II	180

* A1 side area.
**II: Ion-Implantation Type, Li: Lithium Drifted Type.

Table 3.2.3-2 Characteristics of GEOTAIL HEP-BD spectrometer. BD spectrometer consists of three telescopes. Each telescope has rectangular opening.

GEOTAIL HEP-BD

Particle	Electron	0.12 – 2.5 MeV
	Proton + Helium	0.4 – 3.5 MeV/n
	Proton	3.5 – 35. MeV
	Helium	3.5 – 35. MeV/n
Telescope	3 units	
Look Direction	30°, 90°, 150° to spin axis	
Opening Angle	30° x 45°	
Geometrical Factor	0.76 cm^2 sr each telescope.	
Telemetry Bit Rates	3100 bps*, 160 bps**	
Electric Power	2808 W meas.-mode, 936 W save-mode	
Weight	3000 ± 200 g	

* Real mode.
**Recording mode.

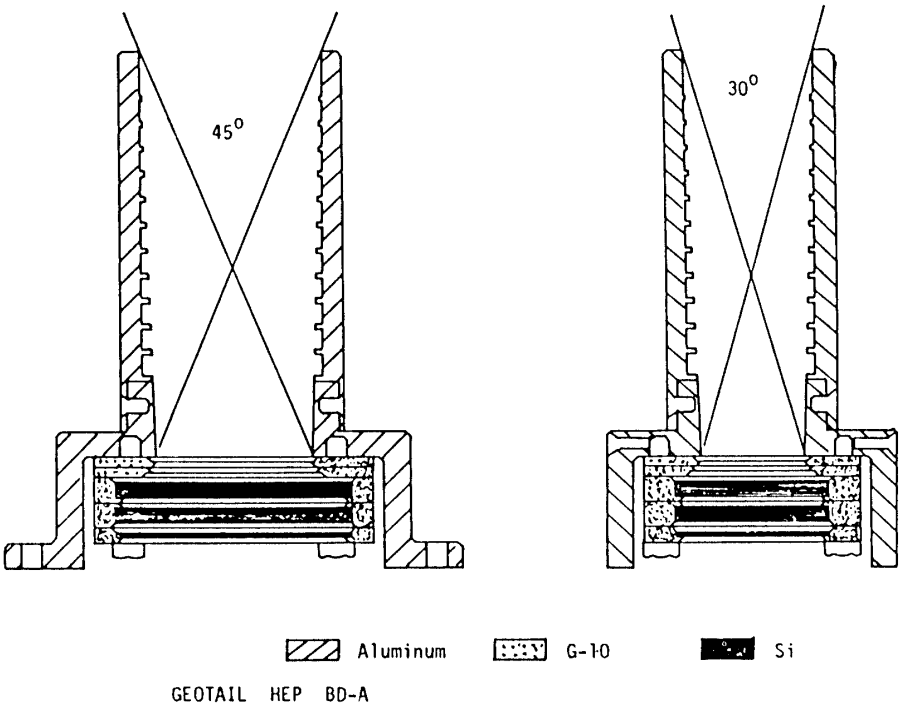

Fig. 3.2.3-1 Cross-sectional view of one of three BD telescopes. Each telescope consists of five silicon detectors; a ΔE detector, three E detectors, and an anticoincidence detector.

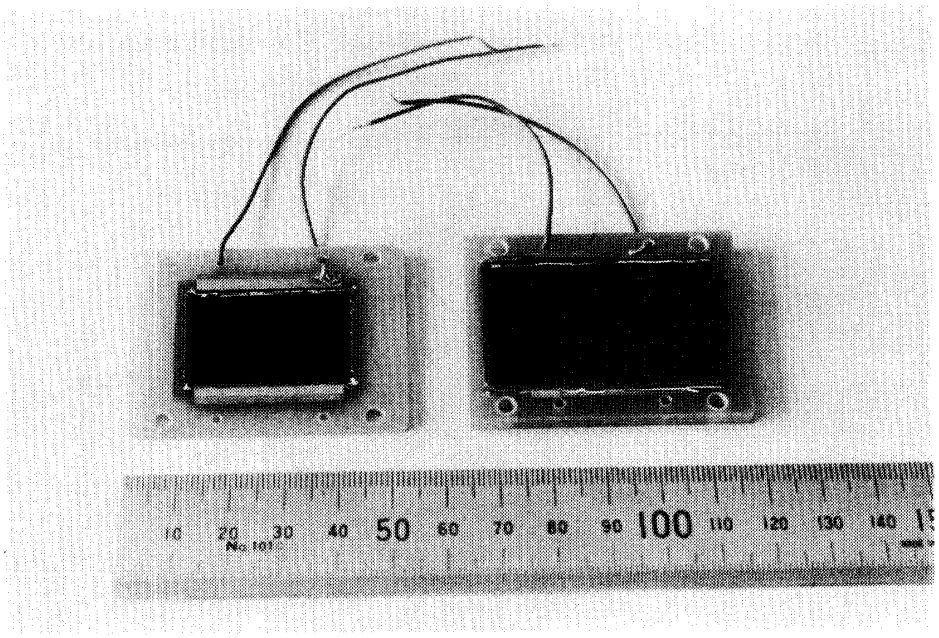

Fig. 3.2.3-2 (Right) 80 μm ΔE silicon surface barrier detector (BD-1) and (Left) 3.0 mm Si(Li) detector (BD-3). Sensitive area of BD-1 is 20 x 30 mm^2, and that of BD-3 is 27 x 43 mm^2.

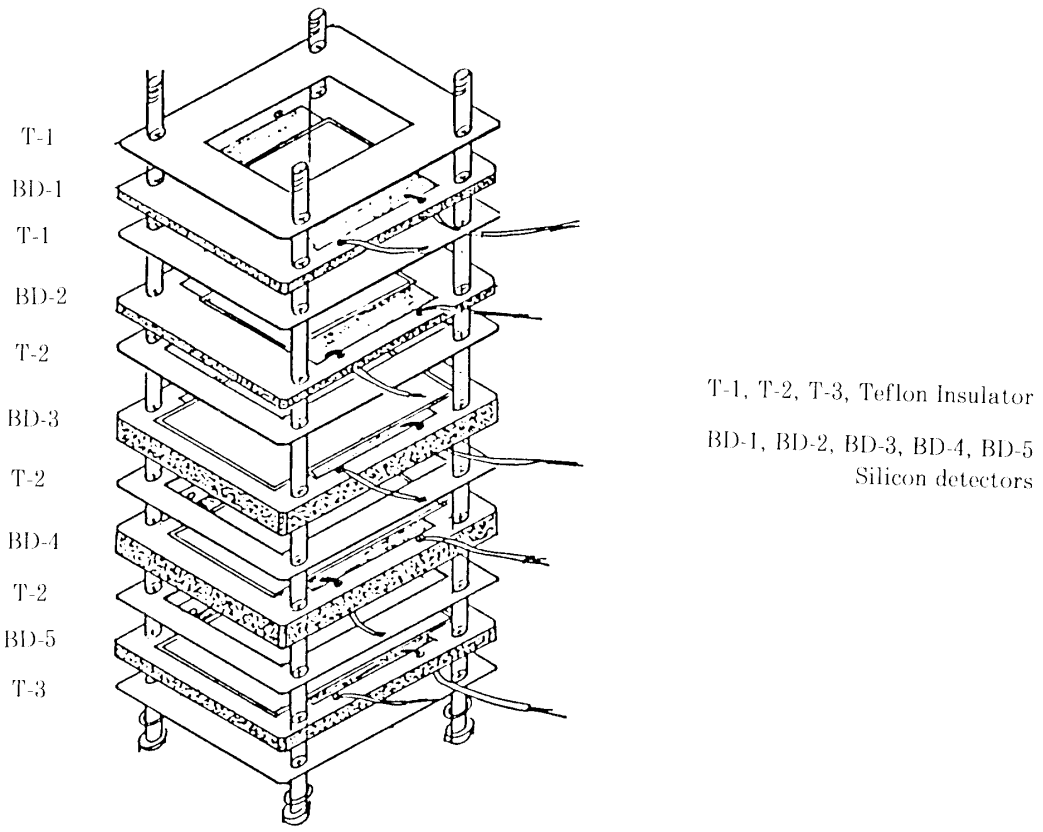

Fig. 3.2.3-3 Structure of one of the BD telescopes. Marked T's are teflon insulators.

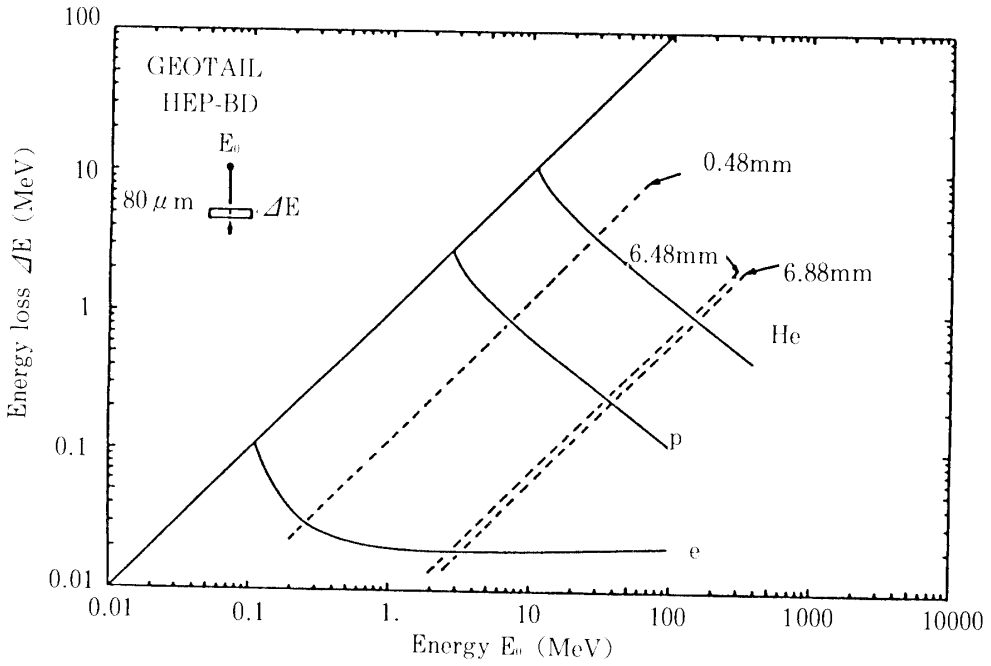

Fig. 3.2.3-4 Energy losses ΔE versus particle incident energy E_0 in 80 μm ΔE detector. The line 0.48 mm shows the total thickness of BD-1 and BD-2 detectors. The line 6.48 mm shows the total thickness of BD-1, BD-2 BD-3, and BD-4.

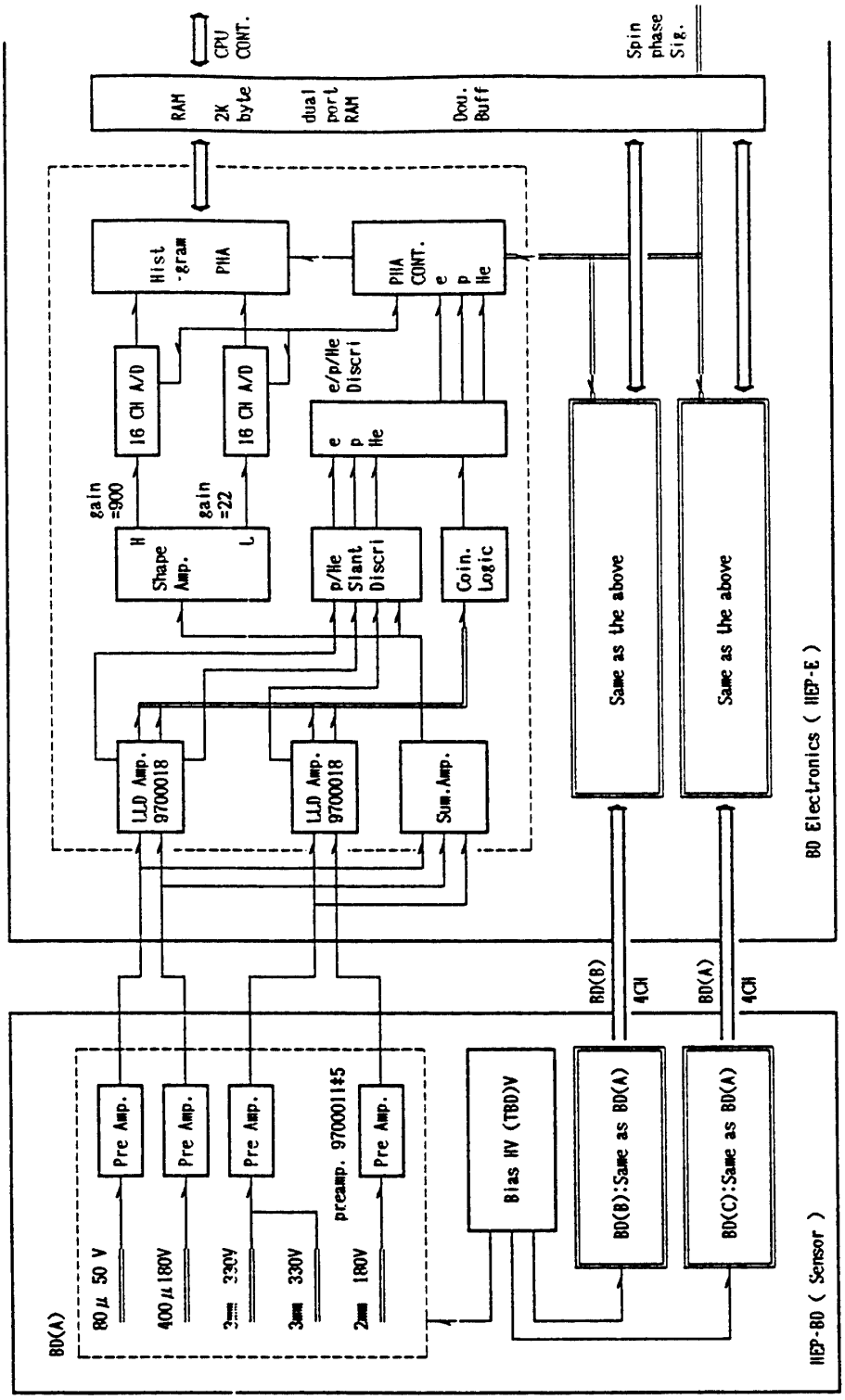

Fig. 3.2.4-1 Functional diagram of HEP-BD system. One of three telescopes is shown in the figure. The left part is telescopes and preamplifier box, and the right box is electronics system and data processing unit HEP-E.

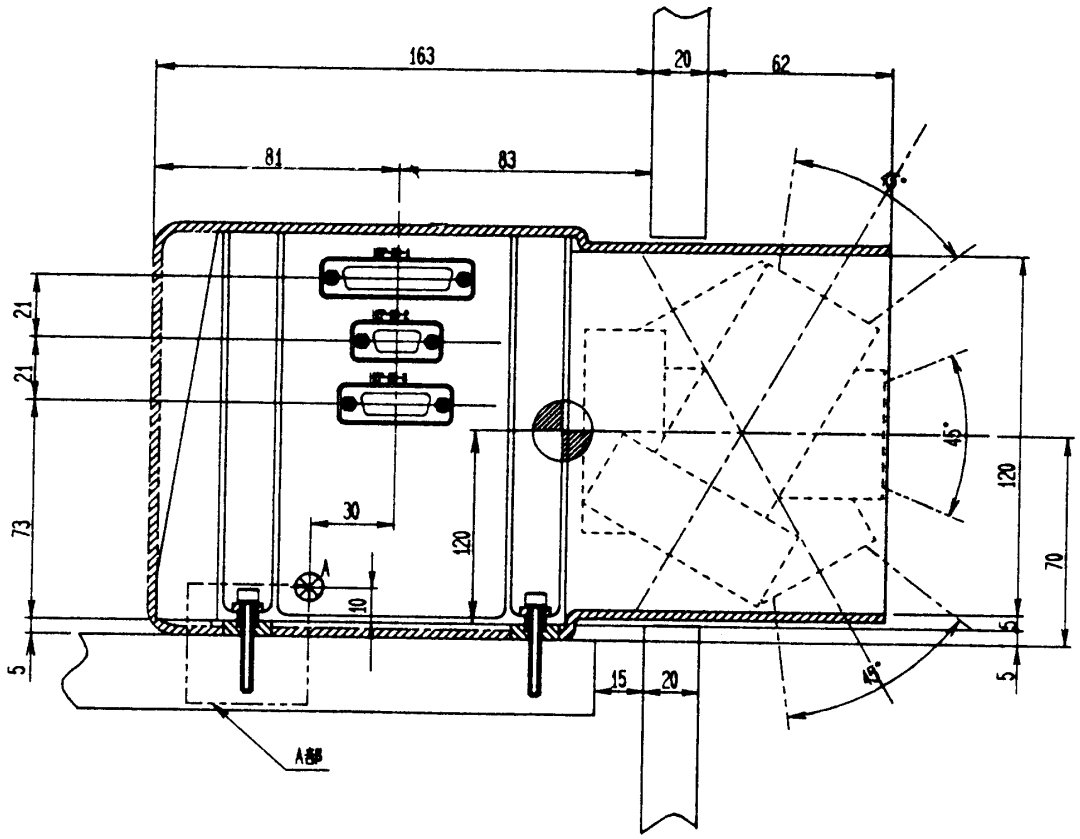

Fig. 3.2.5-1 Mounting structure of BD telescope and preamplifier box. The telescopes look 30°, 90°, and 150°.

3.3 Medium and High Energy Isotope Telescopes (MI and HI)

3.3.1 Introduction

Silicon detector telescope, consisting of ΔE-detector and E-detector, provides ΔE-signals produced by energy loss of an incident particle in the ΔE-detector, and E-signals produced by residual energy deposited in the E-detector. As the ΔE-E plots made by various species give different curves, the ΔE-E method is used for the isotope identification.

In Japan, the particle identification in space has so long history that we must go back to the late '60s (e.g. reviewed by Doke et al., 1986). A few authors in HEP team measured abundance of hydrogen isotopes (p, d, t) in the radiation belt those days, using a silicon-detector telescope on board the L-3H rocket (Doke et al., 1968; Nakagawa et al., 1967). This successful

observation made us the new start of isotope identification of heavy ions in galactic cosmic rays. The mass identification of heavy ions with the energies less than a few MeV/n was a very important thing to achieve scientific objectives in the field of nuclear physics, but it was found in the early '70s that it was technically easy to identify isotopes with the energies around 100 MeV/n if we could use thick silicon detector. From the results of hydrogen isotope observation, moreover, they showed that even iron isotopes might be identified from the calculation of energy loss straggling of the heavy ions in the Si telescope if thick detectors with uniform thickness could be used in the telescope (Doke and Nagata, 1971).

Since the spread of energy losses in ΔE-detector caused by inclined incidences of ions has to be kept as small as possible for the mass identification of heavy ions, the geometric factor of the ΔE-E silicon detector telescope is greatly restricted (Doke and Nagata, 1971; Nagata and Doke, 1973). And the intensities of heavy ions in galactic cosmic rays are extremely weak in comparison with those of proton and helium. A large geometric factor is required in the isotope telescope for the measurement of heavy isotopes. Then, authors proposed the use of position-sensitive Si detector (PSSD) as the ΔE-detector which enabled the correction of the energy losses of the penetrating particles with the inclined incident angles in the ΔE-detector.

They developed charge-division type of circular PSSD with a very large area, three inches in diameter, which was the largest PSSD in the world those days. They proposed an isotope telescope combined with the PSSDs, which had a very large geometric factor of 46 cm^2 sr which was 100 times larger than that of telescopes boarded on the spacecraft (S/C) launched earlier (Nagata and Doke, 1973; Nakamoto et al., 1975). Unfortunately such an excellent isotope telescope could not be used on S/C in Japan, instead an excellent isotope telescope combined with PSSDs, called HIST, was realized by CALTEC-group for the ISEE-3 S/C in 1978. The HIST, which had a geometric factor of 0.43 – 0.8 cm^2 sr, did not have a sufficiently large geometric factor (Althouse et al., 1978). The digital type of the PSSD anode for the HIST was adopted as the method to determine the position of the incident ions. The geometric factor is much smaller than that described above. This is because the spacing between strip-lines as the pick-up electrodes was 1 mm and the two PSSDs used in the HIST had to be arrayed with a wide gap between them to separate isotopes as heavy as iron.

The position resolution for the charge-division type of PSSD is improved with the increase of nuclear charge of ions, while that for the digital type it is determined by the spacing between strip-lines. And the anode structure and the read-out circuit for the charge division type is quite simpler than that for the other. Therefore, in space experiment to identify various

isotopes of heavy ions, the charge division type of PSSD is superior to the digital type.

From the point of view, we adopted the charge division type as the PSSD to be used in the isotope telescope for future mission and have made a great effort to develop more excellent PSSD. Recently we have developed excellent position-sensitive detectors with a very large area and a good position response (Doke et al., 1986; Doke et al., 1987; Kohno et al., 1987; Hasebe et al., 1988; Yanagimachi et al., 1989). Combining these PSSDs with the ΔE-E Si-detector telescope, we have designed isotope telescopes with large geometric factors, which will measure helium through nickel isotopes with a wide energy range from a few MeV/n through a few hundred MeV/n.

Isotope telescopes designed for High Energy Particle (HEP) experiment in the GEOTAIL S/C are called Medium Energy Isotope Telescope (MI) and High Energy Isotope Telescope (HI). HEP-MI instrument measures elemental and isotopic compositions of solar energetic particles and other energetic particles in the heliosphere with $2 \leq Z \leq 28$ in the comparatively low and medium energy region (2.4 MeV/n to 80 MeV/n) and, furthermore, measures the elemental composition of SEP heavier than iron-group. HEP-HI also measures the elemental and isotopic compositions of SEP and galactic cosmic rays with $2 \leq Z \leq 28$ in the high energy region (10 MeV/n to 210 MeV/n).

3.3.2 Principle of Sensors

HEP-MI and -HI instruments are all silicon semiconductor detector telescopes utilizing the well-known dE/dx x E algorithm for isotope identification. For particles passing through the ΔE-detector with a given thickness and stopping at the E-detector, the mass and nuclear charge can be identified by simultaneous measurements of the energy loss, ΔE, and the total energy of E (= ΔE + E'). Both isotope telescopes consist of several layers of Si detectors, of which top two layers are position-sensitive detectors newly developed by GEOTAIL HEP team (Doke et al., 1987; Hasebe et al., 1988; Yanagimachi et al., 1989). Each PSSD provides a two-dimensional position information using charge-division method. The PSSDs determine the trajectory of each particle so that an accurate measurement of path length Δx can be obtained in each layer. Each has a square ion-implanted resistive surface and charge is collected at each corner of the square surface. Distortion in the resultant position linearity has been greatly reduced by a new approach in which the four corners have been connected by an additional ion-implanted strip-line with a low resistivity. The PSSDs also measure the energy loss in those layers. The application of the PSSDs to the ΔE-E detector telescopes greatly improves the geometric factors of the telescopes so

that even rare elements and isotopes in SEPs and GCRs can be observed by the in-flight telescopes.

The other several layers are Si-detectors for measuring energy losses or residual energy of stopping ions, which have graded thicknesses from thin to thick one to optimize the detector system due to the energy loss straggling of ions. The bottom layer is an anti-coincident Si-detector which rejects energetic ions penetrating out of the detector stack. The mass resolution of heavy ions expected for both HEP-MI and -HI spectrometers is designed to be 0.22 amu for the isotopes of nickel, and even better for ligher elements.

3.3.3 The Sensors

[1] HEP-MI Spectrometer

HEP-MI sensor has a wide aperture to observe elemental and isotopic compositions of SEP and other energetic particles in the heliosphere with low and medium energies. HEP-MI consists of single MI-1 and two identical MI-2 units. MI-1 sensor with a relatively small geometric factor (4 cm^2 sr), is dedicated to measure low energy light ions from He to Ne isotopes. Two MI-2s have extremely large geometric factors (2 x 30 cm^2 sr) which can measure not only elements and their isotopes from C to Ni but also elements heavier than iron groups ($Z \leq 45$).

MI-1: The HEP-MI-1 is a very high sensitivity telescope which identifies heavy nuclides in various energy ranges, starting at 2.4 MeV/n for heliums. It measures chemical composition for $2 \leq Z \leq 20$, and the isotopic composition for each element from He through Ne. A cross sectional view is shown in Fig. 3.3.3-1.

To achieve the very high mass resolution required for isotope identification of the incident charged particles, it is necessary to determine the trajectory of the particles through the telescope with high precision. The trajectory information is provided by Si-detectors (PSD1, PSD2), which are position-sensitive silicon detectors of a charge division type developed by GEOTAIL HEP team.

The top layer (PSD1) consists of four PSDs of 50 μm x 15 mm (one wafer is actually divided into four sensitive regions). The second layer is a single PSSD (PSD2) 100 μm x 34 mm x 34 mm. Detectors, D1–D2, for measuring energy losses or residual energy, are 400 μm x 56 mm x 56 mm and 2000 μm x 56 mm x 56 mm, respectively. The last layer D3 is an anti-coincident detector of 1 mm x 56 mm x 56 mm. Detectors D2–D3 are Li-drifted types and others are ion implanted junction types (II).

The information on the incident positions of the particle, its energy losses and residual energy is provided by 14 bit pulse height analysis of signals

from the detectors. The signals from each detector are amplified by a dual-gain shaping amplifier system which selects either low or high gain, depending on the signal size.

The dimension of each detector used for HEP-MI-1 is summarized in Table 3.3.3-1. The characteristics of HEP-MI-1 are shown in Table 3.3.3-2.

Table 3.3.3-1 GEOTAIL HEP-MI-1 consists of 5 Si-detectors. The characteristics of the detectors are shown.

GEOTAIL HEP MI-1 Si Detectors

	t (μm)	L (mm)	W (mm)	No.	Type*	Bias (V)
PSD1	50	15	15	4	II	12
PSD2	100	34	34	1	II	40
D1	400	56	56	1	II	180
D2	2000	56	56	1	Li	220
D3	1000	56	56	1	Li	120

*II: Ion-Implantation Type, Li: Lithium Drifted Type.

Table 3.3.3-2 Characteristics of GEOTAIL HEP-MI-1 spectrometer

GEOTAIL HEP MI-1

	Ions	Energy (MeV/n) Nuclear charge	Nuclear mass
Particle	He	2.4 – 20	2.4 – 15
	C	4.5 – 38	4.5 – 38
	Ne	5.5 – 50	5.5 – 50
	Mg	6.0 – 55	
	Si	6.2 – 60	
	Fe	7.5 – 80	
Telescope		1 unit	
Look Direction		90°	
Opening Angle		90° x 90°	
Geometrical Factor		4 cm^2 sr	
Mass Resolution (rms)		<0.23 amu for M $\leq$ 22	
Telemetry Bit Rate*		TBD	
Electric Power**		4.980 W	
Weight**		3200 ± 640 g	

* 40 words per isotope.
**including MI-2.

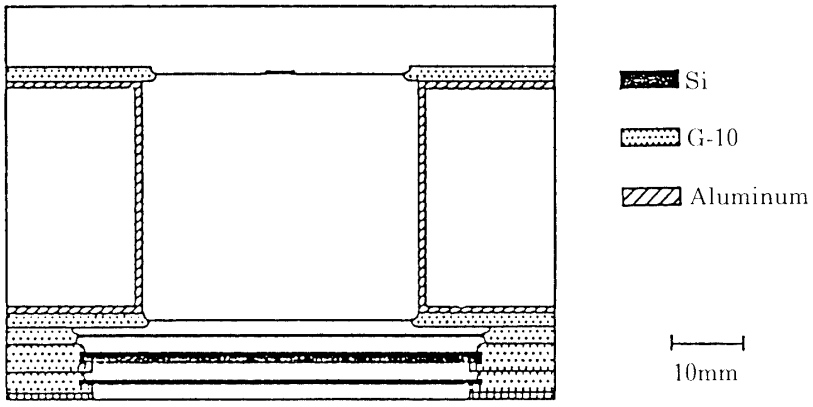

Fig. 3.3.3-1 Cross sectional view of GEOTAIL HEP-MI-1 telescope. It consists of five square-shaped Si-detectors. Two PSSDs, ΔE and E-detectors.

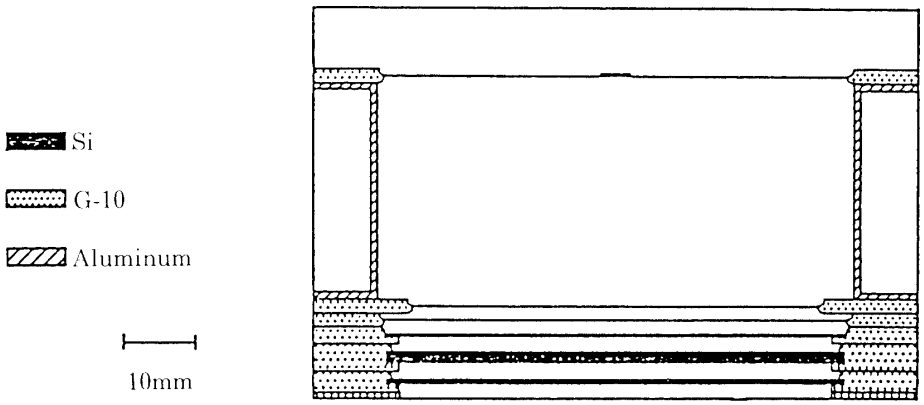

Fig. 3.3.3-2 Cross sectional view of one of two identical MI-2. It consists of six square-shaped Si-detectors. Two PSSDs, ΔE and E-detectors.

MI-2: A schematic drawing of MI-2 is shown in Fig. 3.3.3-2. The top layer (PSD1) consists of four PSSDs of 100 μm x 28 mm x 28 mm (one wafer is actually divided into four sensitive regions). The second layer a single PSD (PSD2) 200 μm x 56 mm x 56 mm. D1–D3, for measuring energy losses or residual energy, are 200 μm x 56 mm x 56 mm, 400 μm x 62 mm x 62 mm and 2000 μm x 62 mm x 62 mm, respectively. The last layer D4 is an anti-coincident detector 1 mm x 62 mm x 62 mm. Detector D3–D4 are Li-drifted types and others are ion implanted junction types.

The dimension of each detector used for HEP-MI-2 is summarized in Table 3.3.3-3. The energy, elemental region and other characteristics for HEP-MI-2 are shown in Table 3.3.3-4. Figure 3.3.3-3 shows mechanical drawing of HEP-MI box which includes one MI-1 and two identical MI-2s

and their preamplifiers and bias voltage supplies. MI-2 can observe isotopic abundances of SEP and GCR from C to Fe/Ni. Two MI-2s have large geometric factor of 60 cm^2 sr that we can expect to make first observation of elemental SEP compositions above Fe/Ni in the coming solar maximum.

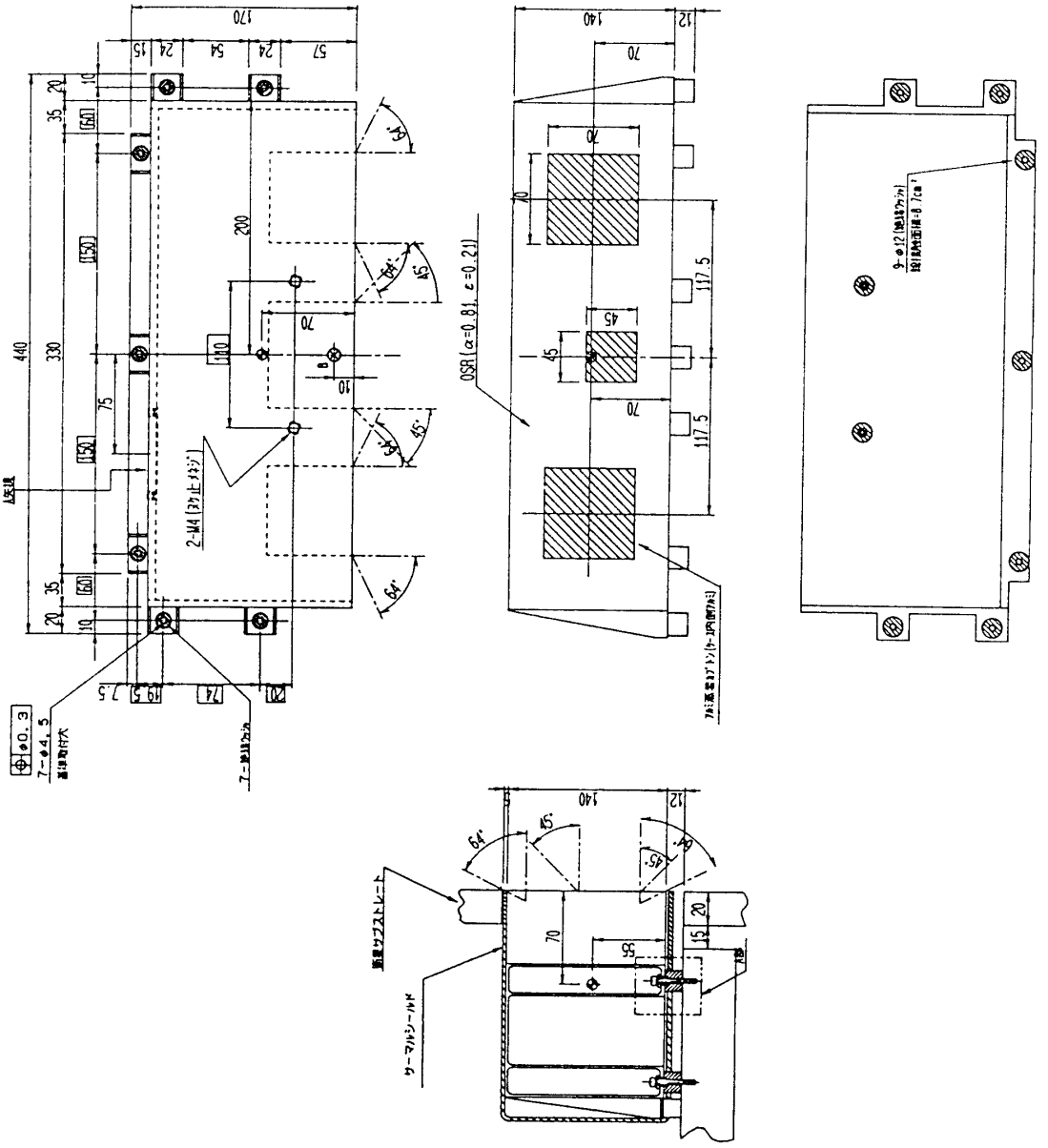

Fig. 3.3.3-3 Mounting structure OF HEP-MI spectrometer (MI-1 and -2).

Table 3.3.3-3 GEOTAIL HEP-MI-2 consists of 6 Si-detectors. The characteristics of the detectors are shown.

GEOTAIL HEP MI-2 Si Detectors

	t (μm)	L (mm)	W (mm)	No.	Type*	Bias (V)
PSD1	100	28	28	4 x 2	II	40
PSD2	200	56	56	2	II	150
D1	200	56	56	2	II	150
D2	400	62	62	2	II	180
D3	2000	62	62	2	Li	220
D4	1000	62	62	2	Li	120

*II: Ion-Implantation Type. Li: Lithium Drifted Type.

Table 3.3.3-4 Characteristics of GEOTAIL HEP-MI-2 spectrometer.

GEOTAIL HEP MI-2

Particle	Ions	Energy (MeV/n) Nuclear charge	Nuclear mass
	C	6.5 – 40	6.5 – 40
	Ne	8.0 – 52	5.5 – 52
	Mg	9.0 – 60	9.0 – 60
	Ca	12.0 – 80	14.0 – 74
	Fe/Ni	13.0 – 80	16.0 – 65
	Z<45	14.0 – 120	
Telescope		2 units	
Look Direction		90°	
Angle		120° x 120°	
Geometrical Factor		30 cm^2 sr x 2	
Mass Resolution (rms)		0.23 amu for $Z \leq 28$	
Telemetry Bit Rate*		TBD	
Electric Power**		4.98 W	
Weight**		3200 ± 640 g	

* 40 words per iostope.
**including MI-1.

[2] HEP-HI Spectrometer

The HEP-HI is a large geometric factor, very high mass resolution telescope which identifies heavy nuclides in various energy ranges, starting at 10 MeV/n for heliums. It measures chemical composition for $2 \leq Z \leq 28$, and the isotopic composition for each element from He through Ni. HI-box consists of Si-detector telescope, preamplifiers and bias voltage supplies. A cross sectional view is shown in Fig. 3.3.3-4.

To achieve the high mass resolution required for isotope identification of the incident charged particles, it is necessary to determine the trajectory of the particles through the telescope with high accuracy. The trajectory information is provided by Si-detectors (PSD1, PSD2), which are position-sensitive silicon detectors of a charge division type developed by GEOTAIL HEP team. These PSSDs are very large silicon detectors with 500 μm x 62 mm x 62 mm in size. Detector D1–D7 are used to measure the energy loss and/or residual energy of stopping particle. Detector D1 is Li-drifted Si-detector with a size of 1000 μm x 78 mm x 78 mm. D2 is also a Li-drifted Si-detector with a size of 2000 μm x 114 mm (dia.). Detector D2 through D6 are Li-drifted Si-detectors with 3.0 mm (thick) x 114 mm (dia.). D6 is employed as an anti-coincident detector.

The information on the incident positions of the particle, its energy losses and residual energy is provided by 14 bit pulse height analysis of signals from the detectors. The signals from each detector are amplified by a dual-gain shaping amplifier system which selects either low or high gain, depending on the signal size.

The dimension and other characteristics of each detector used for HEP-HI are summarized in Table 3.3.3-5. And the features of HEP-HI are shown in Table 3.3.3-6. The HEP-HI has such an exceptionally large geometric factor, 40 cm^2 sr, to be realized by the use of large PSSDs and large Li-drifted Si-detectors that we can expect to measure heavy isotopes up to Fe/Ni nuclei with a high accuracy in the SEP and GCR observations. The mechanical drawing of outside look for HEP-HI is shown in Fig. 3.3.3-5.

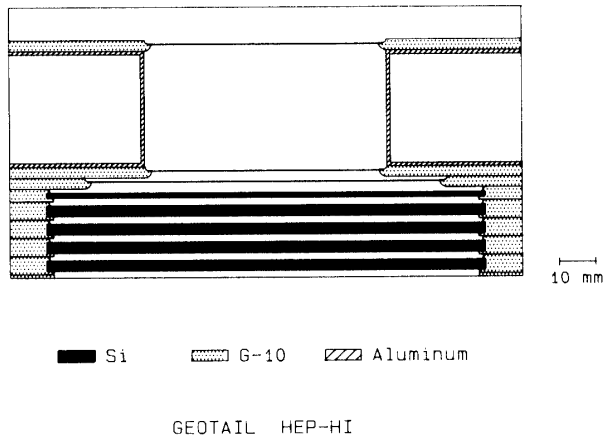

Fig. 3.3.3-4 Cross sectional view of GEOTAIL HEP-HI spectrometer. It consists of eight Si-detectors.

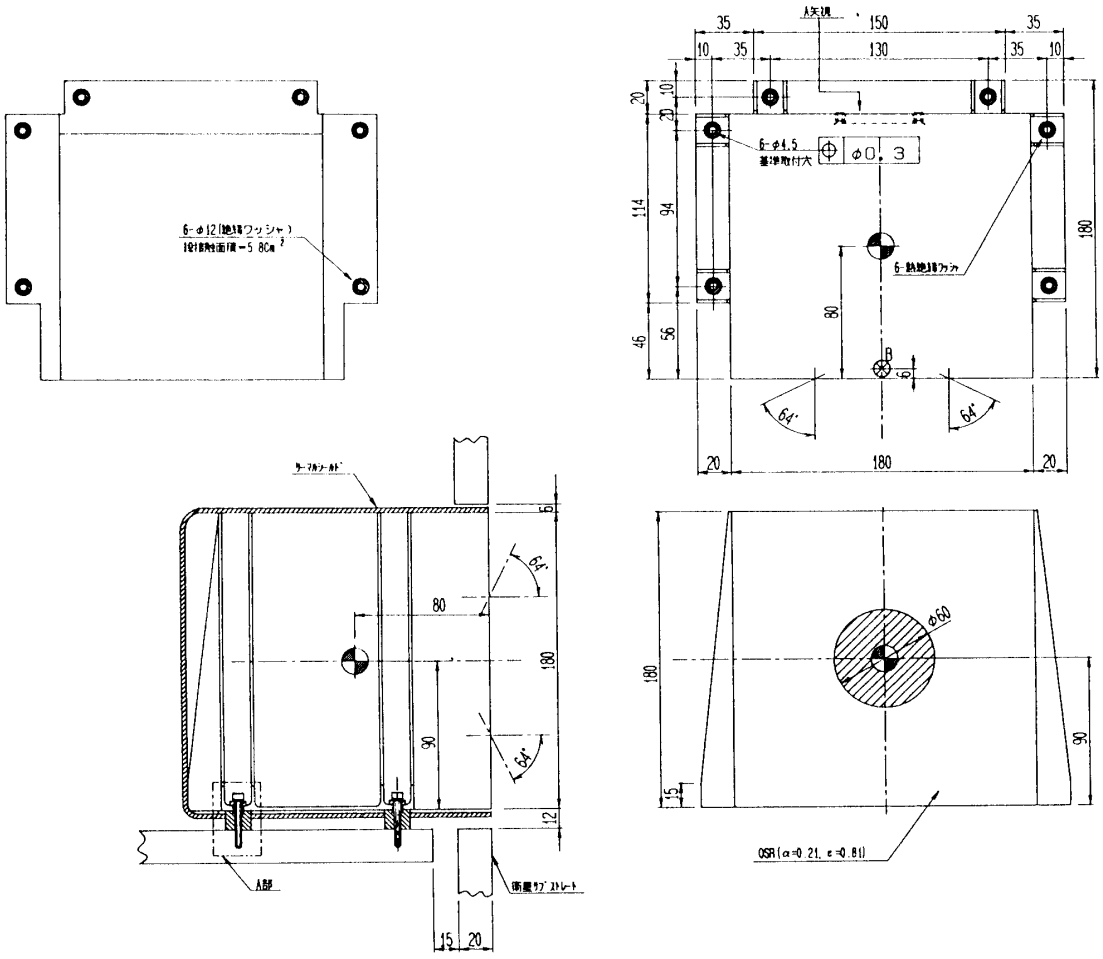

Fig. 3.3.3-5 Mounting structure of GEOTAIL HEP-HI spectrometer and preamplifier box.

Table 3.3.3-5 GEOTAIL HEP-HI consists of eight Si-detectors. The characteristics of the detectors are shown.

GEOTAIL HEP-HI Si-Detectors

	t (μm)	L (mm)	W (mm)	No.	Type*	Bias (V)
PSD1	500	62	62	1	II	180
PSD2	500	62	62	1	II	180
D1	1000	78	78	1	Li	100
D2	2000	114 (dia.)		1	Li	180
D3	3000	114 (dia.)		1	Li	330
D4	3000	114 (dia.)		1	Li	330
D5	3000	114 (dia.)		1	Li	330
D6	3000	114 (dia.)		1	Li	330

*II: Ion-implantation Type, Li: Lithium Drifted type.

Table 3.3.3-6 The Characteristic of GEOTAIL HEP-HI sepectrometer.

GEOTAIL HEP HI

	Ions	Energy (MeV/n) Nuclear charge	Nuclear mass
Particle	He	10 – 55	10 – 40
	C	18 – 110	18 – 110
	Ne	24 – 130	24 – 130
	Mg	26 – 160	26 – 160
	Si	28 – 180	28 – 180
	Ca	34 – 210	34 – 210
	Fe/Ni	38 – 210	21 – 210
Telescope		1 unit	
Look Direction		90°	
Opening Angle		120° x 120°	
Geometrical Factor		40 cm^2 sr	
Mass Resolution (rms)		< 0.23 amu for Z < 28	
Telemetry Bit Rate*		TBD	
Electric Power**		2.448 W	
Weight**		2500 ± 500 g	

*40 words per iostope.

Instrumental Characteristics and Comparisons

To better appreciate the unique and scientifically important studies possible with GEOTAIL HEP-MI and -HI, it is useful to compare it with an alternative sensor used before. Table 3.3.3-7 compares characteristics of the instruments.

Table 3.3.3-7 Comparison of instrumental characteristics.

Spacecraft	VOYAGER & ISEE-3	ISEE-3	ULYSSES	GEOTAIL HEP	
Instrument	HET	HIST	HET	MI	HI
Charge range (Z)	1 – 30	2 – 28	1 – 28	2 – 45	2 – 28
Mass range (M)	1 – 8	4 – 28	1 – 28	2 – 28	2 – 28
Mass Resolution (amu; rms)	O: 0.5 Be: 0.4	Ne: 0.27 Mg: 0.28	<0.25 for Fe	<0.23 for Fe	<0.23 for Fe
Geometrical factors (cm^2 sr)	0.9 – 1.7	0.43 – 0.82	3.6 – 16.2	60	40

To demonstrate the superiority of GEOTAIL HEP instruments, we compare in Table 3.3.3-8 the collecting power as the expected performance of GEOTAIL HEP instruments with the actual performance of the HIST experiment on board ISEE-3 during a flare of importance 2B on July 23 to 27, 1978.

The outstanding high resolution of GEOTAIL HEP allows precise measurement of elements and isotopes. Table 3.3.3-9 lists elements and isotopes resolvable by the GEOTAIL HEP sensors and Table 3.3.3-10 shows the counts of SEPs and GCRs per year, expected for the GEOTAIL HEP instruments.

Table 3.3.3-8 Comparison of collecting power between ISEE-3 HIST and GEOTAIL HEP-MI and -HI.

		ISEE-3 HIST		GEOTAIL HEP	
Element/ Isotope	Energy range MeV/n	No. Ptcls	Mass res. amu	No. Ptcls	Mass res. amu
He	6 – 38	1.2×10^{5}	0.13	7.2×10^{6}	0.1
C	6 – 42	1.1×10^{3}		6.6×10^{4}	
^{12}C		Main Comp.		Main Comp.	
^{13}C		12		7.2×10^{2}	
^{14}C		1		6.0×10^{1}	
N	9 – 42	300		1.8×10^{4}	
O	7 – 11	2300	0.23	1.4×10^{5}	0.12
	11 – 14	2400		1.5×10^{5}	
^{16}O		Main Comp.		Main Comp.	
^{17}O		0		7.1×10^{1}	
^{18}O		7		3.9×10^{2}	
Ne	8 – 11	136	0.27	8.2×10^{3}	0.13
	16 – 51	164		9.8×10^{3}	
^{20}Ne		Main Comp.		Main Comp.	
^{21}Ne		3		5.0×10^{1}	
^{22}Ne		15 – 18		2.0×10^{3}	
Mg	12 – 36	191	0.28	1.1×10^{4}	0.14
^{24}Mg		Main Comp.		Main Comp.	
^{25}Mg		28		1.2×10^{3}	
^{26}Mg		25		1.3×10^{3}	

Table 3.3.3-9 Observable species expected for GEOTAIL HEP-MI and -HI.

Item	Observed	GEOTAIL HEP-MI & -HI
Elements	H, He, C, N, O	He, (Li, Be, B), C, N, O
	Ne, Na, Mg, Si, A1	F, Ne, Na, Mg, Si, A1
	S, Ar, Ca	P, S, C1, Ar, K, Ca
	Fe	Ti, (V), Cr, Mn, Fe
	Ni	Co, Ni
Isotopes	^{3}He, ^{4}He	^{3}He, ^{4}He
	^{12}C, ^{13}C	^{12}C, ^{13}C, (^{14}C)
	^{14}N, ^{15}N	^{14}N, ^{15}N
	^{16}O, ^{18}O	^{16}O, ^{17}O, ^{18}O
		^{19}F
	^{20}Ne, ^{22}Ne	^{20}Ne, ^{21}Ne, ^{22}Ne
	Na	^{23}Na
	^{24}Mg, ^{25}Mg, ^{26}Mg	^{24}Mg, ^{25}Mg, ^{26}Mg
	A1	^{27}A1
	Si	^{28}Si, ^{29}Si, ^{30}Si
		^{31}P
	S	^{32}S, ^{33}S, ^{34}S
	C1	^{35}C1, ^{37}C1
	Ar	^{36}Ar, ^{38}Ar
		^{39}K
	Ca	^{40}Ca, ^{44}Ca
		^{48}Ti
		^{52}Cr, ^{53}Cr
		^{55}Mn
	Fe	^{54}Fe, ^{56}Fe, ^{57}Fe, ^{58}Fe
		^{59}Co
	Ni	^{58}Ni, ^{60}Ni, ^{62}Ni

Table 3.3.3-10 Expected counts of SEPs and GCRs for GEOTAIL HEP-MI and -HI.

Elements		Solar system Si=100	SEP (Note-1) cnts/flare	GCR (Note-2) cnts/year
2	He	180000	190000	260000
3	Li	--	--	790
4	Be	--	--	410
5	B	--	--	220
6	C	1110	5500	16000
7	N	231	1900	3800
8	O	1840	6200	37000
9	F	0.078	1.5	400
10	Ne	240	690	2600
11	Na	6	84	660
12	Mg	106	1300	3600
13	Al	8.5	100	660
14	Si	100	1100	2800
15	P	0.65	7.0	120
16	S	50	210	490
17	Cl	0.47	5.1	110
18	Ar	10.6	100	200
19	K	0.35	3.4	170
20	Ca	6.25	61	450
21	Sc	0.003	0.006	100
22	Ti	0.24	2.3	380
23	V	0.025	0.24	250
24	Cr	1.27	12	410
25	Mn	0.93	8.0	280
26	Fe	90.0	790	2400
27	Co	0.22	1.8	8
28	Ni	4.78	38	130

Note-1: GF = 100 cm^2·sr; Period, T = 1 day/Flare.
Flux = $2xE^{-2.5}/(cm^2 \cdot sr \cdot sec \cdot MeV/n)$ for He,
Counts = GFxAbundxf(FIP)xTxInt(Flux).
Note-2: Solar Max; GF = 100 $cm^2 \cdot sr$; Period T = 1 year

3.3.4 The Electronics

The functional diagram of HEP-MI and -HI system is shown in Fig. 3.3.4-1 and -2. Preamplifiers and bias voltage supplies as well as silicon-detector telescope are mounted in the boxes of MI and HI telescope. Other analog circuits and digital circuits are in the box of HEP-E Unit (Electronics System and Data Processing Unit).

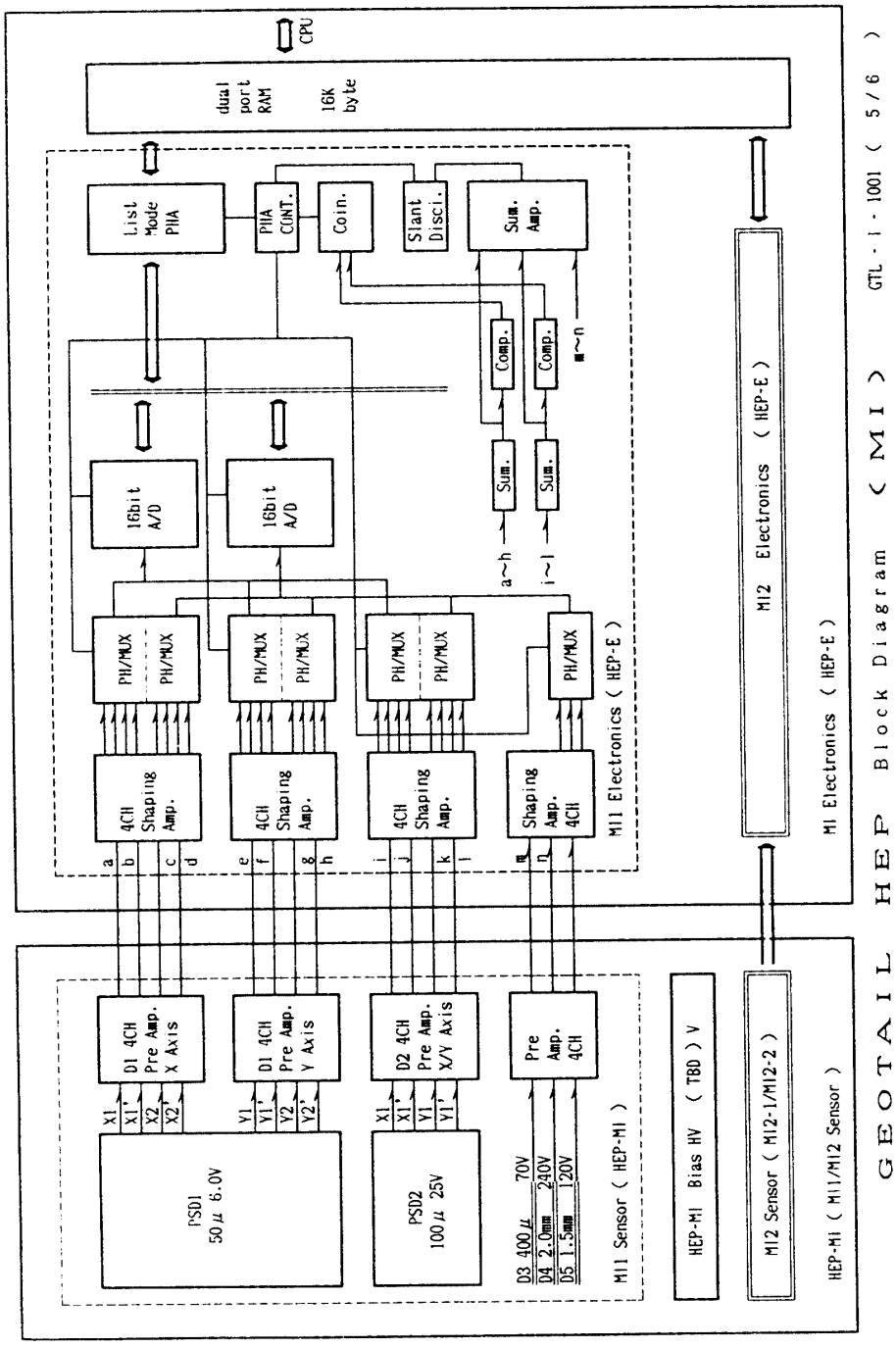

Fig. 3.3.4-1 Functional diagram of HEP-MI system. The left part is telescope and amplifier box (HEP-MI), and the right box is electronics system and data processing unit (HEP-E).

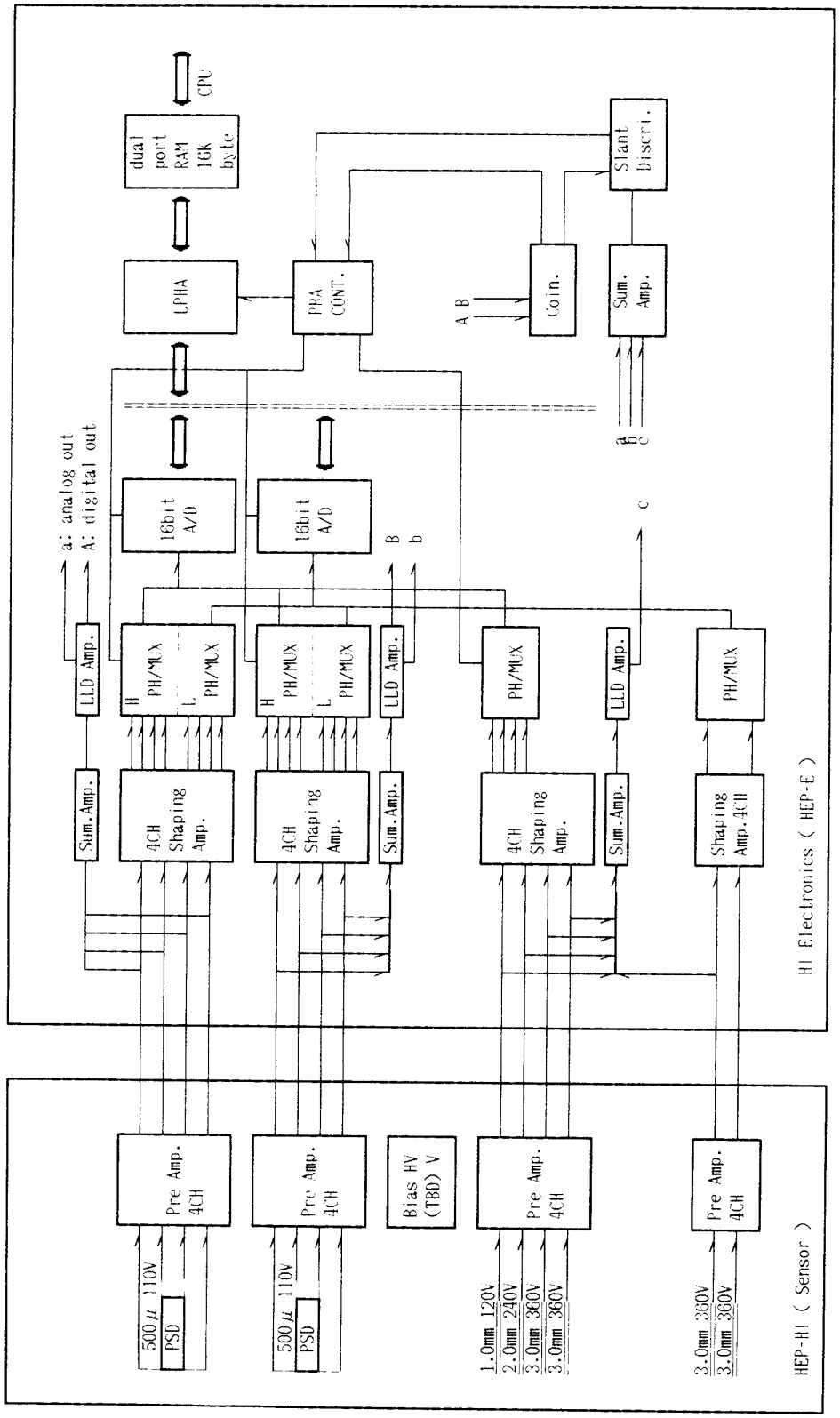

Fig. 3.3.4-2 Functional diagram of HEP-HI system. The left part is telescope and amplifier box (HEP-HI), and the right box is electronics system and data processing unit (HEP-E).

[1] Preamplifier System

This consists of hybrid ICs which include four low noise charge sensitive preamplifiers.

Specification of Preamplifier HIC

Integral Nonlinearity	< 0.01%
Temperature Instability	< +50 ppm/°C from −20°C to 20°C
Open Loop Gain	> 5000
Charge Sensitivity	Nominally 0.4 mV/MeV
Output Voltage Range	−11.0 to 4.0V
Energy Range	100 keV to 10 GeV
Rise Time	< 200 ns @ 1000 pF
Decay Time	Nominally 1000 μs
Input Capacitance (Det. Cap.)	200 pF to 5000 pF
Noise (Si eq.)	18 keV @ 1000 pF (Note 1)
Power Requirements	50 mW/channel nominally
Weight	16 g
Dimensions	1" x 1.5"

Note 1: assuming that electric noise expressed in FWHM is roughly
E noise = 3 keV + 15 eV x C(pF)
HICs is hybridized by AVIONICS company.

Specification of Bias Voltage Power Supply HIC for HEP-MI-1

Bias Voltage Outputs	40, 120, 180 and 220 V
Bias Polarity	Neg.
Bias Current	50 μA

Specification of Bias Voltage Power Supply HIC for HEP-MI-2

Bias Voltage Outputs	40, 120, 150, 180 and 220 V
Bias Polarity	Neg.
Bias Current	50 μA

Bias Voltage power supply is fabricated by MEISEI company.

Specification of Bias Voltage Power Supply HIC for HEP-HI

Bias Voltage Outputs	100, 180 and 330 V
Bias Polarity	Neg.

Bias Current 50 μA

Bias Voltage power supply is fabricated by MEISEI company.

3.3.5 Size, Weight and Power

The figures of the MI and HI sensor boxes are shown in Fig. 3.3.3-3 and 3.3.3-5. The size, weight and power of those sensors are shown in Tables 3.3.3-2, 3.3.3-4, and 3.3.3-6.

3.3.6 Special Requirements

The following precautions must be paid because of the characteristics of silicon detectors which are highly sensitive to humidity, temperature and surface contamination.

Dry nitrogen (or dry air) purge (on-ground).

Temperature	operating	$-20°C<T<20°C$,
	non-operating	$-40°C<T<30°C$,
	survival	$-50°C<T<30°C$.
Switch on temperature in-orbit		$T<20°C$.
Humidity		$<60\%$.

No water, no vapor and no other chemical gases on silicon surface.

Thermal Design: Technical Approach

Sensors thermally isolated from S/C
- Mounting on insulator (POLYARAMID)

Minimizing heat input from outside
- Surrounding by thermal blankets

Front surface of sensors used as radiator surface
- On the surface: OSR (PEI)

Electronics in sensors closely coupled to sensor box

Power for pre-amplifiers used as heat power during eclipse
- Pre-amplifiers are always on in orbit

Thermal test for each instrument independently required
- before thermal test for S/C system

Summary

Two instruments called HEP-MI and -HI will be dedicated to measure elemental and isotopic compositions in SEPs, GCRs and other energetic particles in the heliosphere. These instruments have following three key features;

exceptionally high sensitivity,
excellent isotope resolution, and
wide ranges of energy and observable species.

Geometric factor, mass resolution and energy ranges where elements and isotopes are observable, are shown in Table 3.3.7-1, and Fig. 3.3.7-1 and -2. These distinguished features can be realized by silicon detector telescopes combined with newly- developed position-sensitive detectors with a high position accuracy and by the use of very large silicon wafers.

Schematic drawings on HEP-MI and -HI are shown in Fig. 3.3.3-1 through Fig. 3.3.3-5. They are all Si-detector telescopes using the well-known ΔE-E algorithm for the mass identification of heavy ions.

Top two layers of them are two-dimensional position- sensitive Si-detectors (PSSD) which determine the trajectory of incident heavy ion as well as its energy losses. The PSSD with a good linear response, consisting of a square-shaped ion-implanted resistive anode with the boundary of additional resistive-strip electrodes, was newly developed. The following several layers are Li-drifted Si-detectors for the measurement of energy losses or residual energy of stopping ions. HEP-MI consists of one MI-1 and two identical MI-2 units. MI-1 puts emphasis on the measurement of low energy ions lighter than Mg isotopes. MI-2s are dedicated to observe nuclear charge of heavy ions from C through Rh as well as isotopic composition of heavy ions from C through Ni in the medium energy region. The geometric factor for MI-2 is extremely large, 2 x 30 $cm^2 \cdot sr$, which is about 100 times larger than that for HIST on board ISEE-3 and 4–10 times larger than COSPIN-HET on ULYSSES. HEP-HI measures elemental and isotopic compositions of ions from He through Ni in the high energy region.

The characteristics of these instruments are summarized in Table 3.3.3-1 through Table 3.3.3-6.

The instruments will allow to measure even rare isotopes as well as elemental composition for SEPs and GCRs. And precise identification of these ions in space will give us the essential information for understanding physical processes, such as stellar nucleosynthesis, the mechanism of solar flare, stellar activity, injection/acceleration and propagation of energetic ions, which occur at the Sun, heliosphere, stars and interstellar space.

REFERENCES

Althouse, W. E. et al., *IEEE Trans. Geosci. Electr.*, **GE-16** (1978) 204.
Doke, T. et al., *ISAS-Report*, **33** (1968) 193.
Doke, T., and K. Nagata, *ISAS Report*, **36** (1971) 475.
Doke, T. et al., *RIKEN*, 1986.
Doke, T. et al., *Nucl. Instr. Meth.*, **261** (1987) 605.
Gloeckler, G., and K. Hsieh, *Nucl. Instr. Meth.*, **165** (1979) 537.
Hasebe, N. et al., *Jpn. J. Appl. Phys.*, **27** (1988) 816.
Kohno, T. et al., *RIKEN*, 1987.
Nagata, K., and T. Doke, *Bull. Sci. and Eng. Res. Lab., Waseda Univ.*, No. 61 (1973) 69.
Nakagawa, S. et al., Cosmic-Ray-Research 1967.
Nakamoto, A. et al., *Nucl. Instr. and Meth.*, **130** (1975) 475.
Wilken, B., *Rep. Prog. Phys.*, **47** (1984) 767.
Yanagimachi, T. et al., *Nucl. Instr. and Meth.*, **275** (1989) 307.

Table 3.3.7-1 Characteristics of HEP-MI and -HI.

Instruments	MI-1	MI-2	HI
Telescope (unit)	1	2	1
Field of View	90° x 90°	120° x 120°	120° x 120°
Geometrical Factor ($cm^2 \cdot sr$)	4	2 x 30	40
Mass Resolution (amu; rms)	<0.23	<0.23	<0.23

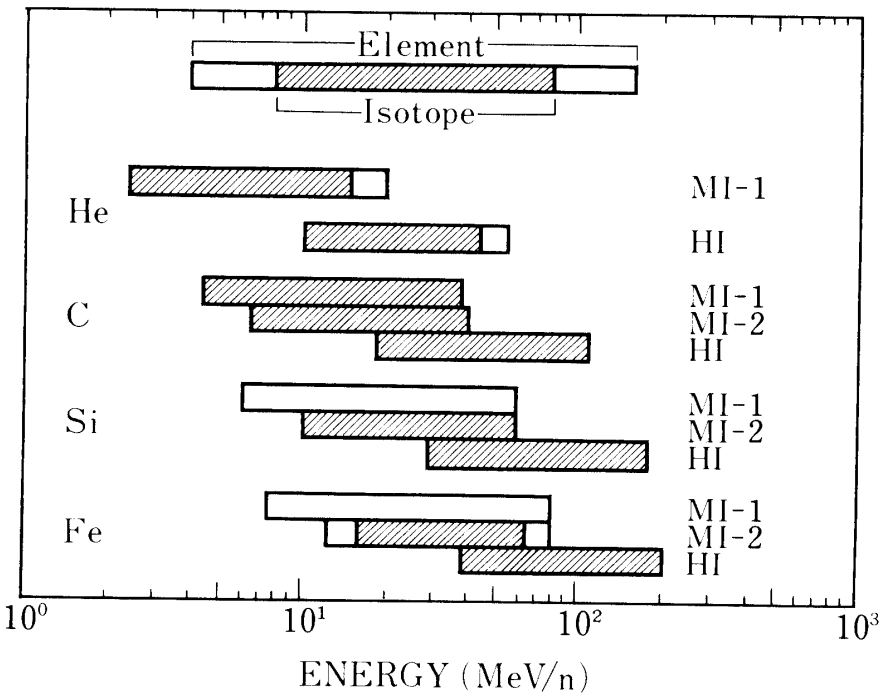

Fig. 3.3.7-1 Energy ranges where elements and isotopes are separable.

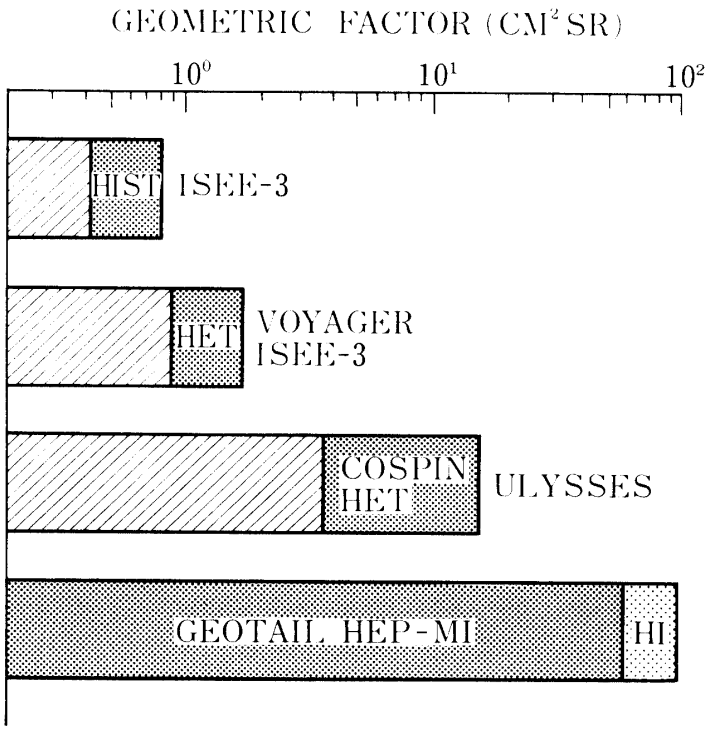

Fig. 3.3.7-2 Comparison of geometrical factors for some instruments.

3.4 Electronics System and Data Processing Unit

As shown in Fig. 3.4-1, HEP electronics (HEP-E) system consists of an analogue signal processing unit, a pulse height analyzing unit and a digital signal processing unit. Charge sensitive pre-amplifiers and bias voltage supplies for SSDs of BD, MI and HI are contained in the sensor unit. Other parts of electronic system are contained in HEP-E. For LD, however, both analogue and digital parts are contained in the sensor unit and observed signals are converted to digital data in it and is fed to HEP-E digital data processing unit.

Signal Processing of BD

BD sensor consists of three telescopes which detect electrons, protons, and helium ions. The analogue signal processing part and ADC part of pulse height analyzing unit stand alone for each sensors. Histograms of observed data are made as a function of the energy of each particle, the angular distribution and the spin of satellite. The schematic block diagram of BD is shown in Fig. 3.2.4-1. The pre-amplifier is a custom-made hybrid IC including buffer amplifier, whose size is 39 mm x 26 mm. The LLD amplifier is a custom-made hybrid IC including a shaping amplifier and two sets of two

level discriminator. The 16 channel ADC is also a custom-made hybrid IC, whose size is 51 mm x 44.5 mm, which analyze and divide a pulse peak into eight divisions for one decade equally by a logarithmic scale of the pulse height. Identification of particles is made by a ΔE-E slant discriminator (ΔE + AE1 + BE1).

Signal Processing of MI and HI

The signal processing systems of MI and HI have the same feature, but are different in the number of detectors and in the thickness of detectors, as shown in Tables 3.2.3-1, 3.3.3-1, 3.3.3-3 and 3.3.3-5. The charge signals caused by heavy ions passing through the detectors are amplified by the charge sensitive pre-amplifiers and the shaping amplifiers. The dynamic range of the signal from position sensitive detector is very large, so the shaping amplifier is divided into two sections of a high gain- and low gain-sections. The signals due to the particles which pass through the first detector and reach the second detector, are selected by LLD amplifiers and slant discriminator and their peak pulse heights are held by a peak hold circuits and converted to digital data by a 16 bit ADC. The output data from the list mode PHA is not analyzed on board and sent to the ground system directly. And then, all analysis such as corrections of incident angle of particles, identification of particles, energy distributions of particles, etc. are done by the analysis system on the ground. Only the rough identification of particles and the priority of transmitting of the data are decided by the slant discriminator on board.

Digital Signal Processor

The digital signal processor consists of the satellite system (DHU) interface, the command interpreter and executing system and two micro-computer systems. The command and the telemeter data are transmitted through DHU of the satellite. The interface between DHU and HEP-E is a standard interface module (PIM). Two kinds of telemeter data, which are the real mode data and the recorded mode data, are transmitted to the ground. The recorded data from the GEOTAIL mission are obtained for 24 hours per day with the bit rate of 16 kbit/sec, in which 1664 bits/sec is allocated to HEP. The real mode data from the GEOTAIL mission are transmitted for 8 hours per day with the bit rate of 64 kbit/sec and received at UDSC (USUDA). The bit rate of the real mode data of HEP is 10752 bit/sec. Also the system has another two modes of the contingency mode and RAM check mode. HEP-E has a two PIM for the real mode data and the recorded mode data.

Two kinds of command, one is discrete (DC) and another is block (BC), are used for HEP. HEP uses only 60 items of 256 DC. BC is used for adjusting several parameters for the systems such as RAM address, the discriminator levels, the voltage of detector bias, the observation mode and the modification of program memory. The command interpreter and executing system interprets and executes the command from DHU except for LD. The command for LD is transferred to LD system only through digital signal processor, and interpreted and executed by LD system. HEP uses two micro computer systems (Z80), one is DATA-DPU for data taking and transmitting, another is EDIT-DPU for data editing. The DATA-DPU executes data taking of BD, MI and HI by the observation mode set by the command, control of PHA and editing of data. The data which is editing by DATA-DPU are written on the common memory as a transmitting data set. The data from LD are stored once every 1 second in the memory of EDIT-DPU as a transmitting data set. EDIT-DPU edits and converts the data in the memory to the format of the telemeter. The telemeter data is stored in buffer memory of PIM every 4 frame in real mode and 1 frame in recorded mode.

HEP-E is made as very compact and reliable by using custom-made hybrid ICs. Also the digital signal processing unit is flexible by using the micro computer systems.

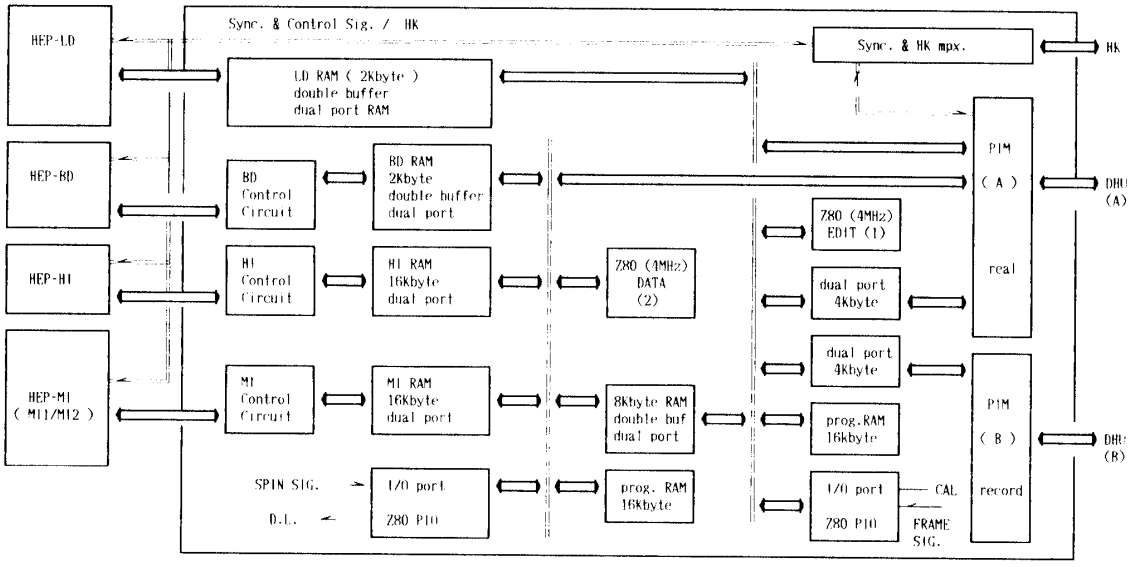

GEOTAIL HEP Block Diagram GTL-1-1001 (1/6)

HEP:	High Energy Particles	HEP-E:	HEP Electronics
LD:	Low Energy Particle Detector	HEP-LD:	LD Sensor
BD:	Burst Detector in Geotail Region	HEP-BD:	BD Sensor
MI:	Medium Energy Isotope Spectrometer	HEP-MI:	MI Sensor
HI:	High Energy Isotope Spectrometer	HEP-HI:	HI Sensor

Fig. 3.4-1 Schematic diagram of HEP-E.

4. KEY PARAMETER DIGITAL FILE (KPDF)

The key parameters are selected data from the observed results by each instrument of GEOTAIL missions, and are delivered to the scientists of the ISTP group. The data of electron and proton observed by the HEP-LD are used as key parameter digital file of the high energy particle experiment.

4.1 Key Parameter Digital Data Volume (Input)

Input data are not required for HEP-LD key parameter file since an inertial system will be used as reference system.

4.2 Key Parameter Digital Data Volume (Output)

The following data sets are provided for the KPDF;

Electrons: 4-channel energy spectrograms for four azimuthal 90° sectors in the S/C equator. Time resolution: 3 min.

Protons: 4-channel energy spectrograms for four azimuthal 90° sectors in the S/C equator. Time resolution: 3 min.

Helium: 4-channel energy spectrograms for four azimuthal 90° sectors in the S/C equator. Time resolution: 3 min.

Oxygen: Integral rate (integrated over energy and angle)
The resolution: 3 min.

4.3 Key Parameter Digital Data Characteristics

Table 4.1 Key parameter digital data characteristics.

Data Set	Format	Size	Frequency (bytes)	(per week)
Electrons	(corrected)	8 bit	1.3×10^4	1
Protons	(corrected)	8 bit compressed	1.3×10^4	1
Helium	(corrected)	8 bit floating	1.3×10^4	1
Oxygen	(corrected)	8 bit point	3×10^3	1

4.4 Key Parameter Digital Processing Algorithm

The HEP-LD KPDF data require:

Decompression
Conversion to flux units
Averaging (Time, Angle, Energy)

4.5 Key Parameter Digital Processing Time Estimates

Will be defined.

4.6 Orbit and Attitude Data in Key Parameter Digital Processing

No requirement.

4.7 Key Parameter Digital Data Storage in the CDHF

Chronologically in 3 hour files.

5. KEY PARAMETER PLOT FILE

The data of electron and proton observed by the HEP-LD are used as key parameter plot file of the high energy particle experiment.

5.1 Key Parameter Plot Data Volume (Input)

Orbital Data.

5.2 Key Parameter Plot Data Volume (Output)

Electron Direction-Spectrogram: 1.1×10^5 bytes/week
Proton Direction-Spectrogram: 1.1×10^5 bytes/week
Helium Direction-Spectrogram: 1.1×10^5 bytes/week
Oxygen Integral Omnidirectional: 3.4×10^3 bytes/week

5.3 Key Parameter Plot Data Set Characteristics

Table 5.1 Key parameter plot data set characteristics.

Type Product Medium	Name of Plot	Format	Volume Plot	Avg. No. of Plots/week	No. of Points plotted/week
Grey Microfiche	Proton Direction-Spectrogram	8 bit integral	1920 bytes	56	1.1×10^5
Grey Microfiche	Helium Direction-Spectrogram	8 bit integral	1920 bytes	56	1.1×10^5
Grey Microfiche	Electron Direction-Spectrogram	8 bit integral	1920 bytes	56	1.1×10^5
Line Microfiche	Oxygen	8 bit integral	60 bytes	56	3.36×10^3

5.4 Key Parameter Plot File Processing Algorithm

The procedure is the same for all three directional data sets. The input consists of count rates in 16 different directions and 8 different energies. Count rates are converted to flux units by subtracting background and multiplying by a conversion factor. The directions are reduced to 4 by averaging. Then for each of these 4 directions, the fluxes are plotted using a grey scale, with energy on the vertical, time on the horizontal axis. Each plot contains 4 such spectrograms (one for each direction), and covers a 3 hour period.

The oxygen data set is similarly treated, expect that it is averaged over all energies and directions, and then plotted as a line plot against time.

5.5 Key Parameter Plot File Processing Time Estimates

Will be defined.

5.6 Orbit and Attitude Data in Key Parameter Plot File Processing

Position data will be added to the time scales.

6. Telemetry Data Format

There are three data acquisition Format for GEOTAIL telemetry operation mode; (1) FORMAT-1 (Record Mode), (2) FORMAT-2 (Real Mode) and (3) FORMAT-3 (Contingency Mode). The HEP data word allocation is shown in Table 6.1-1. The data involve the instrumental status information, the housekeeping information and the scientific data of LD, BD, MI and HI.

The frame allocations of HEP instrumental status information are shown in Table 6.1-2. The status information consists of ON/OFF of the instrument, ON/OFF of high voltage power, and commanding answer. The information of the housekeeping monitor are shown in Table 6.1-3. The data are allocated in word 11, and consist of voltage and current monitor, calibration and discriminator monitor, temperature of the instrument, and some status data of LD sensors.

6.1 Data Formats of Status and Housekeeping Data

Word allocation of HEP telemetry is shown in Table 6.1-1. Format-1 is the case of Record Mode, Format-2 is the case of Real Mode, and Format-3 is the case of Contingency Mode.

Telemetry frame and word allocation mode of status data is shown in Table 6.1-2, and frame allocation of housekeeping data is shown in Table 6.1-3.

6.2 Data Formats of LD

Table 6.2-1 shows the first definition of the HEP-LD Experiment Data Block (EDB) for the Real Time Mode. One EDB contains 960 Byte and the rate is 1 EDB/spin.

A corresponding description of the EDB in the Record Mode is not yet defined.

Abbreviations used in Table 6.2-1.

ID 0, ID 1 = Identifier of EDB, hex 14 GF
DHK = Digital Housekeeping
AHK = Analog Housekeeping
I-SGL = I-SINGLES
I-SPCT = I-SPECT
I-FB = I-FB
I-PTCH = I-PITCH
I-3DS = I-3D slow
I-3DF = I-3D fast
I-MR = I-Matrix
I-DE = I-DE
E-SGL = E-SINGLES
E-SPCT = E-SPECT
E-FB = E-FB
E-PTCH = E-PITCH
E-3D = E-3D

Note:
Frames of the HEP-LD Experiment Data Block (EDB) are not synchronized with the S/C-frames, i.e. HEP-LD-frame 0 dose not appear in S/C-frame 0.

Table 6.1-1 GEOTAIL HEP telemetry word allocations.

	HEP Telemetry Word	
*FORMAT – 1	(Record Mode)	
LD	W48 – W51	4W
BD	W52 – W56	5W
MI, HI	W57 – W60	4W
*FORMAT – 2	(Real Mode)	
LD	W77 – W81	5W
BD	W82 – W87	6W
MI, HI	W88 – W97	10W
*FORMAT – 3	(Contingency Mode)	
LD	W77 – W81	5W
BD	W82 – W87	6W
MI, HI	W88 – W91	4W

Table 6.1-2 GEOTAIL HEP status frame-word-bit allocations.

No.	Status	Frame	Word	Bit	BIT	DISPLAY
1	HEP	32n+18	8	0	1/0	ON/OFF
2	HEP RAM	32n+18	8	1	1/0	ON/OFF
3	HEP CPU1	32n+18	8	2	1/0	ON/OFF
4	HEP CPU2	32n+18	8	3	1/0	ON/OFF
5	LD	32n+18	8	4	1/0	ON/OFF
6	BD	32n+18	8	5	1/0	ON/OFF
7	MI	32n+18	8	6	1/0	ON/OFF
8	HI	32n+18	8	7	1/0	ON/OFF
9	LD HV	32n+18	9	0	1/0	PRESET/RELEASE
10	BD HV	32n+18	9	1	1/0	PRESET/RELEASE
11	MI HV	32n+18	9	2	1/0	PRESET/RELEASE
12	MI HV	32n+18	9	3	1/0	PRESET/RELEASE
13	LD HV	32n+18	9	4	1/0	ON/OFF
14	BD HV	32n+18	9	5	1/0	ON/OFF
15	MI HV	32n+18	9	6	1/0	ON/OFF
16	HI HV	32n+18	9	7	1/0	ON/OFF
17	DATA SYNC. ID0	32n+18	10	0	1/0	ID0
18	DATA SYNC. ID1	32n+18	10	1	1/0	ID1
19	DATA SYNC. ID2	32n+18	10	2	1/0	ID2
20	COVER ENA/DIS	32n+18	10	3	1/0	ENA/DIS
21	LD MCP CAL.	32n+18	10	4	1/0	ON/OFF
22	LD MCP SAFE	32n+18	10	5	1/0	ON/OFF
23	RAM SELECT	32n+18	10	6	1/0	LD/E
24	CAL	32n+18	10	7	1/0	ON/OFF
25	HEP LD BC ANS.	32n+19	8	0	1/0	LD
26	HEP BC 1 ANS.	32n+19	8	1	1/0	1
27	HEP BC 2 ANS.	32n+19	8	2	1/0	2
28	PROGRAM/TABLE	32n+19	8	3	1/0	PROG/TAB
29	TABLE NO ID0	32n+19	8	4	1/0	ID0
30	TABLE NO ID1	32n+19	8	5	1/0	ID1
31	PROG. ADR.SET	32n+19	8	6	1/0	SET
32	PROG. WRI.SET	32n+19	8	7	1/0	SET
33	CPU1 RUN/HALT	32n+19	9	0	1/0	RUN/HALT
34	CPU2 RUN/HALT	32n+19	9	1	1/0	RUN/HALT
35	HEP-E STATUS 1	32n+19	9	2	1/0	1/0
36	HEP-E STATUS 2	32n+19	9	3	1/0	1/0
37	HEP-E STATUS 3	32n+19	9	4	1/0	1/0
38	HEP-E STATUS 4	32n+19	9	5	1/0	1/0
39	LATCH UP FLAG	32n+19	9	6	1/0	ON/OFF
40	RAM OF ENA/DIS	32n+19	9	7	1/0	ENA/DIS
41	BD STATUS 0	32n+19	10	0	1/0	1/0
42	BD STATUS 1	32n+19	10	1	1/0	1/0
43	MI STATUS 0	32n+19	10	2	1/0	1/0
44	MI STATUS 1	32n+19	10	3	1/0	1/0
45	MI STATUS 2	32n+19	10	4	1/0	1/0
46	HI STATUS 0	32n+19	10	5	1/0	1/0
47	HI STATUS 1	32n+19	10	6	1/0	1/0
48	PROG. ADDRESS	135	8	0-7		
49	PROG. ADDRESS	135	9	0-7		
50	BC ANSWER	32n+10	10	0-7		
51	SAVE MODE1	32n+19	10	7	1/0	ON/OFF

Table 6.1-3 GEOTAIL HEP housekeeping data frame allocations.

Housekeeping Telemetry Frame (Word 11)

No.	HK	Frame	Note
1	LD HV1	512n+19	Voltage and Current of Sensors
2	LD HV2	512n+147	
3	BD HVI	512n+20	
4	BD HVV	512n+148	
5	MI HVI	512n+276	
6	MI HVV	512n+404	
7	MI HVI	512n+21	
8	HI HVV	512n+149	
9	HEP MON1	512n+277	
10	HEP MON2	512n+405	
11	CAL REF1	512n+273	Calibration and Discriminaor Level
12	CAL REF2	512n+401	
13	DIS REF1	512n+17	
14	DIS REF2	512n+145	
15	LDS +5V	512n+18	Status of LD Sensors
16	LDS −5V	512n+146	
17	LDS +12V	512n+274	
18	LDS −12V	512n+402	
19	LDS MON1	512n+275	
20	LDS MON2	512n+403	
21	LD-T	128n+89	Temperature of Instruments
22	BD-T	128n+90	
23	MI-T	128n+91	
24	HI-T	128n+92	
25	E-T	128n+93	

Table 6.2-1 HEP-LD Experiment Data Block (EDB) Format 2 and 3 (Real Time Telemetry).

Frame	W77	W78	W79	W80	W81
0	ID 0 (14h)	ID 1 (6Fh)	DHK 0	DHK 1	DHK 2
1	DHK 3	DHK 4	DHK 5	DHK 6	DHK 7
2	AHK 0	AHK 1	I-SGL 0	I-SGL 1	I-SGL 2
3–15	I-SGL				
16	I-SGL 68	I-SGL 69	I-SGL 70	I-SGL 71	I-SPCT 0
17–20	I-SPCT				
21	I-SPCT 22	I-SPCT 23	I-FB 0	I-FB 1	
22–27	I-FB				
28–46	I-PTCH				
47	I-PTCH 95	I-3DS 0	I-3DS 1	I-3DS 2	I-3DS 3
48–84	I-3DS				
85	I-3DS 189	I-3DS 190	I-3DS 191	I-3DF 0	I-3DF 1
86–111	I-3DF				
–115	I-MR				
116	I-MR 20	I-MR 21	I-DE 0	I-DE 1	I-DE 2
117–130	I-DE				
131	I-DE 73	I-DE 74	E-SGL 0	E-SGL 1	E-SGL 2
132–133	E-SPCT				
134	E-SPCT 10	E-SPCT 11	E-FB 0	E-FB 1	E-FB 2
135–152	E-FB				
153	E-FB 93				
	E-FB 94	E-FB 95	E-PTCH 0	E-PTCH 1	
154–162	E-PTCH				
163	E-PTCH 47	E-3D 0	E-3D 1	E-3D 2	E-3D 3
164–191	E-3D				

6.3 Data Formats of BD

Observations of the on-board HEP-BD instruments have three operational modes: Mode-A (Real and Contingency), Mode-B and Mode-C (Record Mode). In the Mode A-1, the energy spectrum of electron, proton and Helium are obtained in 16 sector steps for every 3 sec spin period. In the Mode A-2, the energy spectrum of the particles and the counting rate of detectors are obtained in 8 sector steps for 96 sec 32 spin periods.

In the Mode-B, the energy spectrum of electron, proton and Helium are obtained in 8 sector steps for every 6 sec (2 spins), and in the Mode-C, in 16 sector steps for every 12 sec (4 spins). The difference between Mode-B and -C is the sampling time 6 sec or 12 sec.

The first frame of every BD data group is the spin synchronized format frame. The format is 16 x bit 1 and 8 x bit 0, this means the word representation FF FF 00.

6.4 Data Formats of MI and HI

One data set of MI or HI observed event consists of 40 words. First 2 words are identification words: Hex codes FF F1 ..... show the MI-1 data, FF F2 ..... show the MI-2 data, and FF F3 ..... show the HI data. Frame and word allocations are shown in Fig. 6.4-1. Particle data from telescope are shared in 3W-40W. In case of no data, frame and word are null.

Telemetry Data Format of MI & HI

	1W	2W	3W	...	40W
MI-1	F F F 1	Data of MI-1			
MI-2	F F F 2	Data of MI-2			
HI	F F F 3	Data of HI			

Note:
1. One data set constitutes of 40 words.
2. First 2 words are identification words shown above.
3. Telemetry data format is independent of Format-1, -2, and -3.
4. The 1st word is W57 (Format-1) or W88 (Format-2 and -3).
5. Frame and word are blank in case of no data.

Fig. 6.4-1 Frame and word allocations for HEP-MI and -HI. The first two frames are identification frames of sensor MI-1, MI-2 or HI.

7. Test and Calibration Plans

Test and calibration plans of the HEP instruments will be made under the following plan.

7.1 Onground Experiment Test and Calibration

7.1.1 Calibration Plan for LD

Environmental and qualification tests will be executed on MPAe facilities or in facilities available elsewhere in Europe: a. Vibration: MPAe b. Thermal Vacuum: MPAe c. Magnetic cleanliness: Technische Universitaet Braunschweig d. EMC (if required on LD level): Commercial facilities in Germany.

Characterization of the instrument performance with particle beams will be done with the MPAe heavy ion accelerator (for ion energies up to 350 keV/charge). It is planned to use the Goddard-Space-Flight-Center (USA) beam facility for tests with high energy ions or electrons.

7.1.2 Calibration Plan of BD

The silicon detectors of BD will be calibrated individually using radioactive alpha and electron sources at the institute. After integration, energy-channel relations are calibrated using protons and helium ions from the cyclotron accelerator at Riken or the tandem accelerator at Waseda University. The identification test of electrons and protons will be made using radioactive source.

7.1.3 Calibration Plan of MI and HI

[1] Test Plan

Fundamental test of each silicon detector constituting the HEP-MI and -HI sensors, under the room temperature, will be done at the facility of Waseda Univ. by using the alpha-radioactive sources. Thermal test in the temperature of $-50°C \sim 40°C$ for each detector will be made at the ISAS. Vibrational test of those instruments will be made in the facility of ISAS. The whole test (vibrational, sound, vacuum and thermal tests) of the HEP-MI and -HI system will be done at the facilities of ISAS.

[2] Calibration Plan

The development of the sensors, HEP-MI and -HI, will frequently or timely require access to beams of heavy particles of appropriate energies and species. Initially these particle beams will be required to verify the anticipated sensor response during the design phase. Later these particle

beam will be required to calibrate the various electronic threshold and operational characteristics and to establish the limits to which the critical determination of the various isotope abundances can be determined.

The accelerators required to produce these beams are presently available in the Riken and the LBL. GEOTAIL HEP team has easy access to these facilities.

(A) Riken Ring Cyclotron Accelerator

Riken Ring cyclotron accelerator completed in 1986. Now Cu-beam with around 30 MeV/n is already available. Within this fiscal year, the maximum energy will be raised, and various species will be available, for instance, C-beam with 70 MeV/n and Fe-beam with 50 MeV/n will be produced by the accelerator. This machine can cover the essential energy ranges for elements for HEP-MI and -HI instruments. It can cover the lower energy ranges even for the iron-group. The GEOTAIL HEP team can utilize this accelerator facilities easily.

(B) Bevalac at LBL

The Bevalac accelerator is capable of producing particle beams of any masses with high energy range which exceeds the range of iron-group produced by Riken cyclotron accelerator. This machine is especially suitable to examine the response of the HEP-HI instruments against the high energy particles heavier than argon.

These facilities which is ideally suited to testing and calibrating the MI and HI will be utilized by the HEP team. The availability of these accelerator facilities to the HEP instruments is a resource to the GEOTAIL project.

7.2 Inflight Test and Calibration

Procedure of the inflight calibration of HEP instruments is shown in this section.

7.2.1 Inflight Calibration of LD

The LD spectrometer contains an advanced built-in calibrator system which is controlled by the digital processing unit (LD-DPU). The principle of this in-flight calibrator (IFC) is to produce highly accurate (E; T)-pulse pairs to simulate particle events. The injected energy (E) and time (T) signal amplitudes can be selected by the DPU within a prescribed range. The IFC calibrator allows the detailed test of significant parameters in the analog sec-

tion of LD such as energy threshold, conversion factors, multiplexer performance, and ADC conversion gain. Since the injected signals simulate particle events the correct data flow through the DPU will also be verified. Two principle modes of operation will be available for the IFC:

The Automatic IFC Mode (AIFC): On telecommand the DPU initiates the IFC with a high pulse rate (approx. 1 kHz) and steps the calibrator through a pattern of preprogrammed configurations. The total duration of this mode is about 3 min and the instrument returns to its normal operation after completion of AIFC.

The Background IFC Mode (BIFC): For each spin rotation a single (E, T) pulse pair is injected into the system at a fixed phase angle. The DPU cycles the pulse amplitudes and multiplexer positions through a preprogrammed pattern which allows easy confirmation of the general instrument health. This single-shot-per-spin mode is intended as a continuous background calibration which will have negligible interference with real particle events because of the known injection time and short pulse duration. The simulated events are part of the routine on-board and ground data processing and allow therefore an end-to-end test of the LD space and ground segment. This mode can be initiated or inhibited by telecommand.

7.2.2 In-Flight Calibration of BD

In order to ensure the required accuracy of the electrical linearity during in-flight operation, status and housekeeping information will be monitored, and test pulse signals will check the system periodically by command. The check items by the test pulse signals are amplifier gain, discriminator and trigger levels, and logic functions.

7.2.3 Inflight Calibration of MI and HI

In order to ensure the required accuracy of the electrical linearity during in-flight operation, status and housekeeping information will be monitored, and test pulse signals will be sent to check the analog and digital circuit system periodically by commands. The checking items by the test signals generated by Pulse Generator in the HEP-E are noise levels of all Si-detectors and amplifiers, gain-drifts of all amplifiers, discriminators and trigger levels, and logic functions.

8. Data Analysis Scenario

The raw data of HEP observation are stored in the SIRIUS data storage system of the ISAS. The scientific object of this observation is to analyze local spatial and temporal structures in various regions in geotail space and to obtain the elemental and isotopic abundance of energetic particle. The aid of data such as geomagnetic activity data and/or solar activity data are important to resolve the geospace phenomena. The data processing scenario of HEP group is the combination of satellite data and ground based data. In addition to the observed data, the other data set, such as magnetic field line, plasma density and plasma waves must be used to understand the disturbed geotail space.

Software will be developed to produce data set in which HEP data and relevant data are merged according to the scientific objects. The produced outputs are particle flux, energy spectra, isotope distribution, and three dimensional particle distribution as well as the spacecraft orbit data.

The data analysis plans of HEP individual spectrometers are shown in Fig. 8-1.

8.1 Data Analysis Plan

8.1.1 LD Data Analysis Plan

The LD raw science data (if possible together with BD data or the complete HEP data volume) on tapes or optical disks (or via networks) shall be sent to MPAe where they shall be archived and processed to a higher level appropriate for interpretation. The data tapes should be written in a format identical to a format used for system tests to avoid duplication of the software effort. In addition to the experiment data, other data sets such as magnetic field and auxiliary data (orbit, attitude etc.) are required for the analysis phase. Software will be developed to produce working data sets in which the LD data and the other relevant data sets are merged and blocked according to the instrumental data format. The software will be produced for and the tapes will be processed on the MPAe-VAX computer. The software and processed data will be made available to the HEP group on tapes or via computer links.

MPAe will produce data summaries in graphical form on microfiche. The fiche will include the experiment as well as housekeeping data, modes of operation, spacecraft orbital position, plus other relevant information. Together with the HEP group MPAe will check the performance of the instrument and will establish conversion factors and other parameterss needs to convert the measured data into physical quantities. All of these factors will

be built into a service subroutine that can directly read the raw data and deliver the desired quantities. This service subroutine will be provided to the HEP group, who will then be able to include it in their specialized analysis programs according to their main field of investigation.

Specialized programs will be written according to the needs of the investigation being carried out. They will naturally include energy and mass spectra, as well as pitch angle plots and more complicated three dimensional distributions. LD data are multi-dimensional (three-dimensional velocity vector, particle species) and therefore there is no obvious, simple method of representation.

8.1.2 BD Data Analysis Plan

Electron, proton and Helium particles are observed by BD spectrometers. The raw data consist of particle counting rate, energy spectrum as spin synchronized data set. The particle data are summarized in graphical form. The form include time dependence of the particle intensity, energy spectra of each particle, spacecraft orbit data, and other information such as geomagnetic field lines, geospace coordinates, and pitch angles. The next phase of the data analysis is to merge the LD's data with BD's data. The merged data show the three dimensional distribution functions for protons and ions of energy range 2 keV/n – 35 MeVn and for electrons of 20 keV – 2.5 MeV. The large opening angle of BD can show the high time resolution for protons and Helium particles of MeV regions. Physical consideration of the geospace phenomena can be made by exchange HEP data with the other GEOTAIL observation data and SOHO, WIND, POLAR, CLUSTER, and EXOS-D data.

8.1.3 MI and HI Data Analysis Plan

[1] Data Analysis

Both the HEP-MI and -HI consist of two PSDs and several layers of ΔE- and E-silicon detectors. Precise measurements, data reduction and analysis must be done to make an identification of heavy isotopes. Information from the two PSSDs is used for the determination of the trajectory of the incident particle. To know the precise positions where the particle hits the silicon detectors, careful correction of the non-linearity of PSSDs is required. Pulse heights of energy signals sent from the ΔE- and/or E-detector are dependent on the temperature. Slight difference of amplifier gains should also be carefully corrected each other. After these raw data carrying the position and energy information will be calibrated by using the inflight calibration data as well as onground calibration data, they are made into processed data of actual positions and the energies deposited in the detectors.

[2] Scientific Analysis Plan

Processed data of positions determine particle trajectory and the inclination of incident particle to the detector plane is determined. Then, thicknesses of silicon detectors through which the particle passes, and the energy loss in the thickness of the matter can be obtained. The energy losses in the detector thickness and the residual energy provide the total energy, and the nuclear charge and mass of the incident particle by the use of the results of energy loss and its straggling of the heavy energetic particles carried out by the particle accelerator experiments in advance. As for each particle event hitting the telescope, finally mass, charge, energy, time, field alignment and other physical quantities will be stored in the data bank.

The analysis of statistical and experimental uncertainty is made, and the elemental abundance, isotopic abundance, energy spectra and time profit are shown.

Comparison with solar, coronal abundance and SEP's.
Comparison with GCR and SEP.
Correlation with He-3/He-4 and heavy isotopes.
Correlation with electrons and heavy isotopes.
Correlation with Radio and energetic particles.
Correlation with X-rays and energetic particles.
Correlation with gamma-ray and heavy isotopes.

And any other correlations will be examined in detail.

8.2 Instrument Telemetry Bit Rate

Allocated telemetry bit rate for HEP instruments is 1664 bps = 208 bytes/sec in case of record mode. Record mode is 24 hours record. HEP measurements have no special event mode, and no change of allocated bit rate. Energy calibration is made by artificial test pulses, its frequencies are not determined now.

The total science and housekeeping data volumes of all HEP instruments are:

Science data: Spin synchronized mode (1 spin/3 sec)
List mode

Housekeeping data: 9 status words per 32 Frames
5 temperature words per 128 Frames
20 voltage monitor words per 512 Frames

Data volumes (bytes)

	Hour	Day	Month
Science and Housekeeping	7.5×10^5	1.8×10^7	5.4×10^8

8.3 Instrument Commanding

HEP-LD requires Discrete Commands (DC) and Block Commands (BC). Following Power-ON command (DC) to the HEP-E unit (HEP-LD ON) the HEP-LD spectrometer goes into the POWER-ON RESET MODE. This mode allows the engineering check out but scientific data are not available since the instrument is not fully configured. A preliminary list BC-CMDs to configure HEP-LD is as follows:

CMD-Nr.	Purpose	Frequency
1	CHPS-A ON/OFF	Only after Switch-ON
2	CHPS-B ON/OFF	Only after Switch-ON
3	Deflection Voltage step	occasionally
4	Aperture Wide/Small	Typically twice per orbit
5	Trigger Status for E-T events	Typically a few times per mission duration
6	Multiplexer Status Par./Serial	Typically twice per Orbit
7	Channel Selection Energy: $E_1/E_2/E_3$	Only during check-out or in case of emergency
8	Channel Selection Time: $T_1/T_2/T_3$	same as 7
9	Channel Selection Direction: $P_1/P_2P_3/P_4$	same as 7
10	TAC-Slpe	same as 7
11 to 35	Parameter changes for Mass sorting and Submode selection	Only in case of emergency

CMDs 1, 2 and 3 follow the switch-on command after the health of the instrument has been established. CMD 4 to 6 depend on the orbital phase and the plasma environment. CMD 7 to 35 are needed only for check-out, correction or in case of failure.

Calibration modes
purpose: energy channel calibration
frequency: TBD

Instruments ON/OFF modes
purpose: Instruments ON/OFF at eclipse
frequency: TBD

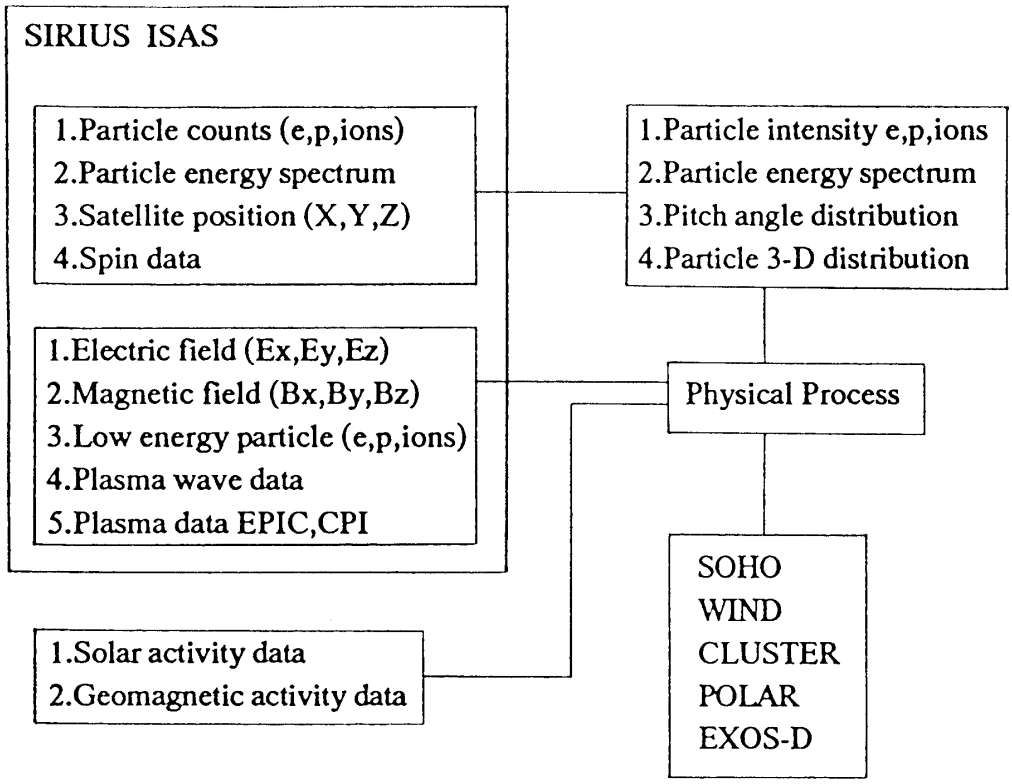

Fig. 8-1 Data analysis flow of LD, BD, MI, and HI data.